Universidad Autónoma de Madrid

Facultad de Ciencias

Departamento de Biología Molecular

Regulation of the expression and function of mitochondrial uncoupling protein UCP3 in response to oxidative stress: involvement of the transcription factor Nrf2 and implications in cardiac ischemia-reperfusion

Elia López Bernardo

Madrid, 2014

Universidad Autónoma de Madrid

Facultad de Ciencias

Departamento de Biología Molecular

Regulation of the expression and function of mitochondrial uncoupling protein UCP3 in response to oxidative stress: involvement of the transcription factor Nrf2 and implications in cardiac ischemia-reperfusion

Memoria presentada por la Licenciada en Biotecnología Elia López Bernardo para optar al grado de Doctora en Biociencias Moleculares por la Universidad Autónoma de Madrid con mención de doctorado internacional

Este trabajo ha sido realizado bajo la dirección de la Dra. Susana Cadenas Álvarez en el Centro de Biología Molecular "Severo Ochoa" (CSIC-UAM) y en el Instituto de Investigación Sanitaria del Hospital Universitario de La Princesa.

TABLE OF CONTENTS

ABBREVIATIONS 1

i. ABSTRACT 7

RESUMEN 11

ii. INTRODUCTION 15

1. MITOCHONDRIAL BIOENERGETICS 17

1.1. Mitochondrial oxidative phosphorylation 17

1.2. Mitochondrial proton leak 18

1.3. The physiological importance of proton leak 20

2. UNCOUPLING PROTEINS 20

2.1. Physiological role of uncoupling proteins 21

2.1.1. Physiological role of UCP1 22

2.1.2. Physiological role of UCP2 22

2.1.3. Physiological role of UCP3 23

2.2. Regulation of uncoupling proteins expression 24

2.2.1. Regulation of UCP1 expression 24

2.2.2. Regulation of UCP2 and UCP3 expression 25

3. OXIDATIVE STRESS 25

3.1. Mitochondrial ROS production 26

3.2. Extra-mitochondrial ROS formation 27

3.3. Oxidative stress induced by ROS 27

3.4. Amplification of oxidative stress by reactive aldehydes 28

3.5. Cellular antioxidant defences 29

3.6. 'Mild uncoupling' as a mechanism to control mitochondrial ROS production 30

4. THE ANTIOXIDANT TRANSCRIPTION FACTOR NRF2 31

5. CARDIAC ISCHEMIA-REPERFUSION INJURY 34

5.1. Cardiac ischemia-reperfusion induces oxidative stress 34

5.2. The phenomenon of ischemic preconditioning 36

5.3. 'Mild uncoupling' and cardiac ischemia tolerance 37

5.4. The Langendorff perfusion system as a tool for the study of the intact mouse heart 38

iii. OBJECTIVES 41

iv. MATERIALS AND METHODS 45

1. CELL CULTURE AND TREATMENTS 47

1.1. Mouse cardiomyocyte HL-1 cells 47

1.2. Mouse myoblast C2C12 cells 47

1.3. Cell treatments 47

2. ANIMALS 47

3. STUDY OF GENE EXPRESSION 48

3.1. Determination of RNA expression by quantitative PCR 48

3.1.1. RNA extraction 48

3.1.2. Determination of RNA concentration and purity 48

3.1.3. Reverse transcription 48

3.1.4. Quantitative real-time PCR 49

3.2. Determination of protein expression by immunoblotting 50

3.2.1. Cellular fractionation for differential protein extraction 50

3.2.2. Immunoblot analysis 51

4. STUDY OF GENE REGULATION 52

4.1. Small interfering RNA (siRNA) transfection 52

4.2. Chromatin immunoprecipitation (ChIP) assay 52

4.3. Plasmid construction and cell transfection 54

4.3.1. Construction of the pGL4.27-ARE and pGL4.27-mARE plasmids 54

4.3.2. Construction of the pGL4.27-Prom and pGL4.27-mProm plasmids 55

4.3.3. Transient transfection and luciferase reporter assay 56

5. DETERMINATION OF OXIDATIVE STRESS AND CELL VIABILITY BY FLOW CYTOMETRY 57

6. ANALYSIS OF CELL VIABILITY BY MICROSCOPY 58

7. MEASUREMENT OF CELLULAR RESPIRATION 58

8. ISOLATED HEART PERFUSION EXPERIMENTS 59

8.1. Langendorff perfusion of isolated hearts 59

8.2. Experimental perfusion protocols 61

8.3. Tissue protein extract preparation 63

8.4. Infarct size measurements 63

8.5. Creatine kinase activity assay 64

9. STATISTICAL ANALYSIS 65

v. RESULTS 67

PART I. STUDY OF UCP3 EXPRESSION AND FUNCTION UNDER OXIDATIVE STRESS. ROLE OF THE TRANSCRIPTION FACTOR NRF2 IN OXIDATIVE STRESS-MEDIATED UCP3 UPREGULATION 69

1. EFFECTS OF HYDROGEN PEROXIDE ON UCP3 EXPRESSION AND FUNCTION 69

1.1. Effects of H_2O_2 on UCP3 expression and Nrf2 nuclear accumulation 69

1.1.1. H_2O_2 treatment increases oxidative stress but does not induce cell death at short exposure times 69

1.1.2. H_2O_2 treatment upregulates UCP3 expression 71

1.1.3. H_2O_2 treatment induces nuclear accumulation of the transcription factor Nrf2 73

1.2. Involvement of Nrf2 in H_2O_2-induced UCP3 upregulation 75

1.2.1. Nrf2 binds to the *Ucp3* promoter after H_2O_2 treatment 75

1.2.2. H_2O_2-induced UCP3 upregulation is mediated by Nrf2 77

1.2.3. Nrf2 silencing prevents H_2O_2-induced UCP3 upregulation 78

1.3. Physiological consequences of UCP3 upregulation induced by H_2O_2 79

1.3.1. Upregulation of UCP3 via Nrf2 after H_2O_2 treatment increases cell survival 79

1.3.2. Effects of H_2O_2-induced UCP3 upregulation on cellular bioenergetics 81

2. EFFECTS OF 4-HYDROXY-2-NONENAL ON UCP3 EXPRESSION AND FUNCTION 85

2.1. Effects of HNE on UCP3 expression and Nrf2 nuclear accumulation 85

2.1.1. HNE treatment does not induce cell death at low micromolar doses 85

2.1.2. HNE treatment upregulates UCP3 expression 86

2.1.3. HNE treatment induces nuclear accumulation of the transcription factor Nrf2 87

2.2. Involvement of Nrf2 in HNE-induced UCP3 upregulation 89

2.2.1. Nrf2 binds to the *Ucp3* promoter after HNE treatment 89

2.2.2. HNE-induced UCP3 upregulation is mediated by Nrf2 90

2.2.3. Nrf2 silencing prevents HNE-induced UCP3 upregulation 91

2.3. Physiological consequences of UCP3 upregulation induced by HNE 93

2.3.1. Upregulation of UCP3 via Nrf2 after HNE treatment increases cell survival 93

2.3.2. Effects of HNE-induced UCP3 upregulation on cellular bioenergetics 94

PART II. ANALYSIS OF THE CARDIOPROTECTIVE ROLE OF UCP3 AGAINST ISCHEMIA-REPERFUSION INJURY: INVOLVEMENT OF THE TRANSCRIPTION FACTOR NRF2 96

1. STUDY OF NRF2-MEDIATED UCP3 INDUCTION AND ITS CARDIOPROTECTIVE ROLE IN THE ISOLATED MOUSE HEART AFTER ISCHEMIA-REPERFUSION 96

1.1. Ischemia-reperfusion (IR) increases UCP3 expression and Nrf2 nuclear accumulation in the isolated mouse heart 96

1.2. Infarct size after IR increases in hearts from UCP3-KO compared to WT mice: cardioprotective role of UCP3 against IR injury 97

1.3. Creatine kinase release after IR is higher in hearts from UCP3-KO mice than in those from WT mice 98

1.4. Infarct size after IR increases in hearts from Nrf2-KO compared to WT mice: cardioprotective role of Nrf2 against IR injury 99

1.5. Creatine kinase release after IR is higher in hearts from Nrf2-KO mice than in those from WT mice 100

2. STUDY OF THE INVOLVEMENT OF NRF2-MEDIATED UCP3 INDUCTION IN ISCHEMIC PRECONDITIONING IN THE ISOLATED MOUSE HEART 102

2.1. Cardiac ischemic preconditioning (IPC) increases UCP3 expression levels and Nrf2 nuclear accumulation 102

2.2. IPC does not reduce infarct size after IR in hearts from UCP3-KO mice: involvement of UCP3 in IPC 104

2.3. Creatine kinase release after IR is higher in preconditioned hearts from UCP3-KO mice than in those from WT mice 105

vi. DISCUSSION 107

1. UCP3 EXPRESSION INCREASES IN RESPONSE TO OXIDATIVE STRESS, AN EFFECT MEDIATED BY THE TRANSCRIPTION FACTOR NRF2 109

2. UCP3 UPREGULATION MEDIATED BY NRF2 PROTECTS AGAINST OXIDATIVE DAMAGE AND INCREASES CELL SURVIVAL 112

3. UCP3 EXPRESSION AND NRF2 NUCLEAR ACCUMULATION INCREASE AFTER ISCHEMIA-REPERFUSION IN THE ISOLATED PERFUSED MOUSE HEART: CARDIOPROTECTIVE ROLE OF UCP3 AND NRF2 113

4. UCP3 IS INVOLVED IN THE CARDIOPROTECTIVE PHENOMENON OF ISCHEMIC PRECONDITIONING 116

vii. CONCLUSIONS 119

CONCLUSIONES 123

REFERENCES 127

ANNEX 147

ABBREVIATIONS

ADP	Adenosine diphosphate
ALDH2	Aldehyde dehydrogenase 2
AMP	Adenosine monophosphate
ANOVA	Analysis of variance
ANT	Adenine nucleotide translocase
ARE	Antioxidant response element
ATP	Adenosine triphosphate
BAT	Brown adipose tissue
BCA	Bicinchoninic acid
BMCP1	Brain mitochondrial carrier protein 1
BSA	Bovine serum albumin
bZIP	Basic leucine zipper motive
CA	Calcein
cAMP	Cyclic AMP
CK	Creatine kinase
CoA	Coenzyme A
CREB	cAMP response element-binding protein
DCF-FA	2,7-Dichlorodihydrofluorescein diacetate
DMEM	Dulbecco's Modified Eagle's Medium
DMSO	Dimethyl sulfoxide
DNA	Deoxyribonucleic acid
DNP	2,4-Dinitrophenol
DTT	Dithiothreitol
e^-	Electron
EDTA	Ethylenediaminetetraacetic acid

EGTA	Ethylene glycol tetraacetic acid
ER	Endoplasmic reticulum
ETC	Electron transport chain
FA	Fatty acid
FAD	Flavin adenine dinucleotide (oxidized)
$FADH_2$	Flavin adenine dinucleotide (reduced)
FCCP	Carbonyl cyanide *p*-trifluoromethoxyphenylhydrazone
FFA	Free fatty acid
GPx	Glutathione peroxidase
Grx	Glutaredoxin
GSH	Glutathione (reduced)
GSR	Glutathione reductase
GSSG	Glutathione (oxidized)
H^+	Proton
HNE	4-Hydroxy-2-nonenal
HO-1	Heme oxygenase 1
IMM	Inner mitochondrial membrane
IMS	Intermembrane space
IPC	Ischemic preconditioning
IR	Ischemia-reperfusion
Keap1	Kelch-like ECH-associated protein 1
KO	Knockout
LDH	Lactate dehydrogenase
MAPK	Mitogen-activated protein kinase
MC	Mitochondrial carrier

Mn-SOD	Manganese superoxide dismutase
mPTP	Mitochondrial permeability transition pore
mRNA	Messenger ribonucleic acid
MTs	Metallothioneins
MyoD	Myogenic regulatory factor
NAC	N-Acetyl-L-cysteine
NAD^+	Nicotinamide adenine dinucleotide (oxidized)
NADH	Nicotinamide adenine dinucleotide (reduced)
$NADP^+$	Nicotinamide adenine dinucleotide phosphate (oxidized)
NADPH	Nicotinamide adenine dinucleotide phosphate (reduced)
NO	Nitric oxide
NOX	NADPH oxidase
Nrf2	Nuclear factor erythroid 2-related factor 2
OCR	Oxygen consumption rate
OMM	Outer mitochondrial membrane
PAGE	Polyacrylamide gel electrophoresis
PBS	Phosphate-buffered saline
PCR	Polymerase chain reaction
PFA	Paraformaldehyde
PGC-1α	Peroxisome proliferator-activated receptor γ coactivator 1α
P_i	Inorganic phosphate
PI	Propidium iodide
PPAR	Peroxisome proliferator-activated receptor
Prx	Peroxiredoxin
RNA	Ribonucleic acid

RNAi	RNA interference
ROS	Reactive oxygen species
RT-PCR	Real time polymerase chain reaction
Scr	Scrambled
SDS	Sodium dodecyl sulphate
SEM	Standard error of the mean
siRNA	Small interference RNA
SLC	Solute carrier
SOD	Superoxide dismutase
Srx	Sulfiredoxin
TBS	Tris-buffered saline
TCA	Tricarboxylic acid
Trx	Thioredoxin
TrxR	Thioredoxin reductase
UCP	Uncoupling protein
UPS	Ubiquitin proteasome system
UQ	Ubiquinone
UQH_2	Ubiquinol
WT	Wild-type
Δp	Protonmotive force
ΔpH	pH gradient
$\Delta\Psi_m$	Mitochondrial membrane potential

i. ABSTRACT

Uncoupling proteins (UCPs) constitute a subfamily of mitochondrial inner membrane carriers that modulate energy efficiency by regulating membrane proton conductance. One of its components, UCP3, is specifically expressed in heart, skeletal muscle and brown adipose tissue (BAT). The physiological function of this protein is not clearly established, although it seems to play an important role in the control of the production of reactive oxygen species (ROS) and in the protection against oxidative stress. UCP3 may also have a function in the metabolism of fatty acids. An efficient response to oxidative damage is crucial for cell survival, and the transcription factor Nrf2 is a master regulator of the cellular defences against this type of stress. In the presence of oxidizing agents or electrophiles, Nrf2 translocates to the nucleus, where it induces the transcription of genes involved in the defence against oxidative damage. In this work, we have studied the regulation of UCP3 expression and function in response to oxidative stress, as well as the possible involvement of Nrf2 in this process. We have found that the treatment with hydrogen peroxide (H_2O_2) or the lipid peroxidation product 4-hydroxy-2-nonenal (HNE), induces UCP3 expression in cells from mouse heart and skeletal muscle. This effect is mediated by the transcription factor Nrf2. Moreover, we have shown that the induction of the UCP3 protein is accompanied by an increase in the proton conductance of the inner mitochondrial membrane, which results in a decreased production of mitochondrial ROS and, consequently, in an increased cell survival. In addition, we have found that both UCP3 and Nrf2 have a cardioprotective role in the intact mouse heart subjected to ischemia-reperfusion (IR), a condition known to increase ROS generation, since mice lacking any of these proteins have increased infarct size and augmented levels of creatine kinase compared to wild-type mice. Finally, our data strongly suggest that UCP3 is involved in ischemic preconditioning (IPC), since the absence of the protein prevents the IPC protective effect against IR damage.

RESUMEN

Las proteínas desacoplantes (UCPs) constituyen una subfamilia de los transportadores de la membrana mitocondrial interna que modulan la eficiencia energética mediante la regulación de la conductancia de la membrana a los protones. Uno de sus componentes, UCP3, se expresa específicamente en el corazón, el músculo esquelético y el tejido adiposo pardo. La función fisiológica de esta proteína no está claramente establecida, aunque parece jugar un papel importante en el control de la producción de especies reactivas del oxígeno (ROS) y en la protección frente al estrés oxidativo. UCP3 también podría tener una función en el metabolismo de los ácidos grasos. Una respuesta eficiente frente al estrés oxidativo es esencial para la supervivencia celular, y el factor de transcripción Nrf2 es un importante regulador de las defensas celulares ante este tipo de estrés. En presencia de agentes oxidantes o electrófilos, Nrf2 se transloca al núcleo, donde induce la transcripción de genes implicados en la defensa frente al daño oxidativo. En este trabajo hemos estudiado la regulación de la expresión y función de UCP3 en respuesta al estrés oxidativo, así como la posible implicación del factor Nrf2 en este proceso. Hemos observado que el tratamiento con peróxido de hidrógeno (H_2O_2) o con el producto de la peroxidación lipídica 4-hidroxi-2-nonenal (HNE), induce la expresión de UCP3 en células de corazón y músculo esquelético de ratón. Este efecto está mediado por el factor Nrf2. Además, hemos mostrado que la inducción de la proteína UCP3 está acompañada de un aumento en la conductancia de la membrana mitocondrial interna a los protones, lo que resulta en una menor producción de ROS mitocondriales y, por consiguiente, en una mayor supervivencia celular. Por otra parte, hemos encontrado que tanto UCP3 como Nrf2 presentan un papel cardioprotector en corazones aislados de ratón sometidos a isquemia-reperfusión (IR), una condición que incrementa la generación de ROS, puesto que los ratones que carecen de alguna de estas proteínas presentan mayor tamaño de infarto y niveles de creatina quinasa aumentados en comparación con los ratones de tipo silvestre. Finalmente, nuestros datos sugieren que UCP3 está implicada en el precondicionamiento isquémico (IPC), ya que su ausencia previene el efecto protector del IPC frente al daño por IR.

ii. INTRODUCTION

1. MITOCHONDRIAL BIOENERGETICS

Mitochondria are double membrane organelles with circular genome only present in eukaryotic cells. Their main function is the generation of adenosine triphosphate (ATP) by oxidative phosphorylation. Mitochondria perform other essential functions including the adaptation of cells to metabolic demands during changes in substrate availability (Liesa and Shirihai 2013), the control of the generation of reactive oxygen species (ROS) and the cellular redox status (Zorov et al. 2014) and the control of cell death (Galluzzi et al. 2012), so that mitochondrial dysfunction has emerged as a key factor in pathophysiology (Nunnari and Suomalainen 2012). Mitochondria efficiently communicate with the cytosol. The outer mitochondrial membrane (OMM) is very permeable, in contrast to the inner mitochondrial membrane (IMM), which is highly selective and comparatively impermeable to almost all ions and molecules. The mitochondrial carriers (MCs) are special membrane transporters that catalyse the transport through the IMM facilitating the exchange of molecules involved in all the processes that take part in mitochondrial function (del Arco and Satrústegui 2013, Gutierrez-Aguilar and Baines 2013, Palmieri 2014). In humans, the MCs comprise 53 proteins of the IMM family of proteins SLC25 (solute carrier family 25).

1.1. Mitochondrial oxidative phosphorylation

The most important function of the mitochondrion is the synthesis of ATP by oxidative phosphorylation. ATP is used as a main source of chemical energy. Catabolic pathways such as the tricarboxylic acid (TCA) cycle, the β-oxidation of fatty acids, and the oxidation of amino acids, generate NADH and $FADH_2$ in the mitochondrial matrix. These electron carriers donate their electrons to the protein complexes of the electron transport chain (ETC), located within the IMM (Fig. I1). The electrons pass along a series of electron carriers to reduce molecular oxygen, which acts as the final electron acceptor, to water (Rich and Marechal 2010). The energy released as the electrons pass along the ETC drives the endergonic proton pumping activities of the respiratory complexes I, III, and IV, which pump protons against their electrochemical gradient into the mitochondrial intermembrane space (IMS). This proton movement generates potential energy across the IMM in the form of an electrochemical gradient of protons or protonmotive force (Δp), which consists of a pH gradient (ΔpH) and an electrical potential ($\Delta\Psi_m$). The energy contained in the gradient is used to form ATP from adenosine diphosphate (ADP) and inorganic phosphate (P_i). ATP synthesis is carried out by a phosphorylation reaction that takes place when protons flow back across the membrane and

down their electrochemical gradient through the ATP synthase, by a mechanism known as rotary catalysis (Noji et al. 1997, Stock et al. 1999). Thus, the oxidation of substrates is coupled to the phosphorylation of ADP, being the electrochemical gradient of protons the connection between both processes, as described by Peter Mitchell in his chemiosmotic theory, by which he was awarded the Nobel Prize in 1978 (Mitchell 1966, Mitchell 2011).

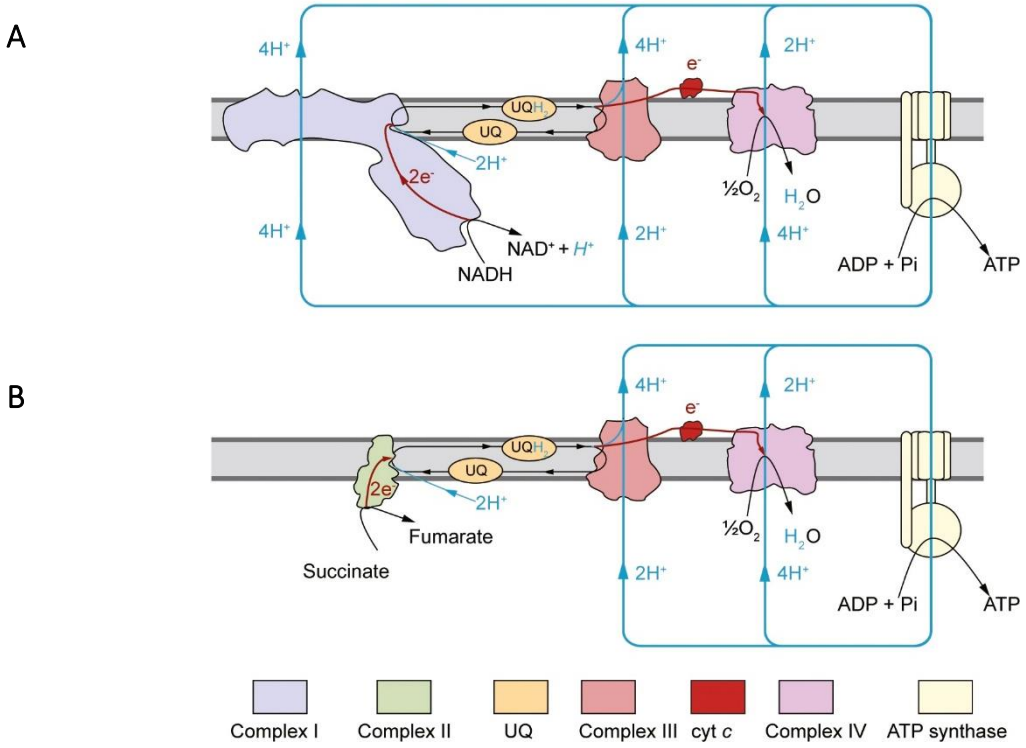

Figure II. Diagram showing the mitochondrial electron transport chain which consists of three proton-translocating complexes (I, III and IV) that act in parallel with respect to the proton circuit and in series with respect to the electron flow. (A) Pathway of electron transfer for NADH-linked substrates through complex I. (B) Pathway of electron transfer through complex II (succinate dehydrogenase), which reduces ubiquinone (UQ) to ubiquinol (UQH_2) without translocating protons. Taken from Nicholls and Ferguson, 2013.

1.2. Mitochondrial proton leak

Oxidative phosphorylation is not fully efficient given the fact that some of the protons return to the matrix through alternative leak pathways (proton leak) causing mitochondrial uncoupling (Brand 1990). Mitochondria rapidly consume oxygen in the presence of oxidizable substrates and ADP to generate ATP (*state 3* respiration). By contrast, respiration is slow in the absence of ADP (*state 4* respiration) and in the presence of the ATP synthase inhibitor oligomycin. *State 4* respiration can be entirely explained by proton leak across the IMM. The proton leak behaves in a non-ohmic manner, which can be evidenced in isolated mitochondria as an approximately exponential increase in the proton leak rate (measured indirectly as

oxygen consumption) as Δp rises (Fig. I2). Importantly, this behaviour is also evident in intact cells, indicating that the proton leak is not caused by damage to the inner membrane during the isolation procedure.

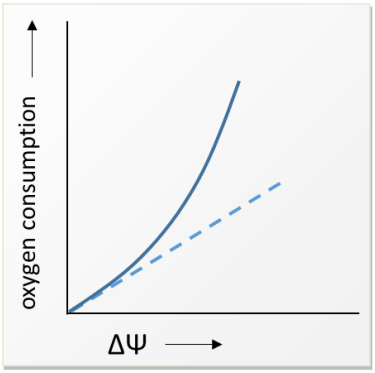

Figure I2. The kinetics of the proton leak (solid line). $\Delta\Psi$, mitochondrial membrane potential.

The total proton leak of a mitochondrion can be considered as the sum of two processes: the basal leak (i), which is unregulated, and the inducible leak (ii), which is catalysed by specific mitochondrial inner membrane proteins and can be activated and inhibited.

i. Basal proton leak. The mechanism of the basal proton conductance is unclear. Proposed mechanisms include the direct movement of protons across the phospholipid membrane (the 'water wires' model) or their diffusion through or around integral membrane proteins (Nobes et al. 1990), as explained below. The contribution of proton conductance through the lipid bilayer is only 5% of the total proton leak in rat liver mitochondria (Brookes et al. 1997). There is a correlation between mitochondrial proton conductance and the fatty acyl composition of the IMM (Brand et al. 2005, Brookes et al. 1998, Hafner et al. 1988, Hulbert et al. 2002, Porter et al. 1996). Thus, the content of n-3 polyunsaturates, particularly docosahexaenoate (C22:6, n-3), correlates with high proton conductance, and the content of monounsaturates, particularly oleate (C18:1, n-9), correlates with low proton conductance. Nevertheless, the proton conductance of phospholipid vesicles prepared from mitochondrial lipids is only 2-25% of the conductance of the mitochondria they are derived from, and does not vary when the composition changes (Brookes et al. 1997, Brookes et al. 1998). Therefore, some other factor apart from membrane surface area and phospholipid composition must make an important contribution to the basal proton conductance of mitochondria. The magnitude of proton conductance also correlates with the abundance of mitochondrial anion carrier proteins, such as the adenine nucleotide translocase (ANT) and the uncoupling protein 1 (UCP1). ANT catalyses the ADP/ATP exchange across the IMM and is the most abundant protein in

mitochondria. In fact, up to two-thirds of the basal proton leak is attributable to the ANT (Brand et al. 2005). Besides, UCP1 contributes to basal proton conductance in BAT (Parker et al. 2009), where it is abundantly expressed. Nevertheless, this proposed role for UCP1 is not supported by other authors (Shabalina et al. 2010). In both cases (ANT and UCP1), the proton leak is not due to protein activity, as it also occurs in the presence of specific inhibitors. Instead, it may be a general property of all the mitochondrial inner membrane carrier proteins, but only the most abundant make a significant contribution to proton leak, and the interface between these proteins and the lipid bilayer may be responsible for the majority of the basal proton leak.

ii. Inducible proton leak. Inducible proton leak is catalysed by the ANT and UCPs. The uncoupling function of the ANT is activated by fatty acids and reactive alkenals, and inhibited by carboxyatractylate (Khailova et al. 2006, Parker et al. 2008b). The proton conductance catalysed by UCPs is controlled at multiple levels: transcriptional, translational, and proteolytic (Azzu and Brand 2010). The uncoupling function of UCPs will be analysed in detail in section 2 of the Introduction.

1.3. The physiological importance of proton leak

Proton leak may be physiologically important. For instance, the energy consumed by proton leak accounts for around 25% of the basal respiration rate of isolated hepatocytes (Nobes et al. 1990). The contribution of proton leak to metabolic rate in muscle is even greater than that observed for isolated liver cells (Rolfe and Brand 1996). Thus, in resting muscle, about 50% of metabolic rate is used to counteract the leak of protons into the mitochondrial matrix. Taking into account the contribution of liver and skeletal muscle to whole-body resting energy consumption, we can estimate that proton cycling in these tissues alone accounts for approximately 20% of the standard metabolic rate of the rat (Rolfe and Brand 1996, 1997). Therefore, proton leak represents the single most energetically important component of basal energy metabolism in the rat.

2. UNCOUPLING PROTEINS

Uncoupling proteins (UCPs) belong to the superfamily of mitochondrial anion carriers. They are located in the IMM and catalyse nucleotide-sensitive proton leak when activated by fatty acids, superoxide, or alkenals derived from membrane lipid peroxidation (Brand et al. 2004, Esteves and Brand 2005), thus regulating membrane proton conductance (Azzu and Brand 2010). The UCP family comprises the proteins UCP1-5, encoded by the genes SLC25A7 (UCP1), SLC25A8 (UCP2), SLC25A9 (UCP3), SLC25A27 (UCP4), and SLC25A14 (UCP5), all

of which have been cloned (Boss et al. 1997, Echtay et al. 2001, Fleury et al. 1997, Nicholls and Locke 1984, Yu et al. 2000b). The amino acid sequence identity of UCPs and the ANT proteins with UCP1 is shown in Table II. In the Introduction of this thesis, we will focus on UCP1, UCP2 and UCP3 only, as they are the most extensively studied.

Protein	UniProt accession number	Amino acid identity (%)	Overlapping residues
UCP1	P25874	100	307
UCP2	P55851	59	300
UCP3	P55916	57	311
UCP5 (BMCP1)	O95258	33	282
UCP4	O95847	30	294
ANT2	P05141	20	298
ANT3	P12236	20	298
ANT1	P12235	19	287

Table II. Comparison of the amino acid sequence identity of UCPs and the ANT proteins with UCP1. The species for all proteins is human. UCP2 and UCP3 have 59% and 57% identity, respectively, with UCP1, and 73% identity with each other. Adapted from Krauss et al., 2005.

UCPs exhibit tissue-specific expression: UCP1 is specific of BAT (Bouillaud et al. 1985), UCP3 is mainly expressed in cardiac, skeletal muscle and BAT (Boss et al. 1997), and UCP4 and UCP5 are primarily expressed in the brain (Yu et al. 2000b). *UCP2* mRNA, unlike that of the rest of the UCPs, is ubiquitously expressed, but its protein has been identified in spleen, hypothalamus, pancreatic β-cells, and macrophages (Fleury et al. 1997, Ricquier and Bouillaud 2000).

2.1. Physiological role of uncoupling proteins

In the presence of specific activators, UCPs are able to uncouple substrate oxidation from ATP synthesis, allowing protons to return to the mitochondrial matrix and dissipating the proton gradient necessary for ATP production. However, in contrast to the well-characterized function and regulation of UCP1, the role of UCP2 and UCP3 in the cell is still uncertain. Nevertheless, these proteins have been involved in a wide range of physiological processes and pathologies, such as insulin resistance, obesity, immunity, neurodegeneration, and cardiovascular diseases.

2.1.1. Physiological role of UCP1

UCP1 dissipates Δp to generate heat during non-shivering thermogenesis in BAT from hibernators, cold-adapted rodents, and newborn mammals (Cannon and Nedergaard 2004). The thermogenic function of the protein is well established and corroborated by the fact that UCP1-KO mice are cold-sensitive (Enerback et al. 1997, Nicholls 2001). UCP1 is subjected to strict regulation: it is activated by fatty acids and inhibited by purine nucleoside di- and triphosphates (Locke et al. 1982). The mechanism by which fatty acids activate the transport of protons through UCP1 is still controversial. Two main models have been proposed:

- *Cofactor model*. This model proposes that fatty acids act as a prosthetic group in UCP1. The carboxylate binds protons and deliver them to a site from which they are translocated to the matrix side of the membrane. Thus, UCP1 is a proton carrier and fatty acids increase its proton conductance (Rial et al. 1983, Rial et al. 2004, Winkler and Klingenberg 1994).

- *Fatty acid cycling model*. Protonated fatty acids flip-flop to the mitochondrial matrix where the pH gradient promotes their dissociation into fatty acid anions, which are then transported back to the IMS by UCP1, driven by the membrane potential. This cycle leads to a Δp net decrease although in this model UCP1 does not translocate protons (Breen et al. 2006, Garlid et al. 1998, Skulachev 1991).

Much of the controversy comes from the use of different experimental systems such as UCP1 reconstituted into liposomes and isolated mitochondria. Although experimental evidence supports both models, the precise molecular mechanism of UCP1 regulation by fatty acids remains unresolved.

2.1.2. Physiological role of UCP2

The role of UCP2 is still unclear but it seems to be involved in a broad range of physiological and pathological processes including cytoprotection (Blanc et al. 2003, Paradis et al. 2003), immune cell modulation (Arsenijevic et al. 2000, Rousset et al. 2006) and regulation of glucose sensing (Parton et al. 2007, Zhang et al. 2001).

UCP2 has been reported to uncouple oxidative phosphorylation in thymocytes (Krauss et al. 2002) and the INS-1E pancreatic β-cell model (Affourtit and Brand 2008), therefore leading to Δp dissipation and to a decrease in ROS production.

In glucose-sensing cells, UCP2 attenuates insulin secretion, possibly acting in two different ways. First, it may act by uncoupling oxidative phosphorylation and lowering the ATP/ADP

ratio, which results in decreased stimulation of K_{ATP} channels and lowered insulin secretion (Chan et al. 2001, Zhang et al. 2001). UCP2 can also act by decreasing ROS production (Krauss et al. 2003), which is an important signal in glucose-sensing systems. Accordingly, UCP2 downregulation or its pharmacological inhibition has been shown to reverse the deleterious effects of obesity- and high glucose-induced pancreatic islet dysfunction (Zhang et al. 2006).

Based on a bioinformatic prediction, UCPs substrates have been proposed to be small carboxylic acids or keto acids, transported in symport with protons (Robinson et al. 2008). Importantly, the first experimental evidence has been recently reported by Vozza and col., showing that UCP2 transports C4 metabolites out of mitochondria, regulating glucose and glutamine oxidation (Vozza et al. 2014).

It is yet uncertain whether UCP2 is also regulated by fatty acids and nucleotides. When reconstituted into liposomes, it does catalyse a fatty acid-inducible, nucleotide-sensitive proton flux (Zackova et al. 2003), but evidence from isolated mitochondria is diverse. UCP2 catalyses an inducible uncoupling in the presence of specific activators such as retinoic acid analogs (Rial et al. 1999), superoxide (Echtay et al. 2002) and reactive alkenals (Murphy et al. 2003).

2.1.3. Physiological role of UCP3

UCP3 is expressed most abundantly in skeletal muscle and, to a lesser extent, in heart and BAT. It was initially suggested that it could mediate thermogenesis in muscle, although experimental evidence indicated this not being the case. For example, fasting, a condition when energy conservation is required, causes UCP3 upregulation in skeletal muscle (Cadenas et al. 1999). Despite upregulation, it does not mediate basal proton leak (Cadenas et al. 1999). Moreover, UCP3 knockout (UCP3-KO) mice are not cold-sensitive nor obese, and have normal energy expenditure (Gong et al. 2000). UCP3 may play a role in fatty acid metabolism. Several conditions associated with a transient rise in plasma free fatty acids (FFA) such as fasting, high fat diet, acute exercise, and exposure to cold, markedly increase the *Ucp3* mRNA levels (Bezaire et al. 2007, Cadenas et al. 1999, Larkin et al. 1997, Schrauwen and Hesselink 2004). Besides, UCP3 over-expression has been shown to increase fatty acid transport and oxidation (Bezaire et al. 2005). Some authors suggested that UCP3 physiologically functions as a fatty acid transporter (Himms-Hagen and Harper 2001, Schrauwen et al. 2006). More recently, however, it has been reported that UCP3 is not a fatty acid transporter, although it is required for the fasting-induced enhancement of fatty acid oxidation rate and capacity, possibly via mitigated mitochondrial oxidative stress (Seifert et al. 2008). Protection from ROS has also been

suggested as a putative role for UCP3. This hypothesis is strongly supported by experimental evidence. Thus, UCP3 has been reported to neutralise protein oxidation in skeletal muscle (Barreiro et al. 2009), and to ameliorate ROS production during exercise (Jiang et al. 2009). Moreover, UCP3-KO mice have higher ROS production and oxidative damage (Brand et al. 2002, Vidal-Puig et al. 2000) and UCP3 over-expressing mice have reduced ROS production during aging (Nabben and Hoeks 2008). Furthermore, UCP3 lowers ROS production in isolated skeletal muscle mitochondria (Toime and Brand 2010). The observation that glutathionylation activates UCP3 and controls proton leak (Mailloux et al. 2013) also suggests a role for this protein against oxidative stress. In addition to increased fatty acid oxidation and reduced ROS production, UCP3-overexpressing mice also have decreased diet-induced obesity and are protected against insulin resistance (Son et al. 2004). Accordingly, mutations in the UCP3-encoding gene have also been correlated with obesity and diabetes (de Luis et al. 2012).

As in the case of UCP2, it is uncertain whether UCP3 is regulated by fatty acids and nucleotides. UCP3 does catalyse a fatty acid-inducible, nucleotide-sensitive proton flux when reconstituted into liposomes (Zackova et al. 2003), which has also been observed in isolated mitochondria (Aguirre and Cadenas 2010, Lombardi et al. 2010). UCP2 and UCP3 may lack the amino acid sequence necessary to confer the high sensitivity to fatty acids that is characteristic of UCP1 (Jimenez-Jimenez et al. 2006). UCP3 catalyses an inducible uncoupling in the presence of specific activators including superoxide (Echtay et al. 2002) and reactive alkenals (Murphy et al. 2003). As mentioned above, glutathionylation also activates UCP3 and controls proton leak (Mailloux et al. 2013).

2.2. Regulation of uncoupling proteins expression

2.2.1. Regulation of UCP1 expression

The expression of UCP1 varies in response to the adaptive status of the animal: it is high at birth but it is repressed afterwards. Recently, it has been recognized that BAT is present in the adult human (Cypess et al. 2009). The *Ucp1* gene is under extensive transcriptional control (Cannon and Nedergaard 2004). Cold-adaptation (or overfeeding under certain conditions) leads to the induction of the protein by a mechanism involving the transcriptional coactivator PGC-1α (peroxisome proliferator-activated receptor γ coactivator 1α) (Nicholls 2006). In response to cold stimulus (or overfeeding), sympathetic inervation in BAT releases catecholamines, such as noradrenaline, which activate β_3-adrenergic receptors, triggering pathways mediated by cyclic AMP (cAMP) that affect *Ucp1* transcription. In addition, cAMP-

dependent protein kinase A stimulates lipolysis, releasing fatty acids that acutely activate UCP1 (Robidoux et al. 2004). FFA also activate a cAMP-responsive enhancer element upstream of the *Ucp1* gene that controls its expression (Cassard-Doulcier et al. 1993, Kozak et al. 1994)

2.2.2. Regulation of UCP2 and UCP3 expression

Like UCP1, UCP2 and UCP3 are subjected to extensive transcriptional control. Several studies have linked *Ucp2* mRNA expression to the hyperglycemia and hyperlipidaemia associated with type 2 diabetes mellitus (Chan and Harper 2006). Transcriptional regulation has also been linked to fatty acid oxidation (Li et al. 2002), oxidative stress (Giardina et al. 2008), and Sirt1 protein (Bordone et al. 2006). UCP2 is also translationally regulated, so increases in mRNA are not necessarily indicative of increased protein concentration. *Ucp2* mRNA is controlled by glutamine, an amino acid implicated in the insulin secretion pathway (Hurtaud et al. 2006).

Ucp3 mRNA is upregulated in response to nutrient deprivation (Cadenas et al. 1999), serum FFA (Samec et al. 1998), cytokines (Busquets et al. 1998), and thyroid hormones (Lanni et al. 1999, Solanes et al. 2005). Sirt1 represses *Ucp3* mRNA expression (Amat et al. 2007). Transcriptional upregulation by fatty acids is mediated by peroxisome proliferator-activated receptors (PPARs) and the myogenic regulatory factor MyoD (Pedraza et al. 2006, Solanes et al. 2003, Villarroya et al. 2007). Moreover, thyroid hormone sensitivity is conferred by a thyroid response element (Solanes et al. 2005).

Like UCP1, UCP2 and UCP3 are also regulated by proteolysis, being rapidly degraded by the cytosolic ubiquitin-proteasome machinery with half-lives of a few hours (Azzu et al. 2010a).

3. OXIDATIVE STRESS

Eukaryotic aerobic organisms cannot exist without oxygen, yet oxygen is inherently dangerous to their existence ('oxygen paradox') (Davies 1995). Oxygen itself is a free radical, as it contains two unpaired electrons, and it can give rise to partially reduced oxygen forms that are highly toxic. Both free radicals and other non-radical reactive molecules derived from oxygen, are collectively known as reactive oxygen species (ROS). To maintain redox homeostasis, living cells engage powerful antioxidant systems to eliminate the intracellular

ROS (Halliwell 2011). Oxidative stress is caused by an imbalance between the production of ROS and the ability of the antioxidant systems to detoxify them.

Although ROS are usually considered toxic by-products of aerobic metabolism, they play a dual role in aerobic cells. On one hand, their uncontrolled production results in oxidative stress that impairs cellular function and contributes to the development of cancer, chronic diseases and toxicity, potentially triggering cell death (Balaban et al. 2005, Ma 2010), but on the other hand, ROS can also be produced in response to physiological cues in a controlled manner. In this case, they may serve useful purposes acting as important signalling molecules to regulate processes such as cell division, inflammation, immune function, autophagy and stress response (Finkel 2011).

3.1. Mitochondrial ROS production

ROS are formed physiologically as by-products during respiration (Brand et al. 2004, Chance et al. 1979), being the mitochondrial electron transport chain (ETC) the most important source (Brand 2010, Brand et al. 2004). Most of the oxygen consumed by a cell is reduced to water in a reaction catalysed by the mitochondrial cytochrome *c* oxidase (complex IV), but the mitochondrial ETC contains some redox centres that may transfer one electron directly to oxygen generating the superoxide radical ($O_2^{\cdot-}$) (Cadenas and Davies 2000). This radical is mainly produced by the transfer of a single electron from complex I or from ubiquinone (UQ) of complex III to O_2 (Guzy et al. 2005, Murphy 2009). Large amounts of superoxide are generated during reverse electron transport from reduced ubiquinone (UQH_2) to NAD^+ at the quinone-binding site in complex I (Brand 2010). Superoxide is a moderately reactive radical that leads to the formation of more reactive ROS. Thus, in the mitochondrial matrix, $O_2^{\cdot-}$ can undergo dismutation by manganese-containing superoxide dismutase (MnSOD), producing hydrogen peroxide (H_2O_2), a stable 'diffusable' non-radical ROS. H_2O_2, in turn, can lead to the formation of the hydroxyl radical ($^{\cdot}OH$), a very dangerous radical due to its highly reactivity. H_2O_2 can react with free transition metals (Fe^{2+} or Cu^+) via the Fenton reaction. Thus, $^{\cdot}OH$ can be generated from an interaction between $O_2^{\cdot-}$ and H_2O_2 (Haber-Weiss reaction), as shown below:

$$Fe^{3+} + O_2^{\cdot-} \rightarrow Fe^{2+} + O_2$$

$$Fe^{2+} + H_2O_2 \rightarrow Fe^{3+} + {}^{\cdot}OH + OH^- \quad \textit{(Fenton reaction)}$$

$$\textit{Net reaction: } O_2^{\cdot-} + H_2O_2 \rightarrow {}^{\cdot}OH + OH^- + O_2$$

The rate of mitochondrial ROS generation depends on Δp, the NADH/NAD^+ and QH_2/Q ratios, and the local O_2 concentration (Murphy 2009). When the mitochondria are actively making ATP (*state 3*) and consequently have a low Δp and NADH/NAD^+ ratio, the extent of ROS generation is almost negligible. On the contrary, when there is no ATP synthesis (*state 4*) in conjunction with a high Δp and a highly reduced Q pool, a condition leading to reverse electron transport, or when there is a high NADH/NAD^+ ratio in the matrix, the production of superoxide, predominantly from complex I, is significant (Murphy 2009).

Few of the ROS produced within mitochondria are released into the cytosol since there are several mitochondrial detoxification systems (Wojcik et al. 2010), and the ROS released into the cytosol are neutralized by cellular antioxidant systems (Freeman and Crapo 1982). Moreover, mitochondria are also able to remove ROS produced by other cellular sources (Andreyev et al. 2005).

3.2. Extra-mitochondrial ROS formation

Although the main source of ROS is the mitochondrial respiratory chain, nearly all the enzymes that utilize O_2 as a substrate, including plasma membrane-bound NADPH oxidase (NOX), microsomal cytochrome P450 (CYP), and cytoplasmic xanthine oxidase, can produce ROS. Indeed, ROS generation has been observed in the cytosol and peroxisomes, as well as in plasma and endoplasmic reticulum (ER) membranes. The contribution of extra-mitochondrial sources to cytosolic ROS concentration can be relevant in several pathophysiological conditions (Andreyev et al. 2005, Jezek and Hlavata 2005, Yu 1994). Thus, even though mitochondria is the main source of ROS during ischemia-reperfusion (IR) (detailed in section 5.1. of the Introduction), experimental evidence suggests an increase in ROS production from extra-mitochondrial sources, such as the aforementioned xanthine dehydrogenase/xanthine oxidase enzyme system, which was early identified as a potential source of cellular $O_2^{\cdot-}$ generation during IR (McCord et al. 1985, Schoutsen et al. 1983).

3.3. Oxidative stress induced by ROS

Under normal conditions, the effects of ROS are counteracted by a variety of antioxidants. As previously stated, oxidative stress is the result of an imbalance of ROS and antioxidants, in which the effects of ROS are more potent than the compensatory capacity of antioxidants. An excess of ROS can damage the main cellular macromolecules affecting their function, which can lead to cellular dysfunction (Sies 1997). Thus, ROS attack polyunsaturated fatty acids in membrane phospholipids causing toxic peroxidative reactions (Halliwell and Gutteridge 1990,

Kehrer 1993). ROS also damage proteins, altering their functions (Stadtman 2006), and DNA, originating DNA strand breaks and mutations (Maynard et al. 2010). ROS can also lead to mitochondrial DNA damage, eventually resulting in an impaired ETC (Indo et al. 2007).

In addition, severe oxidative stress causes an increase in the levels of free cytosolic Ca^{2+} (Orrenius et al. 1989), which can lead to the opening of the mitochondrial permeability transition pore (mPTP) and the consequent loss of $\Delta\Psi_m$ (Halestrap and Pasdois 2009, Yellon and Hausenloy 2007). The subsequent release of cytochrome *c* from mitochondria leads to the execution of cell death processes (Huttemann et al. 2011, Whelan et al. 2010).

3.4. Amplification of oxidative stress by reactive aldehydes

As mentioned before, ROS attack the biomembranes causing toxic peroxidative reactions which can result in the formation of highly reactive aldehydes (alkenals). The hydroxyl radical (·OH) attacks polyunsaturated fatty acids in membrane phospholipids, thereby triggering lipid peroxidation. This process results in the generation of lipid hydroperoxides and α,β-unsaturated aldehydes, including 4-hydroxy-2-nonenal (HNE), one of the most abundant hydroxyalkenals produced by lipid peroxidation, and the most cytotoxic, having biological effects in the low micromolar range (Benedetti et al. 1984) (Fig. I3).

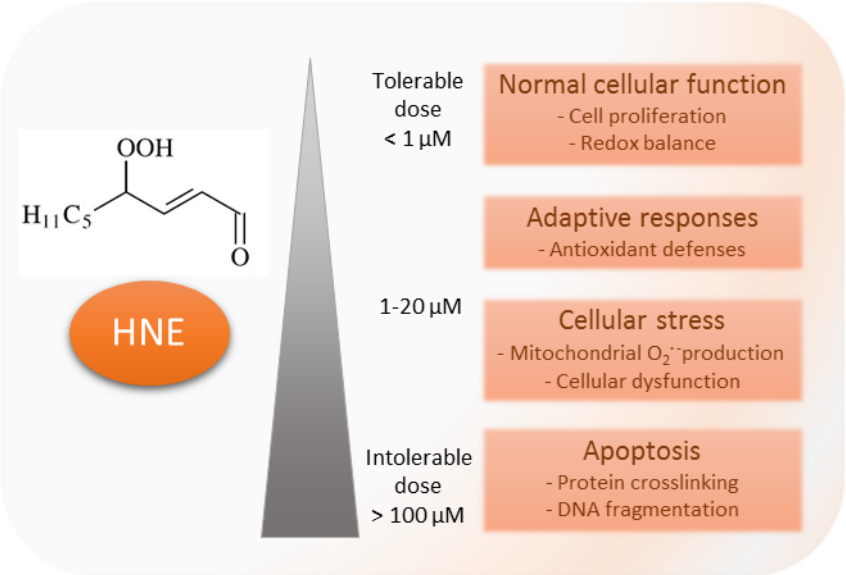

Figure I3. HNE chemical structure and HNE-induced modulation of cell function. Low physiological levels of HNE target cellular pathways for proliferation while maintaining a redox balance. Higher concentrations can be detrimental, and chronic exposure to pathological concentrations can lead to apoptosis. Based on Chapple *et al.* 2013.

HNE results from the oxidation of phospholipids containing ω-6 polyunsaturated fatty acyl chains (Spickett 2013). There are several chemical mechanisms that lead to the cleavage of a carbon-carbon bond in the fatty acyl chain and ulterior generation of HNE, although the process remains unclear. HNE is a bi-reactive compound able to undergo electrophilic reactions such as Michael addition and Schiff base formation (Spickett 2013) and can be metabolized to less cytotoxic compounds such as 1,4-dihydroxynonene-GSH (DHN-GSH), dihydroxynonene-mercapturicacid (DHN-MA) or HNA (Alary et al. 2003, Hill et al. 2009b). An important pathway for detoxification of HNE involves the conjugation to the thiol group of the antioxidant glutathione by glutathione-S-transferases (GSTA) (Balogh and Atkins 2011).

Reactive aldehydes like HNE are highly electrophilic and react with proteins and nucleic acids, generating various adducts (Conklin et al. 2007). These lipid peroxidation products have a very high chemical stability so they can diffuse longer distances than their precursor ROS, and therefore they can disseminate oxidative injury and amplify the damage (Esterbauer et al. 1991). Importantly, the sensing of aldehyde accumulation in injured tissues enables the cell to activate a variety of stress resistance pathways and to counteract oxidative stress-mediated injury. Therefore, similar to ROS, reactive aldehydes have a dual role, since they may be regarded as both toxic products and second messengers that activate protective signalling (Balaban et al. 2005, Chapple et al. 2013, Turrens 2003).

3.5. Cellular antioxidant defences

ROS-induced damage can be neutralized by antioxidant defences, both enzymatic and non-enzymatic, which preserve cellular functionality. Antioxidants are normally balanced with ROS emission to keep ROS within tolerable limits, preserving their role in signalling processes while avoiding their toxic effects. Some of these antioxidant defences are enzymes, such as superoxide dismutase (SOD), which catalyses the dismutation of $O_2^{\cdot-}$ into O_2 and H_2O_2. There are three forms of SOD: cytosolic (Cu/Zn-SOD or SOD 1), mitochondrial (Mn-SOD or SOD 2) and extracellular (SOD 3). Some antioxidant enzymes catalyse the reduction of H_2O_2 into H_2O. These enzymes are catalase, located in the cytosol and peroxisomes, peroxiredoxin (Prx), which requires the thioredoxin (Trx)/thioredoxin reductase (TrxR) system to be regenerated, and glutathione peroxidase (GPx), which requires gluthathione (GSH)/gluthathione reductase (GSR) to be regenerated (Mari et al. 2009). Both Prxs and GPxs enzymes exist in several isoforms that are located differently in either the cytosol or the mitochondria (Hekimi et al. 2011).

There are several low-molecular-weight molecules such as glutathione (GSH), bilirubin and urate, which also form part of the antioxidant system. Some of these molecules (e.g. GSH) act as cofactors for antioxidant enzymes. Others, like vitamins C and E, scavenge free radicals. The antioxidant system also comprises non-catalytic antioxidant proteins such as glutaredoxins (Grxs), metallothioneins (MTs), and Trxs. Redox reactions in cells are enabled by the nicotinamide pairs $NADP^+$/NADPH and NAD^+/NADH. NADPH is used to reduce oxidized Trx (Trx-ox) and glutathione (GSSG) by TrxR and glutathione reductase (GSR), respectively. Sulfiredoxin (Srx) reduces oxidized Prx from sulfinic (inactive) to sulfenic (active) acid in an ATP and GSH-dependent manner (Nickel et al. 2014). Ultimately, there are DNA repair enzymes that remove the DNA lesions (Demple and Harrison 1994) and proteases that degrade free radical-damaged proteins (Grune et al. 1995).

3.6. 'Mild uncoupling' as a mechanism to control mitochondrial ROS production

An exponential correlation between $\Delta\Psi_m$ and mitochondrial ROS (H_2O_2) generation was observed in rat heart mitochondria (Fig. I4) (Korshunov et al. 1997).

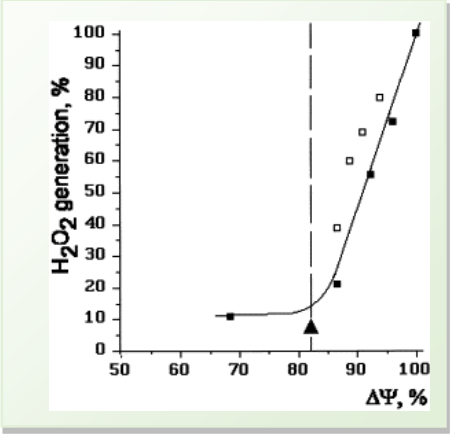

Figure I4. H_2O_2 formation as a function of $\Delta\Psi$. The $\Delta\Psi$ level was varied by adding different concentrations of the uncoupler SF6847 (▪ solid line), malonate (▫) or 100 μM ADP plus 5 mM P_i (▲). Dashed line represents the *state 3* $\Delta\Psi$ level. Taken from Korsunov et al, 1997.

Based on this observation, some authors suggested that the activation of UCPs or ANT by ROS or ROS products, could be protective against oxidative damage by diminishing mitochondrial ROS production (Brand 2000, Brand and Esteves 2005, Mailloux and Harper 2011). The proposed mechanism by which UCP2 and UCP3 decrease mitochondrial ROS production is shown in Fig. I5. The ETC produces superoxide ($O_2^{\cdot-}$) that activates UCPs (Brunelle et al. 2005, Echtay et al. 2002) and the ANT via the formation of lipid peroxidation products such as HNE (Echtay et al. 2003, Murphy et al. 2003). UCP activation allows protons

to return to the mitochondrial matrix independently of the ATPase. This, in turn, causes a slight decrease in $\Delta\Psi_m$ thereby stimulating respiration, without compromising ATP production ('mild uncoupling'). Since ROS production by mitochondria depends greatly on $\Delta\Psi_m$, the activation of UCPs would decrease ROS production as a feedback mechanism in response to ROS overproduction.

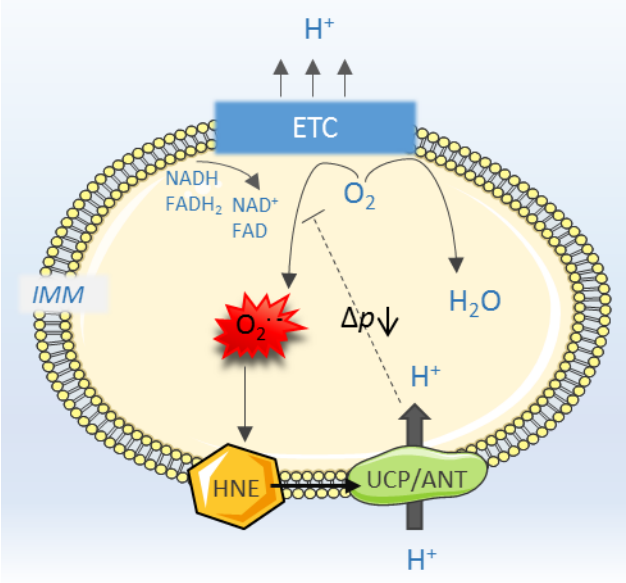

Figure I5. During the oxidation of substrates, specific complexes of the ETC reduce O_2 to H_2O and pump H^+ to the IMS, generating a proton motive force (Δp). However, some electrons in the reduced complexes also react with O_2 to produce superoxide ($O_2^{\cdot-}$), which can peroxidize membrane phospholipids, generating HNE, which in turn induces H^+ transport through UCPs and the ANT. The mild uncoupling caused by this transport, lowers Δp and slightly stimulates electron transport, causing the complexes to become more oxidized, and lowering the local O_2 concentration, effects that decrease $O_2^{\cdot-}$ production. Thus, induction of proton leak by HNE limits mitochondrial ROS production as a feedback response to overproduction of $O_2^{\cdot-}$ by the respiratory chain. Based on Echtay *et al.*, 2003.

In fact, UCP2 and UCP3 have been found to catalyse a proton leak that decreases ROS emission from mitochondria (Duval et al. 2002, Mailloux and Harper 2011, Negre-Salvayre et al. 1997, Toime and Brand 2010). Although there is extensive experimental evidence in favour of this hypothesis, some studies do not support it (Nabben et al. 2011, Shabalina and Nedergaard 2011).

4. THE ANTIOXIDANT TRANSCRIPTION FACTOR NRF2

The nuclear factor erythroid 2-related factor 2 (Nrf2) is a redox-sensitive transcription factor that plays an essential role in the cellular defence against oxidative stress. This protein is a bZIP transcription factor and a member of the Cap 'n' Collar family of regulatory proteins

that also includes NF-E2, Nrf1, Nrf3, Bach1 and Bach2 (Motohashi et al. 2002), and mediates the cellular response to electrophiles and oxidants (collectively referred to as 'inducers') by binding to an enhancer element in the promoter regions of cytoprotective genes (Itoh et al. 1997). Thus, Nrf2 upregulates the transcription of genes encoding defence enzymes and antioxidant stress proteins, such as glutathione S-transferases, NAD(P)H quinone oxidoreductase 1 (NQO1), heme oxygenase 1 (HO-1), γ-glutamyl cysteine synthetase (GCS), and multidrug resistance-associated proteins (MRP) (Bryan et al. 2013). Nrf2 is activated by changes in the redox state of the cell and functions to restore homeostasis by upregulating antioxidant, xenobiotic-metabolising, and other cytoprotective enzymes. The Nrf2 knockout mice are viable and fertile, but show increased sensitivity to numerous xenobiotics and disease conditions associated with oxidative pathology (Motohashi and Yamamoto 2004), highlighting the critical importance of Nrf2 in the cellular stress response. Accordingly, pharmacological boosting of the Nrf2 activity with chemoprotective agents protect animals from oxidative damage (Talalay et al. 2003).

Nrf2 mRNA is expressed broadly and independently of inducers, which suggests a post-transcriptional mechanism for Nrf2 activation. In the presence of ROS and xenobiotic agents, Nrf2 is translocated to the nucleus where it binds to an antioxidant response element (ARE; `TGACnnnGCA`) in the promoter of a battery of cytoprotective genes (Nguyen et al. 2003, Nioi et al. 2003, Rushmore et al. 1991). This activation is controlled by Keap1 (Kelch-like ECH-associated protein 1), a 624-amino acid protein that contains three main domains: a BTB dimerisation domain (*B*road-Complex, *T*ramtrack and *B*ric a` brac), a cysteine-rich IVR domain (intervening region) and a Kelch domain consisting of 6 Kelch repeats through which Keap1 binds to Nrf2. Keap1 negatively regulates Nrf2 and contains a number of reactive cysteine residues that act as the inducer sensors. Thus, inducers chemically react with critical cysteine residues of Keap1, leading to stabilisation and nuclear translocation of Nrf2 (Taguchi et al. 2011). Keap1 is also a substrate adaptor protein for the Cullin3 (Cul3)-containing E3-ligase complex, which targets Nfr2 for ubiquitination and degradation by the ubiquitin proteasome system (UPS) (Kobayashi et al. 2004). The regulation of Nrf2 by Keap1 is shown in Fig. I6.

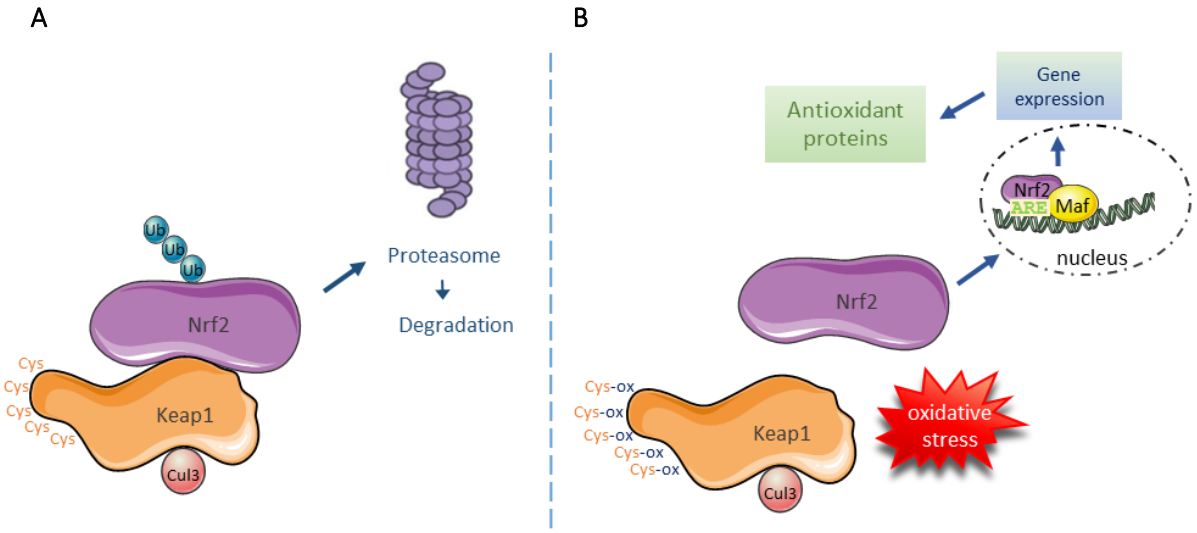

Figure I6. Schematic overview of Nrf2 activation. (A) Basal conditions. Nrf2 is sequestered in the cytosol by a Keap1 homodimer which facilitates the ubiquitination and proteasomal degradation of Nrf2. (B) Oxidant conditions. A conformational change in Keap1 mediated via its reactive cysteine residues results in the release of Nrf2 from Keap1. Nrf2 can no longer be ubiquitinated and degraded, therefore Nrf2 accumulates and translocates to the nucleus. There, Nrf2 heterodimerizes with small Maf proteins and binds to the antioxidant response element (ARE) of target genes. This activates the expression of genes responsible for eliminating the oxidative insult. Based on Bryan *et al.*, 2013.

- *Basal suppression of Nrf2 by Keap1*. Keap1 is a cytosolic repressor of Nrf2 that functions as a homodimer and plays a central role in regulating the Nrf2 response (Dinkova-Kostova et al. 2005, Dinkova-Kostova et al. 2002). Under basal conditions (Fig. I6A), Nrf2 is rapidly degraded by the proteasome, with a half-life of approximately 20 min. Nrf2 degradation is triggered by polyubiquitination through the Keap1/Cul3 ubiquitin ligase complex (Kobayashi et al. 2004, Sun et al. 2007).

- *Oxidant activation of Nrf2 by inducers.* Under oxidant conditions (Fig. I6B), Keap1 functions as a sensor of stress signals. Thus, the stress-induced oxidation of key cysteine residues of Keap1 leads to conformational changes of this protein that prevent its binding to Nrf2 and, consequently, the degradation of this transcription factor (Fourquet et al. 2010, Yamamoto et al. 2008). A variety of chemical inducers, including phytochemicals and derivatives (genistein, quercetin, sulforaphane), therapeutics (oltipraz, auranofin), environmental agents (paraquat, arsenic), and endogenous compounds (NO, nitro-fatty acids, H_2O_2 and HNE), modify the sensors of Keap1 (Ma and He 2012). As a result, Nrf2 accumulates in the nucleus, heterodimerizes with a small Maf protein and binds to an ARE in the promoters of its target genes (Malhotra et al. 2010).

In addition to cysteine-thiol modification by inducers, several other mechanisms have been described to regulate Nrf2 signaling. Keap1-Nrf2 binding can also be prevented in response to oxidative stress by proteins such as the autophagy substrate p62 and p53-regulated p21, which compete with the interaction between Keap1 and Nrf2, and cause the persistent activation of Nrf2 (Chen et al. 2009, Komatsu et al. 2010). Moreover, Nrf2 activation may be also the consequence of post-translational modifications of Keap1 that avoid the Keap1-Nrf2 interaction. Thus, Keap1 phosphorylation at Tyr141 renders the protein highly stable, and its dephosphorylation by hydrogen peroxide, an oxidizing agent, results in Keap1 rapid degradation and Nrf2 activation. (Jain et al. 2008). Furthermore, the phosphorylation of Nrf2 at Ser40 by protein kinase C-□ (Huang et al. 2002, Niture et al. 2009) and its acetylation by CREB-binding protein (Kawai et al. 2011) increase Nrf2 nuclear translocation and the transcriptional activation of genes involved in the antioxidant defence. There are also reports of Nrf2 phosphorylation via MAPK (mitogen-activated protein kinase) (Yu et al. 2000a). Activation of MAPK pathways induces ARE-mediated gene expression via an Nrf2-dependent mechanisms, via PI3K/AKT (phosphatidylinositol 3-kinase/protein kinase B) (Kang et al. 2002), and via PERK (PKR-like endoplasmic reticulum kinase), that mediates Nrf2 nuclear import (Cullinan et al. 2003).

5. CARDIAC ISCHEMIA-REPERFUSION INJURY

5.1. Cardiac ischemia-reperfusion induces oxidative stress

Cardiac ischemia is a condition that occurs when the blood flow, and thus oxygen and nutrients, is restricted or reduced in an area of the heart. As a consequence, the cardiac tissue suffers damage and can even become necrotic, resulting in myocardial infarction. The restoration of the blood flow (reperfusion) is essential for recovery; however, a period of ischemia followed by reperfusion often leads to increased damage. This is known as ischemia-reperfusion (IR) injury.

Mitochondrial ROS generation increases in the myocardium during ischemia (Levraut et al. 2003, Zweier et al. 1987), and it plays a central role in the pathophysiology of myocardial injury (Raedschelders et al. 2012). Under complete anoxic conditions, no ROS are generated (Garlick et al. 1987). However, during ischemia there is a progressive reduction in tissue oxygen levels. Then, in the presence of reduced levels of O_2, the electron transport chain (ETC) malfunctions and superoxide formation occurs (section 3.1.). Due to the lack of oxygen, mitochondrial oxidative phosphorylation, the major source of cellular ATP production, ceases, which disrupts

energy metabolism. There is then a switch to anaerobic glycolysis to compensate for ATP generation (Solaini and Harris 2005). Increased glycolysis causes lactic acid accumulation and hence a decrease in the intracellular pH.

When the tissue is reperfused, and given the fact that during reperfusion there is an overshoot of oxygen levels, massive ROS production easily occurs (Murray et al. 2004, Zweier et al. 1987, Zweier et al. 1989). In this conditions, ROS are mainly produced at complexes I and III of the respiratory chain (Drose et al. 2009). The excessive production of ROS is due to high $\Delta\Psi_m$ values (Huttemann et al. 2008). High amounts of ROS mediate dysfunction of the sarcoplasmic reticulum and intracellular Ca^{2+} overload. The generation of ATP by the re-energized ETC in the setting of increased cytosolic Ca^{2+} concentration leads to the opening of the mitochondrial permeability transition pore (mPTP) and consequently to the loss of $\Delta\Psi_m$ (Halestrap and Pasdois 2009). These events induce cardiomyocyte death by hypercontracture, which is facilitated during reperfusion by the restoration from acidic to physiological pH values (Lemasters et al. 1996, Piper et al. 1998) (Fig. I7).

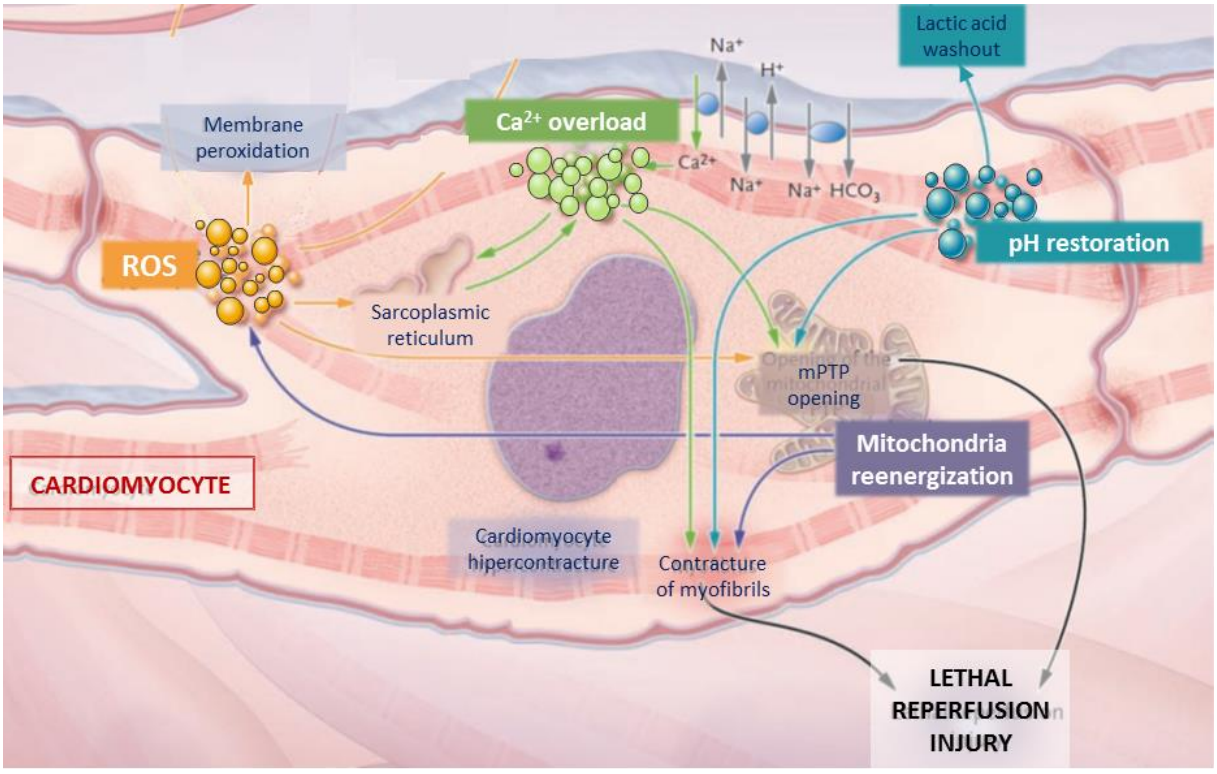

Figure I7. Mediators of myocardial IR injury. Mitochondrial re-energization (purple), generation of ROS (orange), intracellular Ca^{2+} overload (green), and rapid restoration of physiological pH (blue). Adapted from Yellon and Hausenloy, 2007.

ROS also mediate myocardial injury by acting as neutrophil chemoattractants. Neutrophils accumulate in the infarcted tissue, where they mediate cardiomyocyte death by vascular plugging. This causes the release of degradative enzymes, and the generation of ROS, which in turn further damage the cell membrane by lipid peroxidation, induce enzyme denaturation, and cause DNA damage. Finally, cardiomyocyte death occurs, as the pathways leading to cell apoptosis and necrosis are switched on (Galluzzi and Kroemer 2008, Whelan et al. 2010).

5.2. The phenomenon of ischemic preconditioning

The heart can be protected against IR injury by undergoing repetitive short non-lethal periods of myocardial ischemia and reperfusion prior to a prolonged ischemic period, a phenomenon known as ischemic preconditioning (IPC) (Hausenloy and Yellon 2011, Murry et al. 1986, Yellon and Downey 2003). The activation of endogenous cytoprotective pathways that protect the myocardium against IR injury (conditioning) can be applied before (preconditioning), during (perconditioning) or immediately after (postconditioning) the ischemic insult, either directly to the heart or to a distal tissue (remote preconditioning) (Hausenloy and Yellon 2011, Shi and Vinten-Johansen 2012). A wide range of triggers, signalling pathways and potential end-effector mechanisms have been identified (exposed below), which appear common to all forms of conditioning. Moreover, conditioning applies to not only the cardiomyocyte, but to all the constitutive cell types within the myocardium (Bell and Yellon 2012).

IPC protects the heart by reducing oxidative stress during IR and by inhibiting the opening of the mPTP, thus diminishing the shutdown of ATP production and mitochondrial swelling, that in turn decreases cellular damage and death by necrosis and apoptosis (Halestrap 2010, Javadov et al. 2003). IPC induces two windows of cardioprotection: an immediate phase lasting 2-3 h (Murry et al. 1986), and a delayed effect 24-48 h later (Kuzuya et al. 1993, Marber et al. 1993). This latter effect is not as powerful as the previous one but has a longer action. The immediate 'classic' IPC involves preformed factors and confers a powerful protective effect against myocardial necrosis (Kloner et al. 1998). However, the immediate IPC does not protect against the loss of contractility that immediately follows a sub-lethal ischemic insult, called 'stunning' (Bolli and Marban 1999). The second window of protection is probably related to the synthesis of neoformed factors. It protects against myocardial stunning but is less effective against necrosis (Bolli et al. 1997, Sun et al. 1995).

IPC mechanisms are complex and not yet completely understood, but it is known that they involve several triggers, mediators and effectors. Brief episodes of ischemia result in the release

of initiating factors such as adenosine, bradykinin, norepinephrine, and endorphins (Banerjee et al. 1993, Cohen et al. 2001, Liu et al. 1991). During the early phase, these initiators bind to specific receptors coupled to G proteins, which results in message transduction. There are two identified signalling pathways: the reperfusion-induced salvage kinase (RISK) pathway (Hausenloy et al. 2005) and the survivor activating factor enhancement (SAFE) pathway (Suleman et al. 2008). Both of these pathways lead to the inhibition of mPTP opening, which is considered the main effector of IPC. Mitochondrial ATP-dependent potassium channels (mK_{ATP}) are also likely effectors of IPC (Gross and Auchampach 1992). For the second window of protection, an activation of transcription factors occur. Thus, the activation of the nuclear factor-κB (NF-κB) has been reported (Xuan et al. 1999), which induces the expression of proteins that provide myocardial protection such as the NO synthase (iNOS) (Shinmura et al. 2002), and several anti-apoptotic proteins (Stein et al. 2007).

5.3. 'Mild uncoupling' and cardiac ischemia tolerance

As explained before, mitochondrial ROS production increases with a higher (more negative) $\Delta\Psi_m$. On the contrary, mitochondrial depolarization, which implies a reduction in $\Delta\Psi_m$, results in a tighter association between electron transfer and the ETC complexes, thereby limiting random electron disassociation and $O_2^{\cdot-}$ production (Korshunov et al. 1997). Therefore, 'mild uncoupling' could be protective against oxidative damage generated during IR by diminishing mitochondrial ROS generation. Some studies show that tolerance against IR injury is conferred by directly inhibiting the ETC flux with pharmacological agents and diminishing $\Delta\Psi_m$ (Park et al. 1997). This mechanism is also supported by experiments showing modest depolarization after the administration of low concentrations of uncoupling agents such as FCCP (carbonyl cyanide 4-p-trifluoromethoxy phenylhydrazone) or DNP (2,4-dinitrophenol) that evokes protection against ischemic damage in the intact heart (Minners et al. 2000) and in cardiomyocytes (Rodrigo et al. 2002), in parallel with a decrease in mitochondrial ROS production. Therefore, transient modest mitochondrial depolarization, regardless of whether it is achieved via 'mild uncoupling', through modulation of the ETC flux, or by pharmacological uncoupling, confers protection against IR injury. Hence, the question arises as to whether endogenous modulation of mitochondrial uncoupling by UCPs may contribute to the regulatory machinery governing cellular ischemia tolerance.

Taking into account the 'mild uncoupling' effect on mitochondrial ROS generation, and since UCP2 and UCP3 are expressed in the heart (Bezaire et al. 2007, Murray et al. 2004), it seems reasonable to hypothesize that their uncoupling activity could potentially have a major

impact on ischemia tolerance and possibly on cardiac ATP production (Cadenas et al. 2010, Sack 2006). The activation of UCPs would lower the $\Delta\Psi_m$, thereby attenuating mitochondrial ROS production and protecting against oxidative cellular damage (Brand et al. 2004). In fact, the ectopic expression of UCP1 in the mouse heart, mitigates reperfusion-induced damage (Hoerter et al. 2004).

Disturbances in ATP synthesis in the heart have been implicated in cardiac failure pathogenesis, and increased levels of cardiac UCP2 and UCP3 were found in patients with heart failure (Murray et al. 2004). Moreover, *in vitro* studies have shown that preconditioned mitochondria are uncoupled. These mitochondria have lower $\Delta\Psi_m$ and reduced ATP levels, and their oxygen consumption rates are higher than in non-preconditioned mitochondria (Minners et al. 2001). The association of IPC with proton leak has been directly confirmed by measuring oxygen consumption and mitochondrial $\Delta\Psi_m$ in mitochondria extracted from preconditioned rat hearts prior to the onset of a prolonged IR insult (Nadtochiy et al. 2006). Importantly, the upregulation of UCP2 and UCP3 was observed in the delayed preconditioned heart (McLeod et al. 2005). More recently, the role of UCP3 in cardioprotection against IR injury and the induction of IPC has been reported (Ozcan et al. 2013). The mechanism involve the regulation of myocardial energetics and ROS generation.

Another plausible hypothesis for UCP3-mediated cardioprotection could be the involvement of this protein in the attenuation of lipotoxic effects. This is based on the fact that the ischemic heart is exposed to elevated levels of FFA (Opie and Sack 2002) and that UCP3 might play a role in the export of fatty acid anions from the mitochondria to prevent the accumulation of fatty acid metabolic by-products (Himms-Hagen and Harper 2001). The implication of UCP3 in myocardial energetic metabolism has been recently suggested, since UCP3 deletion appears to induce a metabolic shift that favoured glycolytic metabolism in a mouse model of permanent coronary occlusion (Gargiulo et al. 2014).

5.4. The Langendorff perfusion system as a tool for the study of the intact mouse heart

The perfusion system was introduced by Oscar Langendorff in 1895 for the study of the mammalian heart physiology, and became a valuable tool for the analysis of factors such as: contractile function, coronary blood flow regulation and cardiac metabolism (Langendorff, 1895). This system is now broadly used for the study of the isolated mammalian heart (*ex vivo* model). In particular, the Langendorff perfusion system is extremely useful for the study of the pathophysiology of IR and other disease states. This system is also an essential tool for the

study of the impact of pharmacological drugs on heart physiology, as well as for the analysis of the consequences of gene deletion or gene expression regulation on intracellular signalling and adaption to clinically relevant stressful stimuli (Liao et al. 2012).

In this *ex vivo* model, the heart is perfused retrogradely (opposite to normal physiological flow) by cannulating the aorta, which implies that the aortic valve closes under pressure, the perfusate fills the coronary arterial vasculature, passing through the vascular bed, and being drawn off to the coronary sinus into the right atria (Fig. I8). The heart is washed of all blood and perfused with buffer solution all throughout. The preparation can be perfused in either 'constant flow' or 'constant pressure' modes, depending on specific experimental requirements. Each mode has its own advantages and disadvantages that must be taken into account (Bell et al. 2011c).

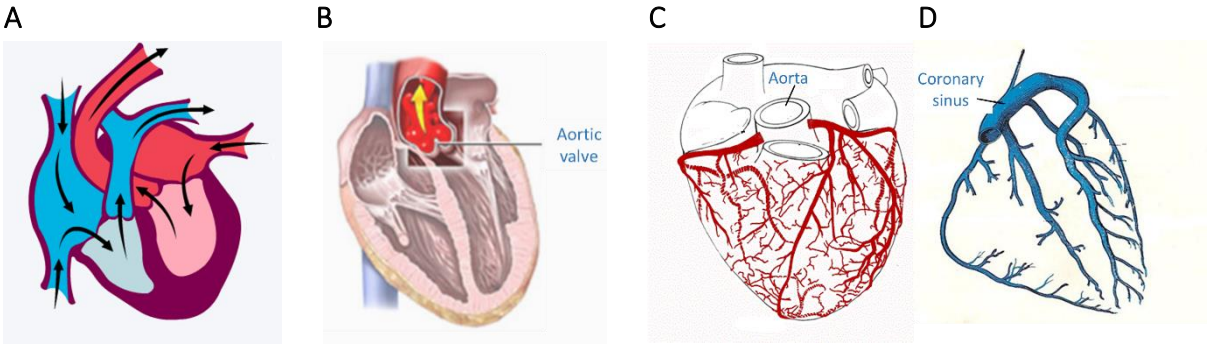

Figure I8. Diagrams showing (A) normal physiological flow, (B) normal valve operation, (C) coronary circulation (arteries) and (D) coronary circulation (veins).

The use of the Langendorff system has some limitations that have to be considered when planning a study. First, the diminutive size and fragility of the mouse heart, as well as its high heart rate add technical difficulties to the experiments. Second, and most important, the isolation of the heart from the whole animal makes the study less clinically relevant than other *in vivo* approaches (Sutherland et al. 2003). Nevertheless, the procedure offers enormous advantages. Thus, as this system provides a tool to study the heart in isolation of other systems and out of exocrine control, the experimental measurements are not interfered by those coming from other physiological processes. Moreover, it can be used to observe protocols that would be lethal to the whole animal if performed *in vivo*. Another important advantage is that treatments and drugs can be used without fear of impacting upon non-cardiac organ function. Hence, in summary, the Langendorff perfusion system is an extraordinary tool for the study of the physiology of the heart.

iii. OBJECTIVES

In this thesis, we seek to achieve the following objectives:

1. To determine the effects of oxidative stress on the expression of mitochondrial uncoupling protein 3 (UCP3).

2. To analyse the possible involvement of the antioxidant transcription factor Nrf2 on UCP3 regulation.

3. To evaluate the influence of UCP3 on mitochondrial function under oxidative stress conditions and the possible antioxidant role of this protein.

4. To investigate the potential cardioprotective role of UCP3 and Nrf2 in isolated perfused mouse hearts subjected to ischemia-reperfusion, as well as the involvement of UCP3 in ischemic preconditioning.

iv. MATERIALS AND METHODS

1. CELL CULTURE AND TREATMENTS

1.1. Mouse cardiomyocyte HL-1 cells

HL-1 cells were grown and maintained on gelatin/fibronectin-coated plates in Claycomb medium (Sigma-Aldrich) supplemented with 10% (v/v) fetal bovine serum (Sigma-Aldrich), 100 µM norepinephrine (Sigma-Aldrich), 1% (v/v) GlutaMAX™ (Gibco, Life Technologies), 100 U/ml penicillin (GE Healthcare, Little Chalfont, UK) and 100 µg/ml streptomycin (GE Healthcare), to maintain a differentiated phenotype and contractile activity. The cells were cultured at high confluence and were passed 1:2 every three days.

1.2. Mouse myoblast C2C12 cells

C2C12 cells were grown and maintained in Dulbecco's modified Eagle's medium DMEM (Lonza, Cambridge, UK) containing 4.5 g/L glucose and supplemented with 10% (v/v) fetal bovine serum (HyClone™ Thermo Scientific, Rockford, IL, USA), 1 mM sodium pyruvate (Sigma-Aldrich), 2 mM L-glutamine (Lonza), 100 U/ml penicillin and 100 µg/ml streptomycin (GE Healthcare). The cells were passed 1:4 every two days. For the experiments, C2C12 myoblasts were differentiated into myotubes after reaching 80-90% confluence, by using for 4 days DMEM supplemented with 2% (v/v) horse serum (Sigma-Aldrich), 1 mM sodium pyruvate (Sigma-Aldrich), 2 mM L-glutamine, 100 U/ml penicillin and 100 µg/ml streptomycin.

1.3. Cell treatments

For most experiments, the cells were treated with 300 µM hydrogen peroxide (H_2O_2; Sigma-Aldrich) for 6 h, or with 20 µM 4-hydroxy-2-nonenal (HNE; Cayman, Ann Arbor, Michigan) for 5 h, unless otherwise stated. In some experiments, the antioxidant N-acetylcysteine (NAC; Sigma-Aldrich) was added at 5 mM, 1 h before the oxidative challenge.

2. ANIMALS

Male UCP3 knockout (UCP3-KO), Nrf2 knockout (Nrf2-KO), and wild-type mice (strain background C57BL/6) were bred and housed in the Animal Services Unit of the Centro Nacional de Investigaciones Cardiovasculares (CNIC, Madrid, Spain). The animals were maintained on normal rodent diet and had *ad libitum* access to food and water. Experiments were performed when mice were 28-30 weeks old. The animals were killed by cervical dislocation before quick excision of the heart.

All procedures used in this thesis were performed in accordance with the guidelines and regulations of the CNIC.

3. STUDY OF GENE EXPRESSION

3.1. Determination of RNA expression by quantitative PCR

3.1.1. RNA extraction

Total RNA from C2C12 and HL-1 cells was extracted using the TRI Reagent RNA Isolation System (MRC, Cincinnati, OH). Cellular samples obtained from 60 mm-plates were lysed and homogenized in 1 mL of TRI Reagent using a mortar. The homogenates were then separated into aqueous and organic phases by the addition of 200 µL chloroform, vigorous mixing, and centrifugation at 12,000 *g* for 15 min at 4°C. The RNA remained exclusively in the upper aqueous phase (600 µL approximately). For RNA precipitation, isopropanol (600 µL) was added and the mix was stored for at least 1 h at -20°C. The samples were then centrifuged at 12,000 *g* for 10 min at 4°C and the pellet containing the RNA was washed twice with 70% ethanol and solubilized in 30-60 µL of RNase-free water for 10 min at 60°C. Finally, the samples were frozen at -80°C overnight and then heated at 60°C for 10 min for a better solubilization previous to the determination of RNA concentration.

3.1.2. Determination of RNA concentration and purity

RNA concentration and purity were determined using a NanoDrop 1000 Spectrophotometer (Thermo Scientific), from 1 µL of sample. RNA concentration was calculated by measuring the absorbance of the sample at 260 nm. 1 OD_{260} unit at 260 nm corresponds to 40 µg/mL of single-stranded RNA. RNA purity was determined by calculating the ratio between the absorbance at 260 nm and 280 nm. An $Abs_{260/280}$ ratio of 2.0 was considered "pure" for RNA.

3.1.3. Reverse transcription

Reverse transcription (RT) was carried out using the GeneAmp® Gold RNA PCR Core Kit (Applied Biosystems, Foster City, CA), with 0.5 µg of total RNA and random hexanucleotides as primers (Table M1). The reaction was carried out in a thermocycler, using the following cycling parameters:

10 min at 25°C
12 min at 42°C

RT-PCR buffer	30 mM Tris-HCl, 20 mM KCl pH 8.3
$MgCl_2$	2.5 mM
dNTP blend	1 mM (250 µM of each dNTP)
RNase inhibitor	10 Units
DTT	10 mM
Hexanucleotides mix	1.25 µM
MultiScribe reverse transcriptase	15 Units
RNase-free H_2O	Up to 20 µL

Table M1. Reverse transcription reaction components.

3.1.4. Quantitative real-time PCR

The resulting cDNA samples (1 µL) were amplified with specific primers, and mRNA levels were determined by real-time PCR (RT-PCR) using Power SYBR® Green (Applied Biosystems) and the StepONEplus™ Real-Time PCR System (Applied Biosystems). The cycling parameters were the following:

10 min initial denaturation at 95°C

x 40 cycles:

15 s denaturation at 95°C

1 min annealing at 60°C

GENE	Forward	Reverse
Ucp3	5'CTGGAGGAGAGAGGAAATACAGAG3'	5'TGGCATTTCTTGTGATGTTGGGCC3'
Nrf2	5'GCAAGTTTGCAGGAGCTATTT3'	5'GCTGCTTGTTTTCGGTATTAAGAC3'
Ucp2	5'GGCCTCTACGACTCTGTC3'	5'GCTCCCGATGCCTGCAT3'
HO-1	5'ACATCCAAGCCGAGAATGCT3'	5'CCAGGGCCGTGTAGATATGG3'
HPRT	5'ATTGTAATGACCAGTCAACAGGG3'	5'GCATTGTTTTGCCAGTGTCAA3'
β-actin	5'CCCAGAGCAAGAGAGG3'	5'GTCCAGACGCAGGATG3'

Table M2. Specific primer pairs used for the amplification of the analysed genes for quantitative real-time PCR.

The relative gene expression level was calculated using *HPRT* mRNA or *β-actin* mRNA as housekeeping genes. The sequences of the primer pairs used for the amplification of the

analyzed genes are shown in Table M2. The primers were designed using the Primer Express® Software 3.0 (Applied Biosystems).

3.2. Determination of protein expression by immunoblotting

3.2.1. Cellular fractionation for differential protein extraction

The following cellular fractionation protocol was based on Fu and Taubman, 2010. Cells were scraped from plates in PBS (phosphate-buffered saline; 137 mM NaCl, 2.7 mM KCl, 10 mM Na_2HPO_4, 1.8 mM KH_2PO_4) and centrifuged at 500 *g* for 5 min at 4°C. The obtained pellet was resuspended in buffer 1 (Table M3) and maintained on ice for osmotic lysis for 15 min. To proceed with the lysis, the samples were subjected to three freeze/thaw cycles of 5 min immersion in liquid N_2 followed by 10 min immersion in a water bath at 37°C. Then, the tubes were centrifuged at 500 *g* for 10 min. At this point, pellets (A) and supernatants (B) were separated to carry out two different cellular fractionations:

- The pellets (A), which contain the nuclei, were resuspended in a supplemented commercial Radio Immune Precipitation Assay buffer (RIPA; Sigma-Aldrich) (Table M3). The samples were maintained on ice for 20 min and centrifuged at 12,000 *g* for 5 min at 4°C, and the obtained supernatants were collected as nuclear protein fractions.

- The supernatants (B) were collected and spun at 12,000 *g* for 20 min at 4°C. The final pellets (mitochondria-enriched fractions) were resuspended in 30 µl of mitochondrial buffer (Table M3). The supernatants were collected as cytosolic fractions.

Buffer 1		Supplemented RIPA buffer		Mitochondrial buffer	
EDTA (pH 8.0)	1 mM	Glycerol	1% v/v	Tris-HCl (pH 7.5)	10 mM
DTT	1 mM	EDTA (pH 8.0)	5 mM	Sucrose	320 mM
NaCl	10 mM	Phosphatase inhibitor cocktail		EDTA (pH 8.0)	1 mM
$MgCl_2$	3 mM	Protease inhibitor cocktail		Protease inhibitor cocktail	
Tris-HCl (pH 7.5)	5 mM				
Phosphatase inhibitor cocktail					
Protease inhibitor cocktail					

Table M3. Composition of buffers for cellular fractionation. All materials were from Sigma-Aldrich, except the phosphatase and protease inhibitor cocktails that were, respectively, *PhosSTOP EASYpack* tablets and *cOmplete Mini* tablets from Roche (Basel, Switzerland).

Protein concentration was determined by the Pierce™ BCA Protein Assay Kit (Thermo Scientific). The protein extracts were stored at -80°C.

3.2.2. Immunoblot analysis

The desired amount of protein extracts (usually 30-70 µg) was mixed 1:1 (v/v) with Laemmli buffer 2X (4% SDS, 20% glycerol, 10% 2-mercaptoethanol, 0.004% bromophenol blue and 0.125 M Tris HCl, pH 6.8; Sigma-Aldrich) and heated at 95°C for 5 min.

The proteins were separated by electrophoresis, using 10-12% SDS-polyacrylamide gels (SDS-PAGE). The gels were usually run at 120 V for 90 min in TGS buffer [25 mM Tris, 192 mM glycine, 0.1 (w/v) SDS, pH 8.3; Bio-Rad Laboratories, Madrid, Spain]. After electrophoresis, the proteins were transferred to nitrocellulose membranes (0.45 µm, Bio-Rad), usually at 380 mA for 90 min, in transfer buffer [25 mM Tris, 192 mM glycine, pH 8.3, plus 20% (v/v) methanol, Bio-Rad], using a Mini-PROTEAN Tetra Blotting Module (Bio-Rad). After transfer, the proteins were stained with a Ponceau S solution [0.1% (w/v) from Sigma-Aldrich, in 5% (v/v) acetic acid] to check protein loading and transfer efficiency.

Antibody	Source	Dilution	Company	Reference
anti-UCP3	Rabbit	1:1000	Thermo Scientific	PA1-055
			Abcam	ab3477
anti-Nrf2	Rabbit	1:1000	Santa Cruz Biotechnology (Santa Cruz, CA)	sc-13032X
anti-Porin	Mouse	1:7500	Invitrogen	456000
anti-Lamin A/C	Mouse	1:1000	Cell Signalling (Danvers, MA)	2032
anti-Hsp90	Mouse	1:2000	Santa Cruz Biotechnology	sc-13119

Table M4. Primary antibodies used for immunoblot analysis. Dilutions were made in blocking solution.

For protein immunodetection, the membranes were washed briefly in a TBS-T solution (10 mM Tris-base, 40 mM Tris-HCl, 150 mM NaCl, adjusted to pH 8.0 and supplemented with 0.1% Tween 20) and then incubated in blocking solution [5% (w/v) skimmed dry milk in TBS-T] for 1 h at room temperature. After blocking, the membranes were incubated overnight at 4°C with the required primary antibody dilution (in 5% milk, TBS-T solution) (Table M4). The membranes were then washed 4 times for 10 min with TBS-T, before incubation for 1 h at room temperature with a horseradish peroxidase-conjugated secondary antibody dilution (in

5% milk, TBS-T solution) (Table M5). The membranes were then washed with TBS-T (4 times for 10 min) and the immunoreactive bands were detected using enhanced chemiluminescence (SuperSignal® West Femto Chemiluminescent Substrate, Thermo Scientific), following the manufacturers' instructions. The specific band intensity was detected using a CCD camera of the ImageQuant LAS 4000 (GE Healthcare). The analysis of the images and the quantification of the bands were carried out using the ImageJ (National Institutes of Health, USA) and Image Quant 5.2 softwares (Molecular Dynamics, Sunnyvale, CA, USA).

Antibody	Source	Dilution	Company	Reference
anti-rabbit	Goat	1:5000	Pierce (Chester, UK)	31460
anti-mouse	Goat	1:8000	Santa Cruz Biotechnology	sc-2005

Table M5. Secondary antibodies used for immunoblot analysis. Dilutions were made in blocking solution.

4. STUDY OF GENE REGULATION

4.1. Small interfering RNA (siRNA) transfection

Once HL-1 cells reached 60% confluence, the supplemented Claycomb medium was replaced by Opti-MEM® medium (Invitrogen, Carlsbad, CA) to perform the down-regulation of *Nrf2* and *Ucp3* gene expression by small interfering RNA (siRNA). The gene silencers used were *Nrf2* siRNA (sc-37049 mouse, Santa Cruz) and *UCP3* siRNA (sc-42685 mouse, Santa Cruz). A non-targeting pool of siRNA or scramble (Scr; Control siRNA-A, sc-37007, Santa Cruz) was used as transfection control. HL-1 cells grown in 60 mm-plates were transfected with 150 pmol RNAi using 15 µL Lipofectamine® 2000 (Invitrogen), according to the manufacturer's instructions. After 4 h incubation with Lipofectamine® 2000, the Opti-MEM® medium was removed from the culture plate and the usual supplemented Claycomb medium (section 1.1. of the Materials and Methods) was added. The cells were used for experiments 48 h after transfection, when silencing was at its maximum.

4.2. Chromatin immunoprecipitation (ChIP) assay

The protocol used was based on Pescador *et al.* 2005. HL-1 and C2C12 cells were grown on 100 mm-plates until they reached 90% confluence. They were exposed to 300 µM H_2O_2 for 3-6 h or to 5, 10 or 20 µM HNE for 3 and 6 h. The cells were then fixed for 12 min at 4°C by adding

formaldehyde to the culture media to a final concentration of 1% (v/v). The cross-linking was stopped by the addition of glycine (0.125 M). The cells were washed with cold PBS and then scraped in 0.5 mL of lysis buffer (Table M6).

Cell lysates were incubated on ice for 10 min and then sonicated to shear the DNA to fragments of 200-1500 bp. After removal of the insoluble material by centrifugation at 12,000 *g* for 5 min, 50 µL of each sample were removed and stored (input), while 450 µL were diluted in 450 µL of immunoprecipitation buffer (Table M6).

Lysis buffer		Immunoprecipitation	
SDS	1% v/v	Triton X-100	1% v/v
EDTA (pH 8.0)	10 mM	EDTA (pH 8.0)	2 mM
Tris-HCl (pH 8.1)	50 mM	Tris-HCl (pH 8.1)	20 mM
Protease inhibitor cocktail		NaCl	150 mM

Table M6. Lysis and immunoprecipitation buffers for ChIP assay.

The lysates were precleared by incubation for 1 h at 4°C with 100 µg of a salmon sperm DNA/protein A agarose 50% slurry (Upstate Biotechnology, Lake Placid, NY). The samples were then immunoprecipitated twice, initially with whole rabbit serum for 4 h at 4°C (Immunoglobulin G, IgG control), and then overnight at 4°C with a rabbit polyclonal anti-Nrf2 (1:100 dilution; sc-13032X, Santa Cruz). The immunocomplexes were recovered by the addition of 200 µg of salmon sperm DNA/protein A agarose 50% slurry to the samples, which were then sequentially washed for 15 min in TSE I, TSE II, and Buffer III (Table M7).

TSE I		TSE II		Buffer III	
SDS	0.1%	SDS	0.1%	LiCl	250 mM
Triton X-100	1%	Triton X-100	1%	NP-40	1%
EDTA (pH 8.0)	2 mM	EDTA (pH 8.0)	2 mM	EDTA (pH 8.0)	1 mM
Tris-HCl (pH 8.1)	20 mM	Tris-HCl (pH 8.1)	20 mM	Tris-HCl (pH 8.1)	10 mM
NaCl	150 mM	NaCl	500 mM	Deoxycholate	1%

Table M7. Immunoprecitation buffers for ChIP assay.

Finally, the immunoprecipitated complexes were washed twice with TE buffer (10 mM Tris, 1 mM EDTA, pH 8.0) and extracted twice with a buffer containing 1% SDS and 0.1 M $NaHCO_3$.

The cross-linking was reversed by the addition of 200 mM NaCl (final concentration) and overnight incubation at 65°C.

PRIMERS	Forward	Reverse
UCP3 ARE1 (positive region)	5'GTATGGTCGCTGTGAAGATCAAAT3'	5'AAGCTTCCATTATGTGCCAAATG3'
UCP3 ARE3 (negative region)	5'TTCCATTCCGTGCCTTCTGT3'	5'GAGGGAACCTCAGGTGATGTTG3'

Table M8. Quantitative PCR (qPCR) specific primers for ChIP assay.

The proteins were removed by the addition of proteinase K (30 µg/sample) for 2 h at 42°C, and the DNA was purified by phenol-chloroform extraction and ethanol precipitation. The immunoprecipitated DNA was amplified by qPCR, using the primers described in Table M8, which target a highly conserved positive region containing an ARE (antioxidant response element) in the *Ucp3* promoter, beginning at position -2002 relative to the transcription start site (UCP3 ARE1), as well as a negative non-conserved region (UCP3 ARE3).

4.3. Plasmid construction and cell transfection

4.3.1. Construction of the pGL4.27-ARE and pGL4.27-mARE plasmids

Gene-specific oligonucleotides were designed based on the GenBank database for the *Ucp3* 5′ flanking region (Accession No. AB011070.1). Forward and reverse single strands of a 71-bp fragment of the 5′-upstream region of the *Ucp3* gene containing the 9-bp ARE (shown in blue) located at the -2002 position in the *Ucp3* promoter were designed (Table M9).

Wild-type (ARE) FW 5′-TCGAGTGGTCGCTGTGAAGATCAAATGGGACATTTCTGAAAATGCTTCGCTGGCATTTGGCACATAATGGA-3′
Mutant, for negative plasmid control (mARE) FW 5′-TCGAGTGGTCGCTGTGAAGATCAAATGGGACATTTCACTAAATTTTTCGCTGGCATTTGGCACATAATGGA-3′

Table M9. Oligonucleotides used to construct a DNA fragment containing the ARE or the mutated ARE (mARE).

Specific mutations (shown in red) in the ARE were introduced by site-directed mutagenesis using the QuikChange Site-Directed Mutagenesis Kit (Agilent Technologies, Santa Clara, CA), following the manufacter's instructions, to generate the negative plasmid control.

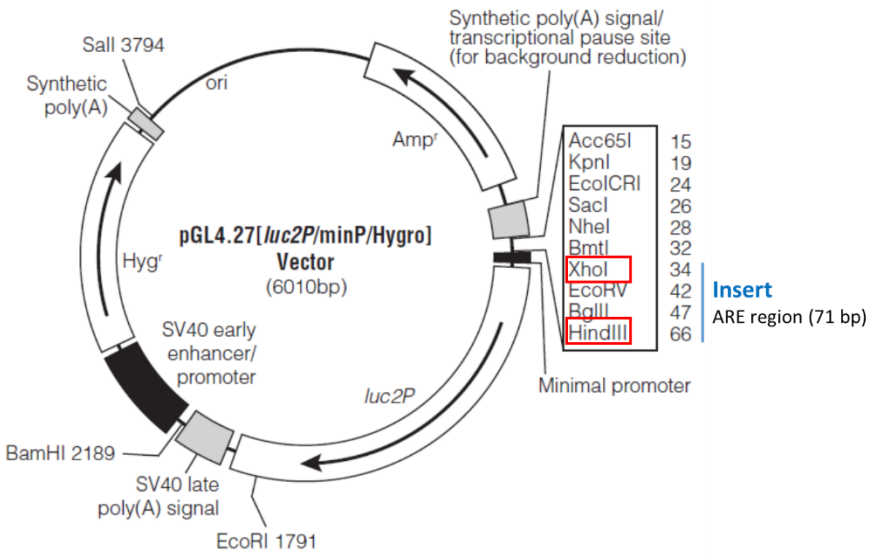

Figure M1. pGL4.27 firefly luciferase reporter vector. The restriction sites used to insert the DNA fragment containing the ARE are marked in red.

The oligonucleotides for both designs included extensions for the *Xho*I and *Hind*III restriction sites at their 5′ and 3′ ends, respectively, and were synthesized by Metabion International AG (Martinsried, Germany). The synthetic oligonucleotides were annealed, phosphorylated, purified, and ligated into the *Xho*I and *Hind*III sites of the pGL4.27 firefly luciferase reporter vector (Promega Biotech Ibérica) (Fig. M1). The construction was amplified using *Escherichia coli* DH5α cells. Positive clones were selected after DNA digestion followed by electrophoresis in 1.5% agarose gel. The resulting clones were named pGL4.27-ARE and pGL4.27-mARE. The reporter constructs were confirmed by DNA sequencing performed by Secugen S.L. (Madrid).

4.3.2. Construction of the pGL4.27-Prom and pGL4.27-mProm plasmids

We defined and cloned a longer DNA fragment (2205 bp, from -2145 to +60 relative to the transcription start site) of the *Ucp3* promoter (Fig. M2), based on the GenBank database for the *Ucp3* 5′ flanking region (Accession No. AB011070.1). The sequence, containing the ARE, was obtained from mouse genomic DNA by PCR, using the primers described in Table M10, which were synthesized by Metabion International AG.

Forward	5′ AAAGGGGTACCACAGCTGCAAAGAGAACAGAG 3′
Reverse	5′ TTCTTTCTCGAGTCCACTCCATTAGGTAGCAGC 3′

Table M10. Primers used to clone the *Ucp3* mouse promoter fragment. The *Kpn*I (forward) and *Xho*I (reverse) restriction sites are marked in blue.

Figure M2. Cloned fragment (2205 bp) of the *Ucp3* promoter region. The sequences shown in magenta and green hybridize, respectively, with the Fw and Rv primers used to amplify the whole *Ucp3* promoter. The +1 transcription start site is shown in red, and the transcription direction is indicated by an arrow. The wild-type ARE is shown in yellow.

4.3.3. Transient transfection and luciferase reporter assay

HL-1 cells were cultured in 6-well plates using supplemented Claycomb medium (section 1.1.). The transfection was carried out when the cells reached 70% confluence, using Lipofectamine® 2000, with a 1:1 ratio of DNA (µg) to Lipofectamine® 2000 (µL). The cells from each well were transfected with 1.5 µg of one of the reporter vectors (pGL4.27-ARE, pGL4.27-mARE, pGL4.27-Prom, pGL4.27-mProm, or empty pGL4.27) in a total volume of 150 µl Opti-MEM® (Invitrogen). As internal transfection control, 30 ng of the *Renilla* pRL-TK plasmid (Promega Biotech Ibérica) were used. For standard promoter activity experiments, transfected

cells were incubated for 48 h and then harvested for their use in reporter gene assays. The cells were lysed with passive lysis buffer (Promega), and the supernatant was assayed for reporter gene activity. The firefly and *Renilla* luciferase activities were measured using the Dual-Luciferase Reporter Assay System (Promega) with a GloMax®-Multi Detection System (Promega). The ratio between firefly and *Renilla* luciferase activities from duplicated determinations was normalized to that of the empty pGL4.27 vector.

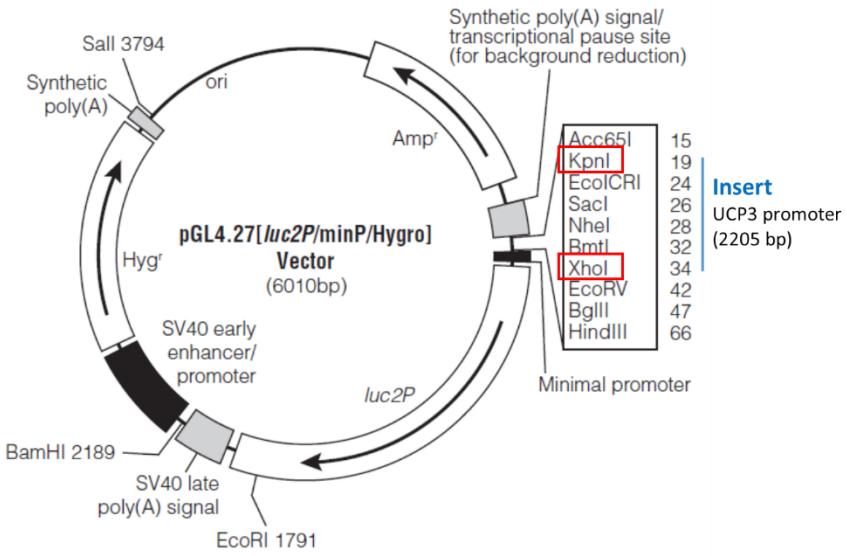

Figure M3. pGL4.27 firefly luciferase reporter vector. The restriction sites used to insert the PCR products containing the cloned promoter fragment are marked in red.

5. DETERMINATION OF OXIDATIVE STRESS AND CELL VIABILITY BY FLOW CYTOMETRY

The fluorescent probes 6-carboxy-2'-7'-dichlorodihydrofluorescein diacetate (DCF-DA; C369, Molecular Probes-Invitrogen, Carlsbad, CA) and propidium iodide (PI; P3566, Molecular Probes-Invitrogen) were used as indicators of reactive oxygen species (ROS) and cell death, respectively. After treatment with 300 µM H_2O_2 for 3-24 h, C2C12 and HL-1 cells were washed with PBS, trypsinized and centrifuged at 335 *g* for 5 min at room temperature. The pellets were resuspended in PBS at a concentration of 10^6 cells/mL and incubated in the presence of 10 µM DCF-DA and 1 µg/mL PI for 30 min at 37°C in the dark. The samples were washed twice with PBS and the fluorescence was analysed at excitation/emission wavelengths of 485/535 nm for DCF-DA and 536/620 nm for PI, using a FACSCalibur flow cytometer (Becton-Dickinson, NJ).

6. ANALYSIS OF CELL VIABILITY BY MICROSCOPY

Viability assays were performed 5-16 h after the treatment with 20 µM HNE, using the calcein-AM and propidium iodide (PI) method for simultaneous fluorescence staining of viable and dead cells. HL-1 cultures were stained for 15 min in the dark with 1 µM calcein (CA; C3100MP, Molecular Probes-Invitrogen) and 2 µM PI (P3566, Molecular Probes-Invitrogen). The cells were then analysed using an Axiovert 200 epifluorescence Microscope (Zeiss) coupled to a monochrome-colour CCD camera, and 4 images were taken for every treatment using a 10X dry objective in red and green channels. Finally, red (PI positive) and green (calcein positive) cells were counted in 4 fields per treatment and condition, and a dead/total cell percentage was calculated and compared between conditions.

7. MEASUREMENT OF CELLULAR RESPIRATION

Oxygen consumption in HL-1 cells was measured using an XF24 Extracellular Flux Analyser (Seahorse Bioscience, North Billerica, MA) after silencing as described in section 4.1. To obtain a homogeneous monolayer of cells, 80,000 transfected cells per well were plated in XF24 cell culture microplates (Ref.100850-001, Seahorse Bioscience) the day before the experiment.

To study the effect of H_2O_2 and HNE on cell respiration, the experiments were performed as follows. HL-1 cells were exposed to 300 µM H_2O_2 for 3 h. The cells were then incubated in unbuffered DMEM supplemented with 25 mM glucose, 1 mM pyruvate and 2 mM glutamine, and the cells were incubated at 37°C in a CO_2-free incubator for 1 h for equilibration before the experiment. For HNE experiments, HL-1 cells were exposed to 20 µM HNE for 4 h and then, the Claycomb medium was replaced by supplemented unbuffered DMEM. In this case, the HNE treatment was maintained in the unbuffered DMEM medium. The cells were incubated at 37°C in a CO_2-free incubator for 1 h. An overnight-equilibrated calibration cartridge (Ref.100777-004, Seahorse Biosciences) was then loaded with unbuffered DMEM (port A), 5 µg/mL oligomycin (port B), 300 nM FCCP (carbonyl cyanide-p-trifluoromethoxyphenylhydrazone; port C), and 1 µM antimycin A plus 1 µM rotenone (port D), all obtained from Sigma-Aldrich. This allowed determination of the basal respiration, the amount of oxygen consumption linked to ATP production, the proton leak, the maximal respiration capacity, the reserve capacity, and the non-mitochondrial oxygen consumption. In all experiments, the protein concentration in each well was determined at the end of the measurements, using the Pierce™ BCA Protein Assay Kit (Thermo Scientific) after cell lysis in

RIPA buffer (Sigma-Aldrich) supplemented with protease inhibitor cocktail (*cOmplete Mini* tablets from Roche), and was used to calibrate the oxygen consumption data.

8. ISOLATED HEART PERFUSION EXPERIMENTS

8.1. Langendorff perfusion of isolated hearts

Mice were killed by cervical dislocation, and the hearts were immediately excised, rinsed, and arrested in ice-cold Krebs-Henseleit buffer solution (Table M11). The hearts were then cannulated via the aorta (Ø = 0.8 mm cannula), and perfused retrogradely with warm (37°C) Krebs-Henseleit buffer using a Langerdorff setup.

Krebs-Henseleit buffer solution	
NaCl	120 mM
$NaHCO_3$	25 mM
Glucose	11 mM
KH_2PO_4	1.2 mM
$MgSO_4$	1.2 mM
KCl	4.8 mM
$CaCl_2$	2 mM

Table M11. Krebs-Henseleit buffer solution composition.

The system (Fig. M4 and Fig. M5) consisted of a peristaltic pump (REGLO *Digital* MS-4/8, ISMATEC International, Wertheim, Germany), a pressure transducer (CIBERTEC S.A., Madrid, Spain), a pressure transducer amplifier (CIBERTEC), and a circulating water bath (Digiterm 100, JP Selecta). The glassware was kindly provided by Prof. M. Saadeh Suleiman (University of Bristol, Bristol, UK). Recordings were obtained using a PowerLab 2/20 (ADInstruments, Oxfordshire, UK) and the PowerLab Chart software (ADInstruments).

The heart was immersed at all times in perfusion solution (Krebs buffer) that was kept at 37°C via water jackets. The solution was previously bubbled with 95% O_2/5% CO_2 to maintain pH 7.4.

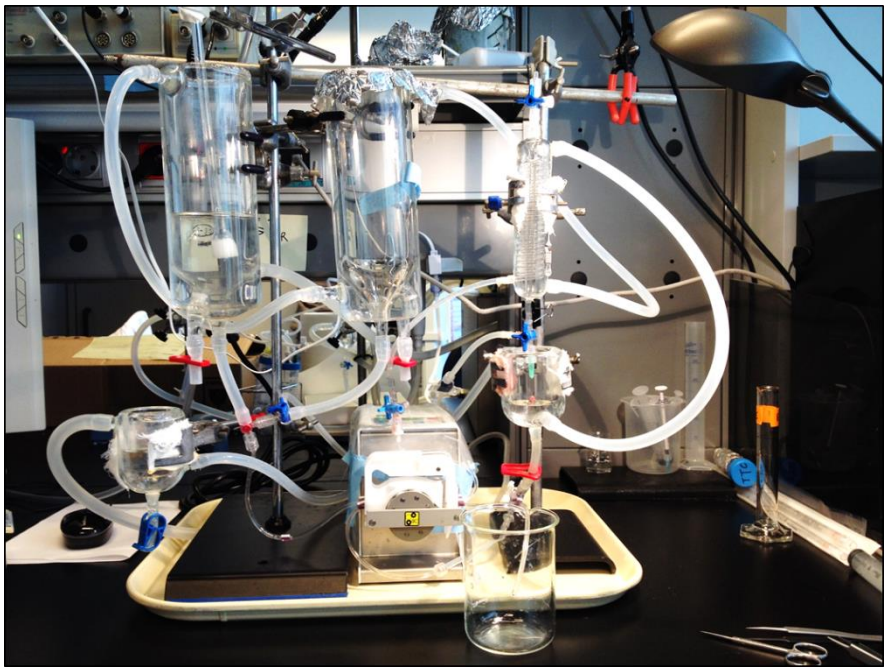

Figure M4. The Langendorff setup used for the experiments described in this thesis.

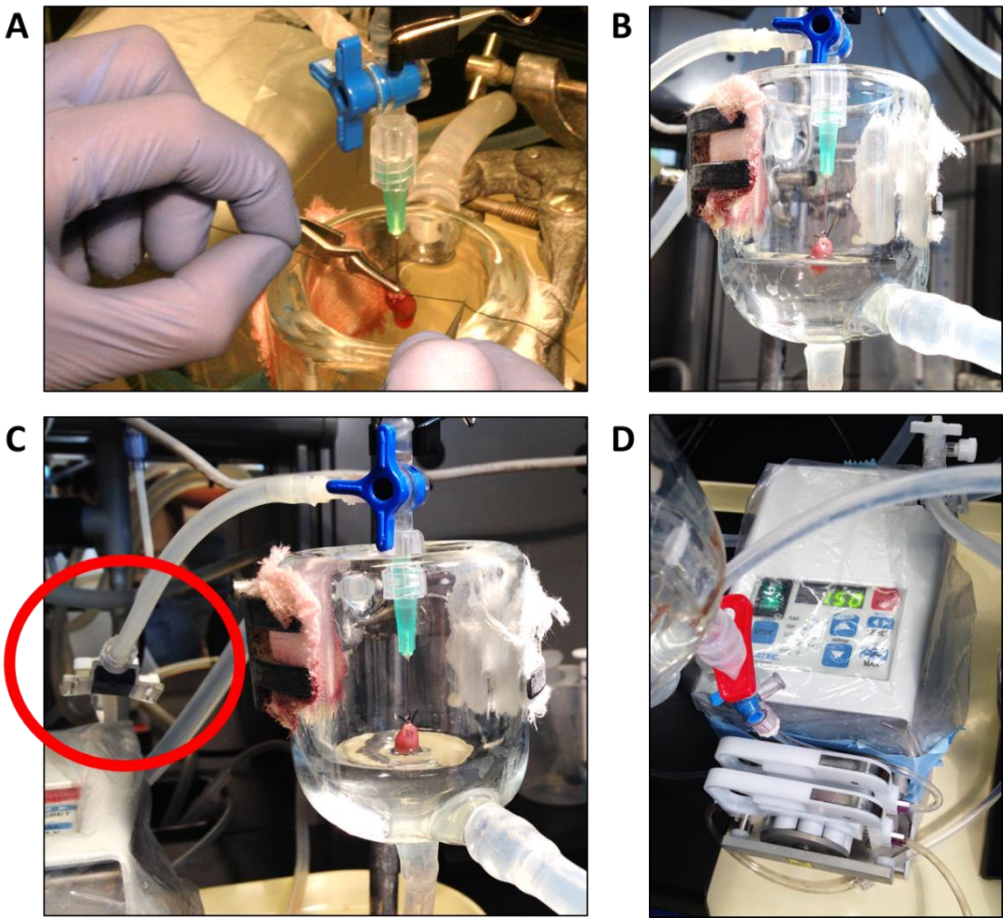

Figure M5. (A) Silk suture was used to secure the cannulated mouse heart and ensure placement. (B) The heart during perfusion, immersed in warm Krebs buffer. (C) The pressure transducer (circled in red) to monitor perfusion pressure was set just above the aortic cannula. (D) The peristaltic pump controls the perfusion flow.

The aortic pressure was monitored continuously by a pressure transducer located above the cannula (Fig. M5C). For cannulation, the flow was set at 0.8 mL/min. At the beginning of the stabilization, the flow was manually increased in order to build up pressure to approximately 70 mmHg. The flow necessary to achieve this aortic pressure varied between experiments, but was usually 1.5-2.5 mL/min. For exclusion criteria, all experiments in which the flow was lower than 1 mL/min or higher than 3 mL/min were discarded. The flow was then maintained constant throughout the experiment.

8.2. Experimental perfusion protocols

Once the hearts were securely attached to the cannula and successfully beating, different perfusion protocols were applied, as described below (schematically depicted in Fig. M6):

- *Control (C)*: hearts were perfused with standard oxygenized Krebs solution at 37°C for 120 min.

- *Ischemia (I)*: hearts were allowed to stabilize for 20 min before the flow was completely stopped to generate global normothermic ischemia for 40 min.

- *Ischemia-reperfusion (IR)*: hearts were allowed to stabilize for 20 min before generating global normothermic ischemia for 40 min. Then, the flow was restored and the hearts were reperfused for 60 min.

- *Ischemic preconditioning control (IPC+C)*: hearts were allowed to stabilize for 20 min before applying 2 cycles of 5 min global normothermic ischemia plus 5 min reperfusion. Then, they were perfused for 60 min.

- *IPC+I*: hearts were allowed to stabilize for 20 min before 2 cycles of 5 min global normothermic ischemia plus 5 min reperfusion. Then, they were subjected to a 40 min period of ischemia.

- *IPC+IR*: hearts were allowed to stabilize for 20 min before 2 cycles of 5 min global normothermic ischemia plus 5 min reperfusion. Then, they were subjected to a 40 min period of ischemia followed by 60 min of reperfusion.

During the perfusion experiments, the aortic pressure was continuously monitored. As shown in Fig. M7, a sharp drop was observed at the beginning of ischemia when the flow is stopped, which was restored at reperfusion.

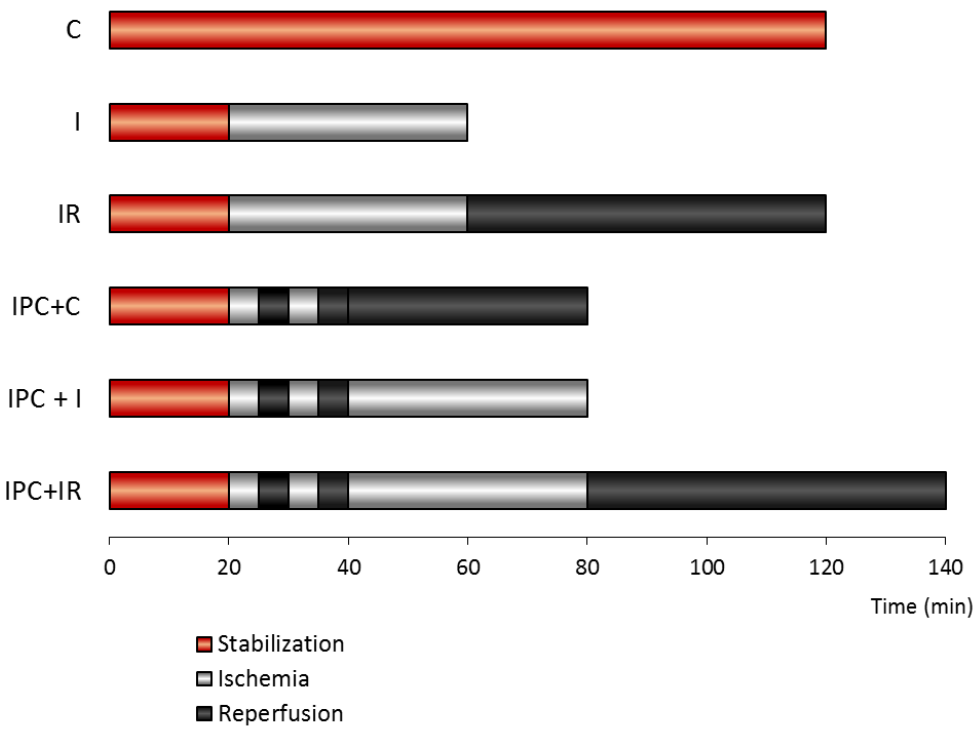

Figure M6. Diagrams showing the perfusion protocols performed for the Langendorff experiments.

Upon completion of the perfusion protocols, the hearts were either removed off the cannula, the ventricles rapidly frozen in liquid nitrogen, and stored at -80°C until processing for analysis of protein expression (section 8.3.), or subjected to triphenyltetrazolium chloride (TTC) staining for infarct size measurements (section 8.4.)

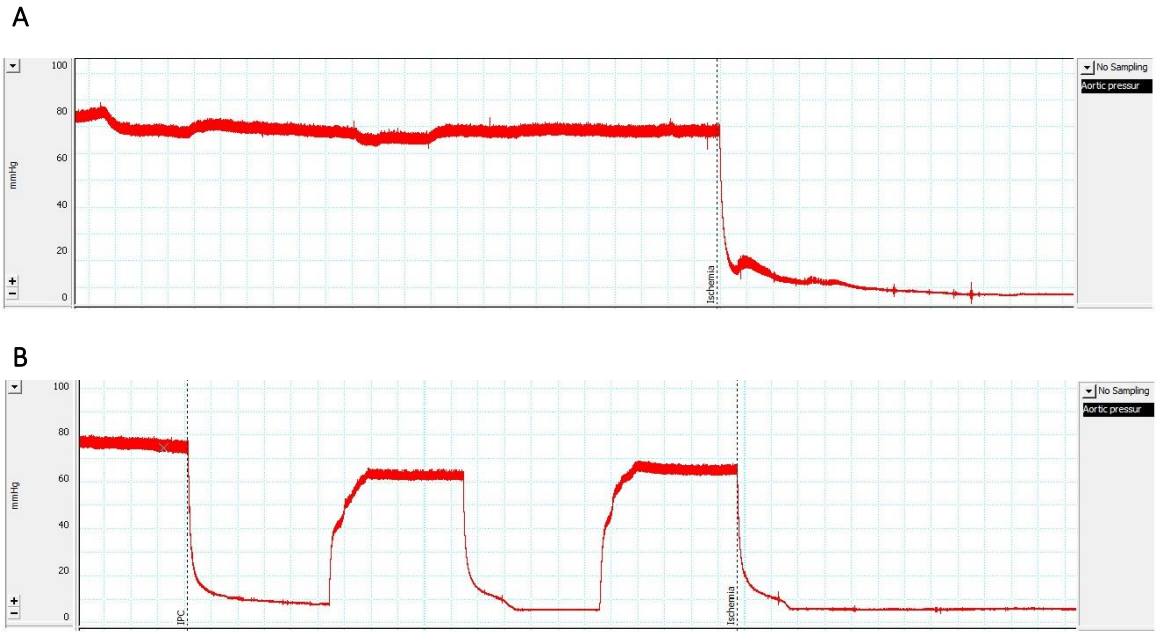

Figure M7. Representative recordings of the aortic pressure (mmHg) during 35 min showing the beginning of ischemia after (A) stabilization, and (B) an IPC protocol. The aortic pressure drops to minimum when the flow is stopped for an ischemia period. Recordings were obtained using a PowerLab Chart software (ADInstruments).

8.3. Tissue protein extract preparation

Frozen hearts were finely minced with sharp scissors in supplemented RIPA buffer (6 mL/g heart tissue, Table M12), and then lysed on ice for 25 min. The lysates were separated into two equal parts to obtain total and nuclear cellular fractions.

Supplemented RIPA buffer	
DTT	1 mM
Pefabloc	1 mM
Phosphatase inhibitor cocktail	
Protease inhibitor cocktail	

Table M12. Supplemented RIPA buffer for heart protein extraction. All materials were from Roche, except RIPA and DTT that were from Sigma-Aldrich.

A) For total extracts, the lysates were centrifuged at 12,000 *g* for 10 min at 4°C. The supernatants were collected and stored at -80°C.

B) For nuclear extracts, the lysates were centrifuged at 500 *g* for 10 min at 4°C. The supernatants were discarded and the pellets were resuspended in 50 µL supplemented RIPA buffer and allowed to lyse for another 10 min on ice. Afterwards, the samples were centrifuged at 12,000 *g* for 10 min at 4°C, and the supernatants were collected as nuclear extracts and stored at -80°C.

Protein concentration was determined by the Pierce™ BCA Protein Assay Kit (Thermo Scientific). UCP3 and Nrf2 protein expression levels were analysed by immunoblot as previously described (section 3.2.2.).

8.4. Infarct size measurements

For infarct size measurements, perfused hearts were stained with 2,3,5-triphenyltetrazolium chloride (TTC; Sigma-Aldrich). Upon completion of the experimental perfusion protocol, 1% TTC in PBS was perfused through the cannula at 1 mL/min for 12 min at 37°C. The heart was then removed from the cannula, immersed in PBS and kept at 37°C for 5 min. Afterwards, the heart was wrapped in cling film, frozen at -20°C for 30 min, and cut into 6-7 slices (approximately 2 mm thick). The slices were fixed overnight in 4% formaldehyde, washed with water, photographed by both sides, allowed to dry for 24 h over desiccant paper, and weighted.

TTC is a white crystalline powder that works as a redox indicator, since it is enzymatically reduced to red TPF (1,3,5-triphenylformazan) in living tissues due to the activity of several dehydrogenases, while it remains white in areas of necrosis (Fig. M8).

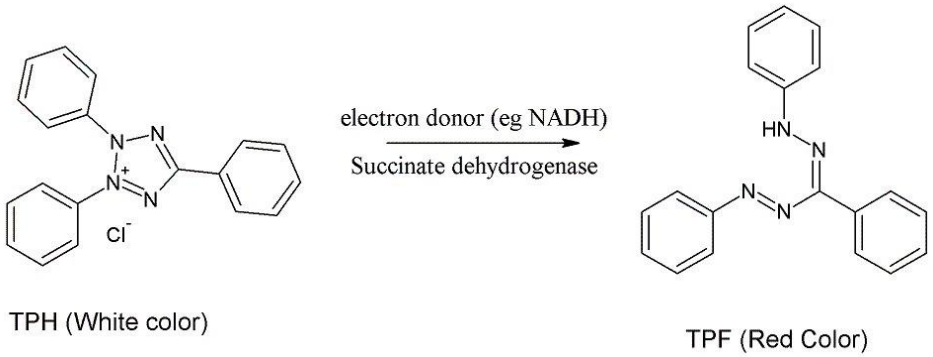

Figure M8. TTC structure in both oxidized and reduced states.

.

The images were analysed for infarct size using AlphaEaseFC software (Alpha Innotech, San Leandro, CA). The percentage of infarcted volume of the whole heart was calculated taking into account the images from both sides of each slide, and the contribution of each particular slice to the total dried weight of the heart.

8.5. Creatine kinase activity assay

Creatine kinase levels in the coronary effluent were measured to determine reperfusion injury. CK is primarily found in muscle, brain and heart tissue. The determination of CK activity provides a sensitive marker for the diagnosis of myocardial infarction. Aliquots of coronary effluent were collected prior to ischemia for basal levels, and during reperfusion. The samples were maintained at 4°C and analysed for CK activity on the same day of the experiment. It is worth noting that there was a "dead volume" in the perfusion chamber that delays the release of effluent. This "dead volume" was measured at the end of the experiment, when all the effluent that remains in the chamber was manually released, and it was taken into account for the calculation of the total effluent volume.

CK activity in the effluent was determined by the CK-NAC kit (CK113, Randox, Belfast, UK). The determination of CK activity was made by using creatine phosphate and ADP as substrates (Fig. M9). The enzyme is very unstable due to the oxidation of sulphydryl groups in its active site, and for this reason NAC is included in the test. The absorbance of samples was measured at 340 nm every 1 min for 4 min at room temperature, and the absorbance increment (ΔAbs) was registered. For calculation, the following equation was used following manufacter's instructions: *CK activity (units/L)= 4127 x ΔAbs* (at 25°C). To estimate total CK

release, the area under the curve (AUC) was calculated using the trapezium rule (Abdul-Ghani et al. 2014).

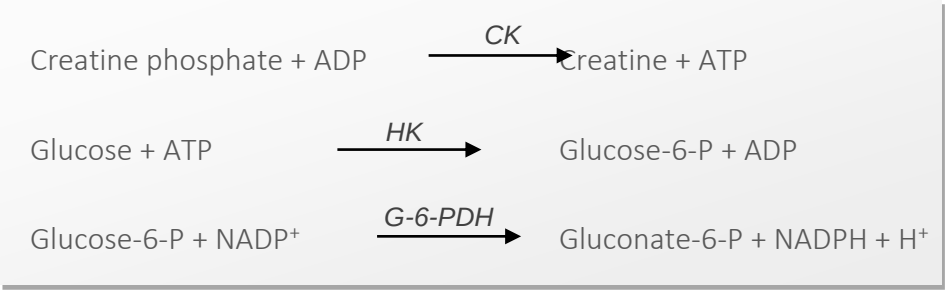

Figure M9. Principle for the creatine kinase (CK) activity measurement with the CK-NAC Randox kit. The determination of CK was made by using creatine phosphate and ADP as substrates for faster reaction and improved sensitivity than the use of creatine and ATP.

9. STATISTICAL ANALYSIS

The data are presented as mean ± SEM. The statistical significance of the differences between means was calculated using a two-tailed Student *t* test or one-way ANOVA followed by a Tukey post hoc test. A P value < 0.05 was considered statistically significant.

v. RESULTS

PART I. STUDY OF UCP3 EXPRESSION AND FUNCTION UNDER OXIDATIVE STRESS. ROLE OF THE TRANSCRIPTION FACTOR NRF2 IN OXIDATIVE STRESS-MEDIATED UCP3 UPREGULATION

1. EFFECTS OF HYDROGEN PEROXIDE (H_2O_2) ON UCP3 EXPRESSION AND FUNCTION

1.1. Effects of H_2O_2 on UCP3 expression and Nrf2 nuclear accumulation

UCP3 has been proposed to protect against oxidative damage (Brand and Esteves 2005, Mailloux and Harper 2011). To investigate whether UCP3 expression was regulated in response to oxidative stress, we first studied UCP3 expression after hydrogen peroxide (H_2O_2) treatment in two different cell lines: C2C12, a mouse myoblast cell line, and HL-1, a mouse cardiomyocyte cell line. Moreover, we analysed the nuclear accumulation of the antioxidant transcription factor Nrf2 under the same challenging conditions.

1.1.1. H_2O_2 treatment increases oxidative stress but does not induce cell death at short exposure times

To induce oxidative stress, we treated C2C12 and HL-1 cells with 300 µM H_2O_2 for 3, 6 or 24 h. The extent of oxidative stress was determined by analysing DCF-DA fluorescence by flow cytometry. The fluorescence signal increased significantly after a 6 h exposure to H_2O_2 in both C2C12 and HL-1 cell lines (Fig. R1), indicating enhanced oxidative stress levels.

Cell death was determined by incorporation of propidium iodide (PI), which was also analysed by flow cytometry (Fig. R2). Our data showed that the treatment with 300 µM H_2O_2 for up to 24 h did not significantly increase cell death in C2C12 cells, as the fluorescence intensity was not modified (Fig. R2A). However, a significant increase in cell death was observed after 24 h of H_2O_2 treatment in HL-1 cells, but not after 3 or 6 h exposure (Fig. R2B).

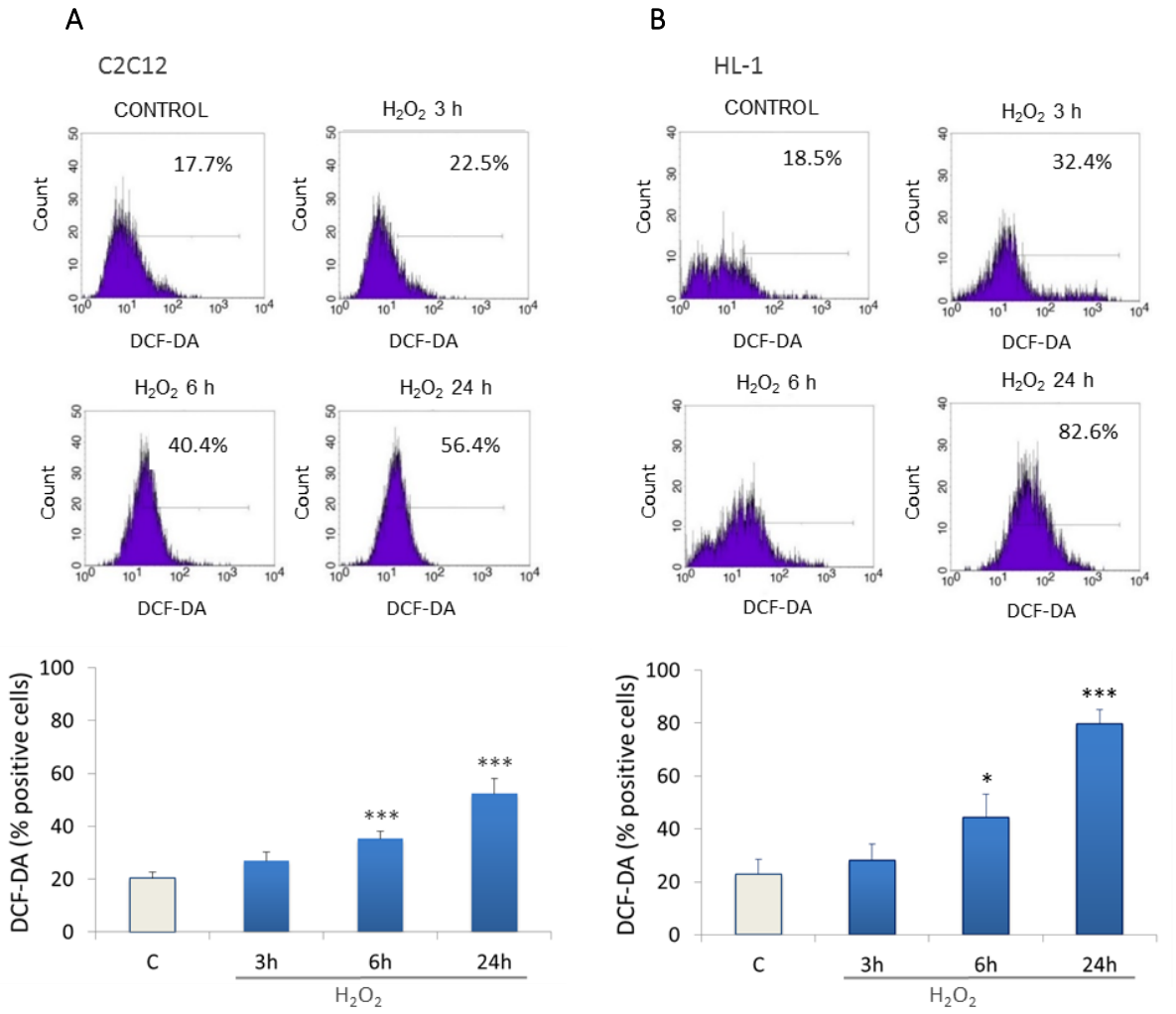

Figure R1. Time-dependent oxidative stress induced by H_2O_2 treatment. Oxidative stress was determined by flow cytometry (upper panels) using the fluorescent probe dichlorofluorescein diacetate (DCF-DA) in (A) C2C12 and (B) HL-1 cells treated with 300 µM H_2O_2 for 3 to 24 h. The percentages of positive cells are indicated. Histograms (bottom panels) show the mean ± SEM of the ROS levels relative to the basal conditions from 6-8 independent experiments. C, control untreated cells. **P* < 0.05, ****P* < 0.001.

Accordingly, the estimation of apoptotic cells, as determined by analysis of cleaved caspase 3 expression levels, was not altered in C2C12 cells but increased in HL-1 cells at 24 h (Fig. R3). These results allowed us to establish the timing conditions under which H_2O_2 treatment caused oxidative damage but not cell death.

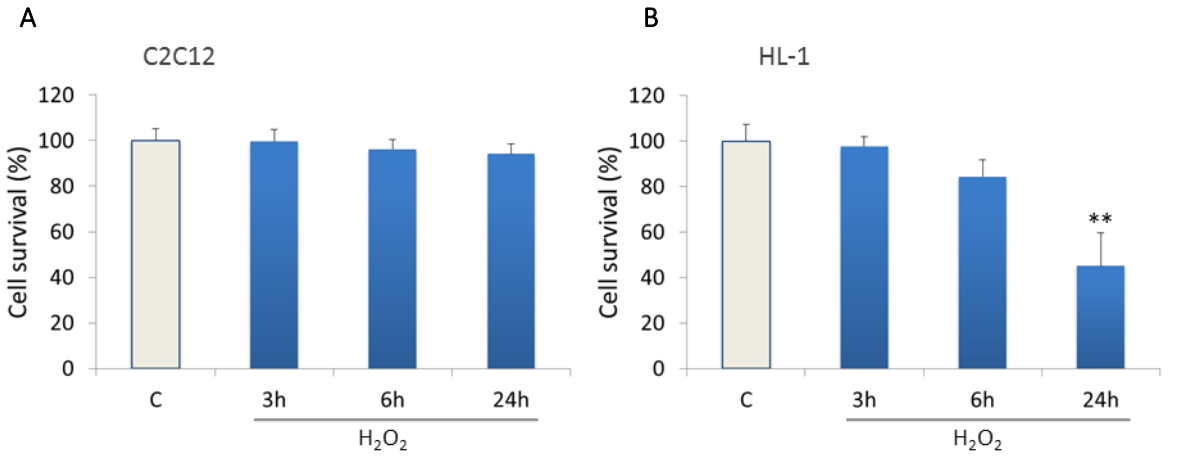

Figure R2. Time-dependent cell death induced by H_2O_2. Flow cytometry analysis of propidium iodide (PI) incorporation by (A) C2C12 and (B) HL-1 cells treated with 300 µM H_2O_2 for 3, 6 or 24 h. Histograms show the means ± SEM of cell death compared to the basal conditions from 6-8 independent experiments. C, control untreated cells. $^{**}P < 0.01$.

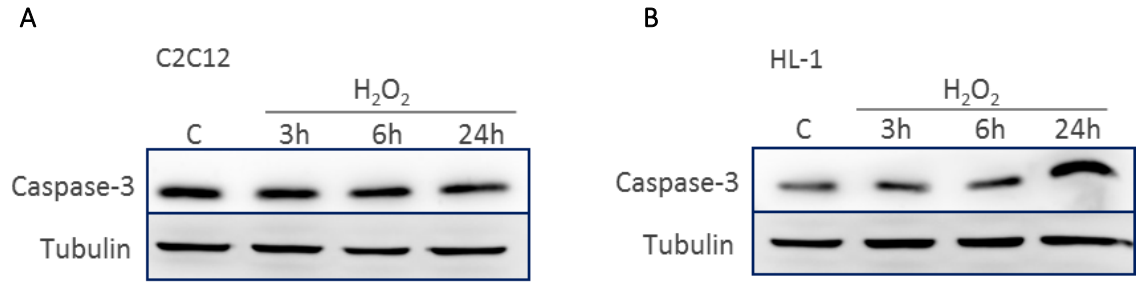

Figure R3. Time-dependent apoptotic cell death induced by H_2O_2. Representative immunoblots of caspase 3 protein in cytosolic extracts from (A) C2C12 and (B) HL-1 cells exposed to 300 µM H_2O_2 for 3, 6 or 24 h. Tubulin was used as protein loading control. C, control untreated cells.

1.1.2. H_2O_2 treatment upregulates UCP3 expression

We next studied the effects of H_2O_2 treatment on UCP3 expression in C2C12 and HL-1 cells. As shown in Fig. R4A and B, the exposure to 300 µM H_2O_2 for 3 or 6 h significantly increased UCP3 protein levels in the mitochondrial fraction of C2C12 and HL-1 cells. A more detailed time-course experiment (Fig. R4C) showed that the observed increase in UCP3 levels was not immediate but required 3 h to become significant.

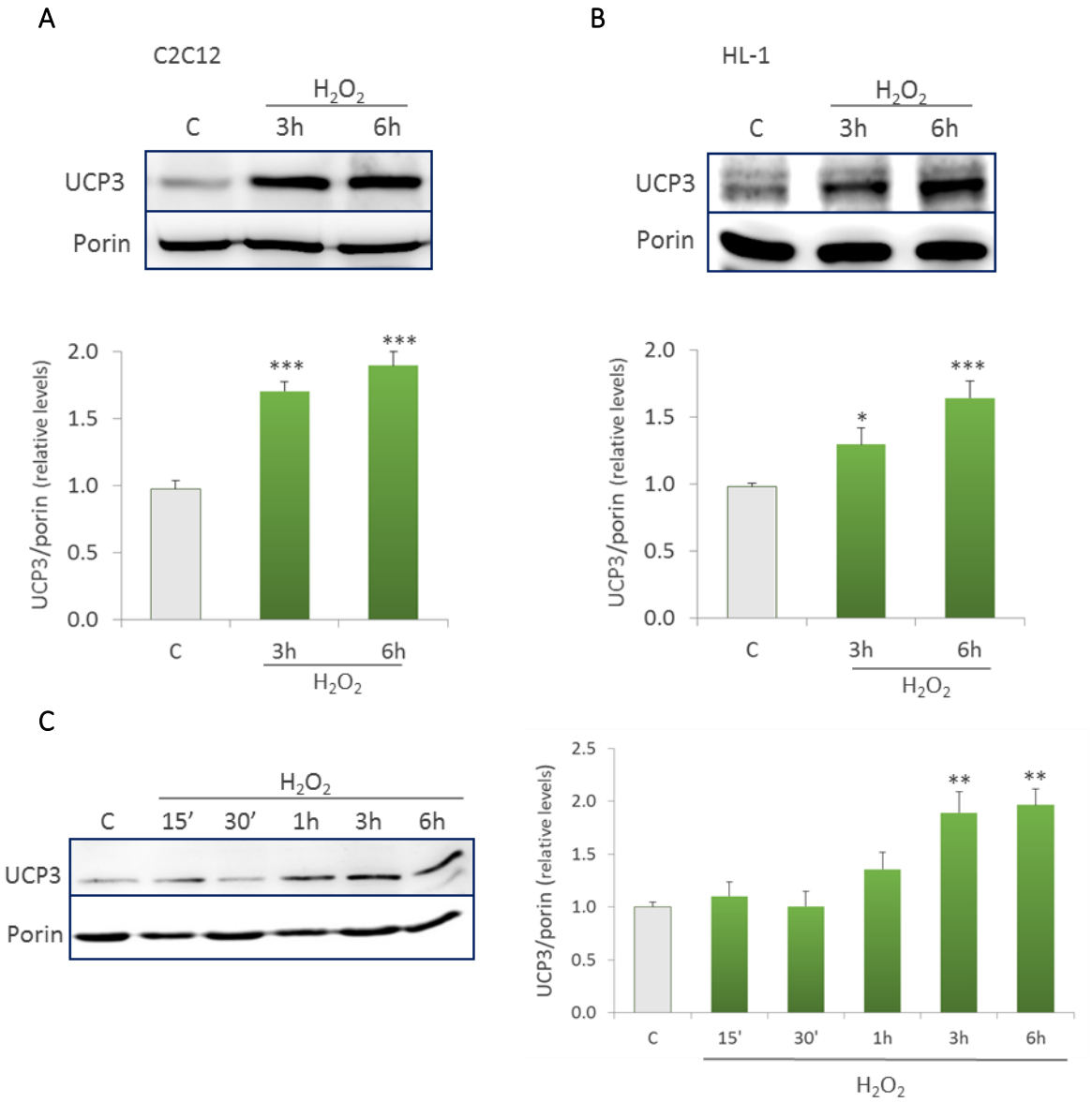

Figure R4. Effects of H_2O_2 on UCP3 expression levels. (A, B) Representative immunoblots and histograms of UCP3 protein levels in mitochondrial extracts from (A) C2C12 and (B) HL-1 cells exposed to 300 µM H_2O_2 for 3 or 6 h. (C) Representative immunoblot and histogram of a time-course experiment to analyse UCP3 protein levels in mitochondrial extracts from C2C12 cells exposed to 300 µM H_2O_2 (15 min-6 h). Porin was used as mitochondrial protein loading control. Histograms show the means ± SEM from 7-8 independent experiments. C, control untreated cells. *P < 0.05, **P < 0.01, ***P < 0.001.

To study whether these elevated UCP3 protein levels after H_2O_2 treatment correlated with an increase in *Ucp3* gene expression, we analysed *Ucp3* mRNA levels under the same oxidative stress conditions. Supporting the protein expression data, the mRNA levels of *Ucp3* were slightly but significantly increased by 300 µM H_2O_2 treatment at 3 and 6 h in both cell lines (Fig. R5). We also studied the mRNA levels of *Ucp2*, the other UCP expressed in skeletal muscle and heart, and found that they remained unaffected in both C2C12 and HL-1 cells (Fig. R5). These results indicate that the enhanced *Ucp3* expression after H_2O_2 treatment is a specific

response. Therefore, the elevated UCP3 protein levels can be explained, at least in part, by an increase in the expression of the *Ucp3* encoding gene. Taken together, these results indicate that UCP3 expression is upregulated in response to oxidative stress.

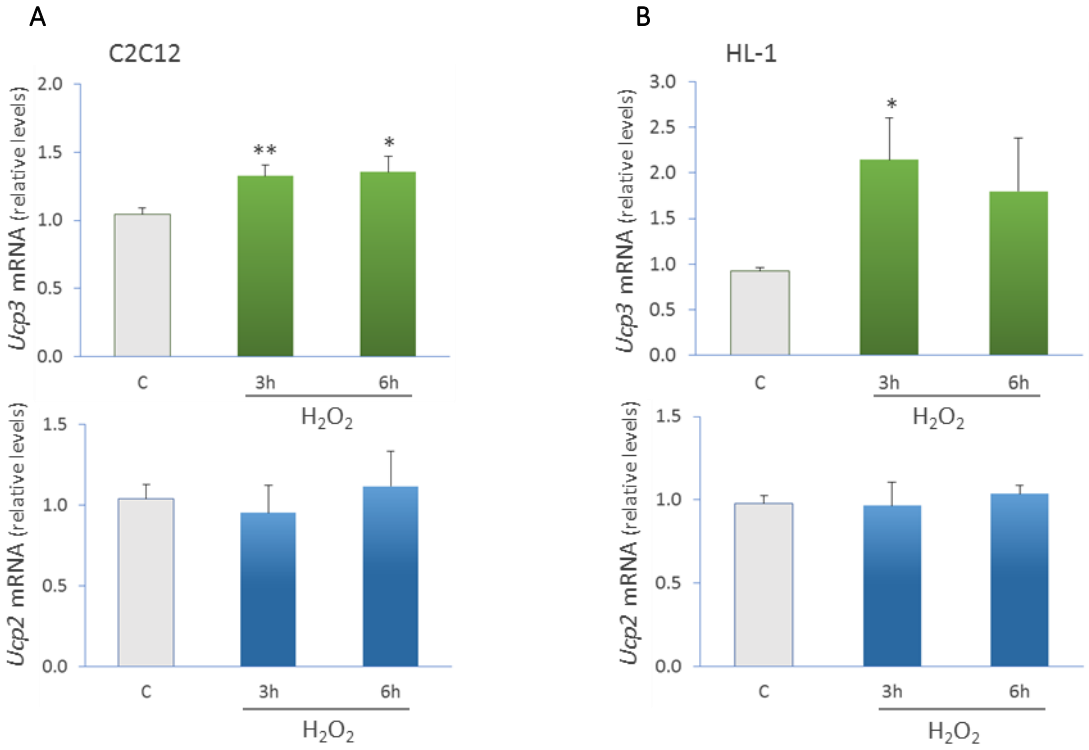

Figure R5. Effects of H_2O_2 on *Ucp2* and *Ucp3* mRNA levels. mRNA levels of *Ucp2* and *Ucp3* in (A) C2C12 and (B) HL-1 cells exposed to 300 µM H_2O_2 for 3 or 6 h. *HPRT* and *β-actin* were used as housekeeping genes for internal normalization Histograms show the means ± SEM from 9 (C2C12) and 6 (HL-1) independent experiments. C, control untreated cells. **P* < 0.05, ***P* < 0.01.

1.1.3. H_2O_2 treatment induces nuclear accumulation of the transcription factor Nrf2

The transcription factor Nrf2 is a master regulator of the antioxidant response in the cell (Jaiswal 2004, Kobayashi et al. 2006). It is known that this protein accumulates in the nucleus after an oxidative insult and then promotes the transcription of several genes involved in the defence against oxidative damage (Ishii et al. 2002, Itoh et al. 1999). It could be expected that, upon H_2O_2 treatment, Nrf2 would also accumulate in the nucleus of the cell lines we used. Figs. R6A and B show that Nrf2 accumulation was indeed observed in the nuclear fraction of both C2C12 and HL-1 cells after 3 and 6 h exposure to 300 µM H_2O_2. This increase was significant at 1 h and was also time dependent (Fig. R6C).

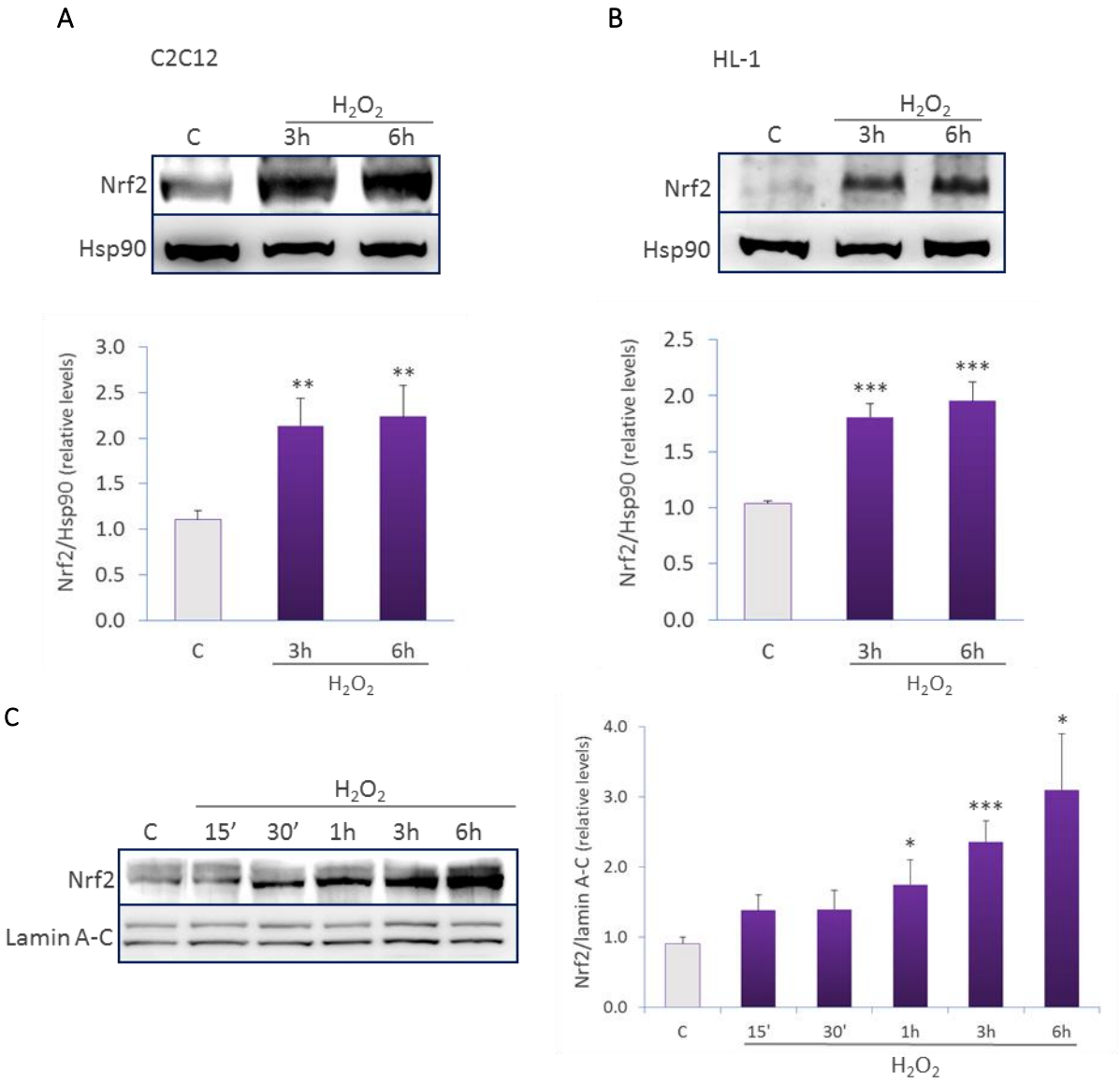

Figure R6. Effects of H_2O_2 on Nrf2 expression levels. (A, B) Representative immunoblots and histograms of Nrf2 protein levels in nuclear extracts from (A) C2C12 and (B) HL-1 cells exposed to 300 µM H_2O_2 for 3 or 6 h. (C) Representative immunoblot and histogram of a time-course experiment to analyse Nrf2 protein levels in nuclear extracts from C2C12 cells exposed to 300 µM H_2O_2 for 15 min to 6 h. Lamin A/C and Hsp90 were used as nuclear protein loading controls. Histograms show the means ± SEM from 8 independent experiments. C, control untreated cells. **P* ‹ 0.05, ***P* ‹ 0.01, ****P* ‹ 0.001.

Consistently, there was an increase in *Nrf2* mRNA in H_2O_2-treated C2C12 and HL-1 cells, which paralleled that of its target gene *HO-1* (Fig. R7). Therefore, Nrf2 accumulates in the nucleus of both C2C12 and HL-1 cells under oxidative stress conditions.

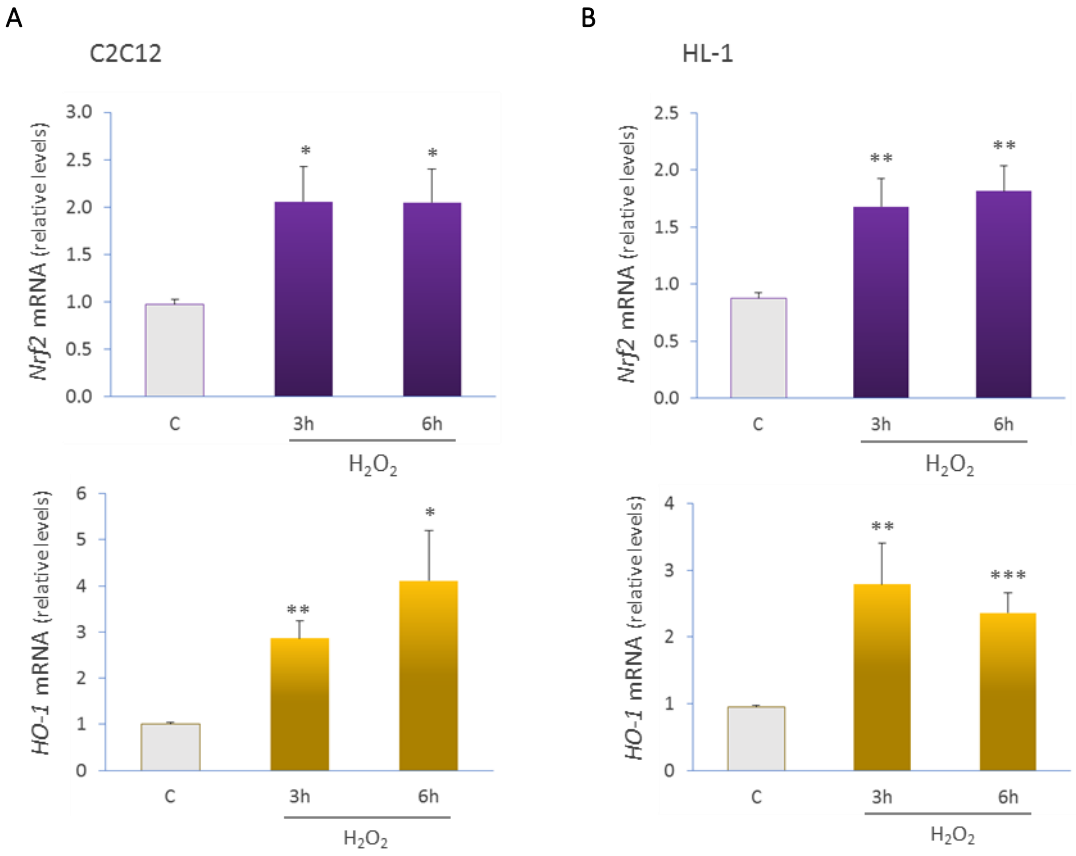

Figure R7. Effects of H_2O_2 on *Nrf2* and *HO-1* mRNA levels. mRNA levels of *Nrf2* and *HO-1* in (A) C2C12 and (B) HL-1 cells exposed to 300 µM H_2O_2 for 3 or 6 h. *HPRT* and *β-actin* were used as housekeeping genes for internal normalization. Histograms show the means ± SEM from 9 (C2C12) and 6 (HL-1) independent experiments. C, control untreated cells. **P* < 0.05, ***P* < 0.01, ****P* < 0.001.

1.2. Involvement of Nrf2 in H_2O_2-induced UCP3 upregulation

1.2.1. Nrf2 binds to the *Ucp3* promoter after H_2O_2 treatment

Since the antioxidant transcription factor Nrf2 accumulates in the nucleus of H_2O_2-treated C2C12 and HL-1 cells in parallel with the increase in the UCP3 protein in mitochondria, we tested the possibility that Nrf2 could regulate UCP3. First, we investigated the possible binding of Nrf2 to the *Ucp3* promoter under oxidative stress. For this, we identified and defined in the *Ucp3* promoter a highly conserved region containing an ARE (antioxidant response element) and beginning at position -2002 relative to the transcription start site. We also defined a non-conserved ARE region that was used as a negative control (Fig. R8).

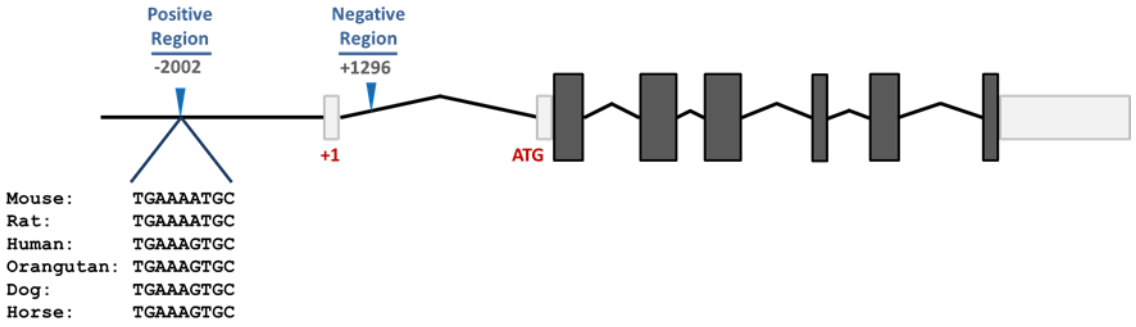

Figure R8. Identification of a conserved ARE within the *Ucp3* promoter. Schematic representation of the mouse *Ucp3* gene showing the nucleotide sequences matching the consensus antioxidant response element (ARE) from six mammalian species within the positive region and a non-conserved ARE within the negative region, as analysed by ChIP assay.

We then analysed the potential binding of Nrf2 to the *Ucp3* promoter by a ChIP assay. Using this technique, we found that Nrf2 binds to the ARE region of the *Ucp3* promoter in C2C12 cells after treatment with H_2O_2 for 3 or 6 h (Fig. R9A) and in HL-1 cells after a 6 h exposure (Fig. R9B). These data suggested that the enhanced UCP3 expression induced by H_2O_2 treatment may be due to Nrf2 binding to the *Ucp3* promoter.

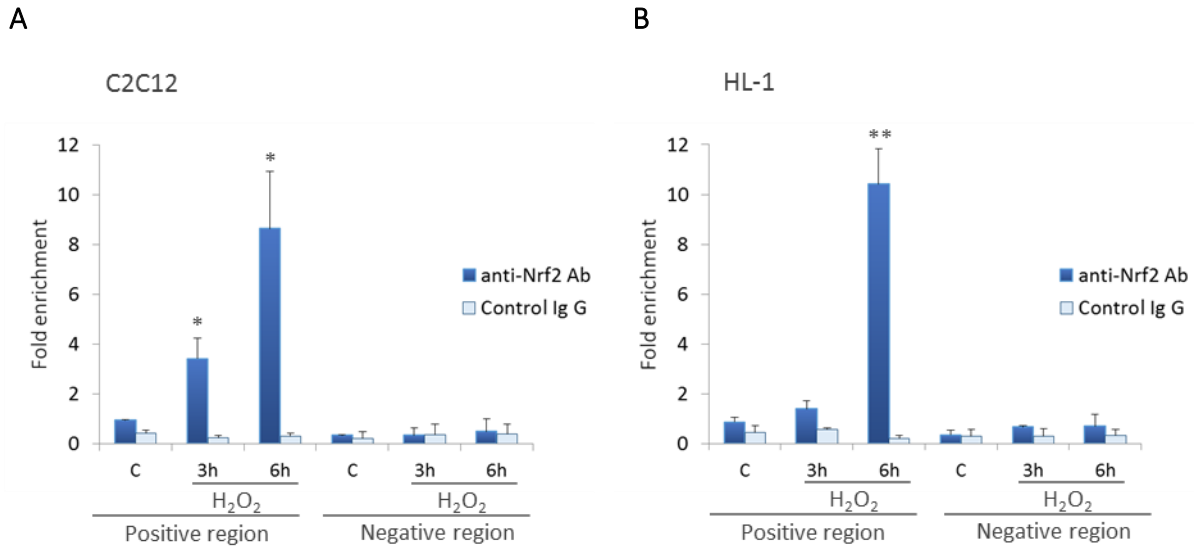

Figure R9. ChIP assay of Nrf2 binding to the *Ucp3* promoter after H_2O_2. ChIP assay of Nrf2 binding to the mouse *Ucp3* promoter in (A) C2C12 and (B) HL-1 cells exposed to 300 µM H_2O_2 for 3 or 6 h. RT-PCR quantification and enrichment of positive and negative regions after immunoprecipitation with Nrf2 or control IgG antibodies are shown. Histograms show the means ± SEM from 3 independent experiments. C, control untreated cells. *$P < 0.05$, **$P < 0.01$.

1.2.2. H_2O_2-induced UCP3 upregulation is mediated by Nrf2

Next, we examined whether the binding of Nrf2 to the *Ucp3* promoter induced the transcription of the *Ucp3* gene and the subsequent increase in UCP3 protein levels. For this, we conducted luciferase reporter assays in HL-1 cells. To perform these experiments the cells were transfected with a plasmid (pGL4.27) containing a 71 bp fragment of the *Ucp3* promoter, which included either the ARE or a mutated ARE (mARE) upstream of the luciferase gene (Fig. R10, and section 4.3. of the Materials and Methods).

Figure R10. Nucleotide sequence of the DNA fragments from the *Ucp3* promoter that were used for luciferase reporter assays after H_2O_2 treatment. Nucleotide sequences (71 bp) containing the ARE (shown in blue) or the mutated ARE (mARE) with the substituted nucleotides shown in red. These sequences were cloned into the pGL4.27 vector, and each of the resulting plasmids (pGL4.27-ARE and pGL4.27-mARE) were used to transfect HL-1 cells.

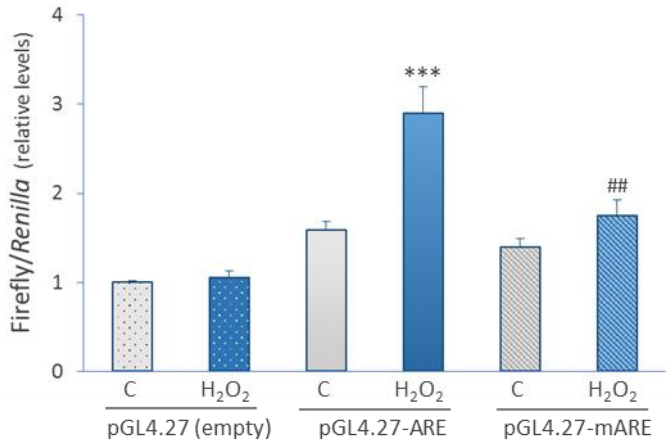

Figure R11. Luciferase reporter assay after H_2O_2-induced Nrf2 activation in HL-1 cells transfected with the plasmids pGL4.27-ARE or pGL4.27-mARE. Luciferase expression in HL-1 cells transfected with the pGL4.27 plasmid containing the ARE (pGL4.27-ARE) or the mARE (pGL4.27-mARE) and treated with 300 µM H_2O_2 for 6 h. Cells transfected with the empty pGL4.27 vector were used as a internal control. Histograms show the means ± SEM of normalized firefly/*Renilla* luciferase expression from 7 independent experiments. C, control untreated cells. ***$P < 0.001$ with respect to control pGL4.27-ARE, ##$P < 0.01$ with respect to H_2O_2 pGL4.27-ARE.

As shown in Fig. R11, H_2O_2 treatment (300 µM for 6 h) increased luciferase expression around two-fold in cells transfected with the ARE but not in those transfected with the mARE. This result indicates that Nrf2 increases *Ucp3* expression through its binding to the ARE region in the promoter of this gene.

1.2.3. Nrf2 silencing prevents H_2O_2-induced UCP3 upregulation

To further confirm that the increase in UCP3 expression under conditions of oxidative stress is mediated by Nrf2, we silenced Nrf2 expression using RNA interference (siNrf2) in HL-1 cells. Fig. R12A and B show that Nrf2 interference was effective, since *Nrf2* mRNA and Nrf2 protein levels, as well as the mRNA expression of the Nrf2 target gene *HO-1*, were clearly reduced in H_2O_2-treated siNrf2 cells compared to control scrambled cells (Scr).

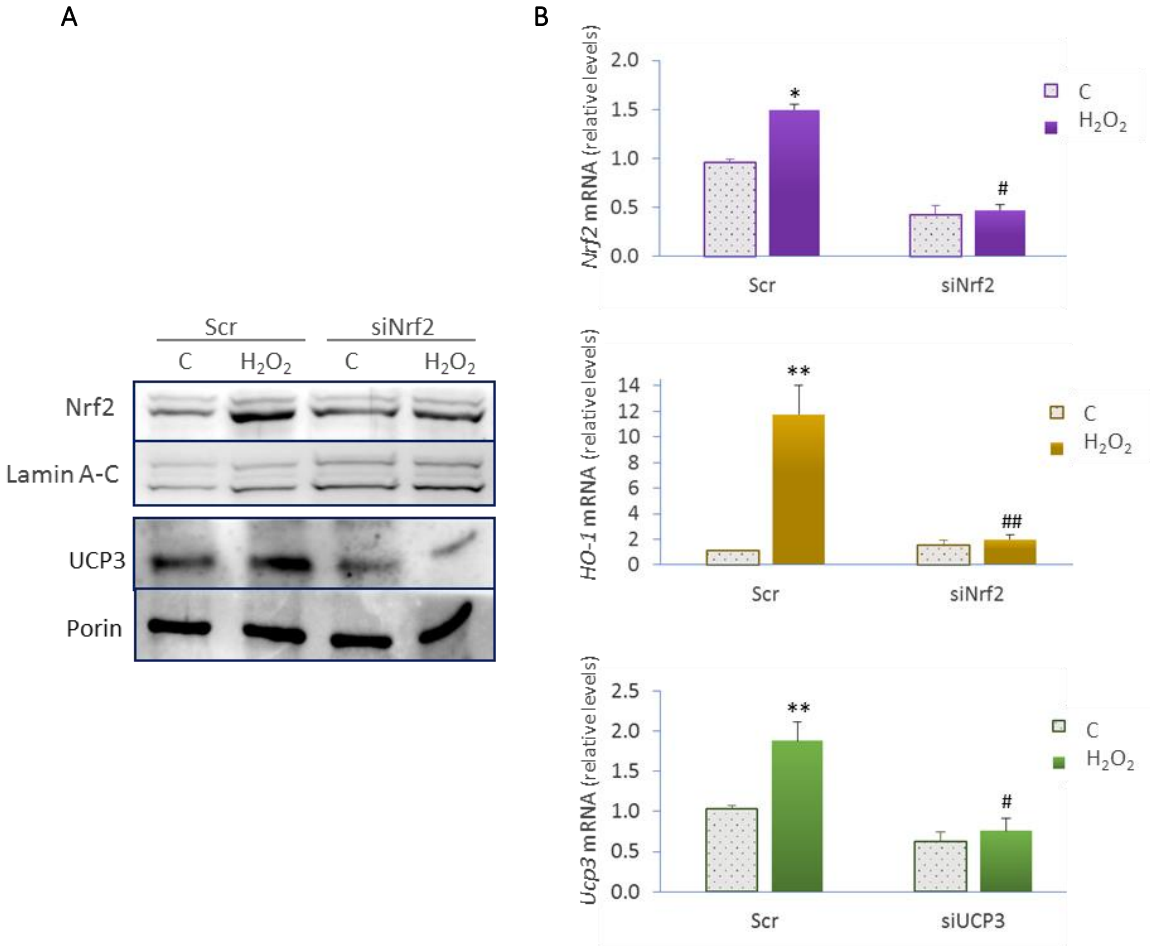

Figure R12. Effects of *Nrf2* RNA interference on Nrf2, UCP3 and HO-1 expression after H_2O_2. (A) Representative immunoblot of Nrf2 and UCP3 protein levels in nuclear and mitochondrial extracts, respectively, from scrambled control (Scr) and Nrf2-interfered (siNrf2) HL-1 cells exposed to 300 µM H_2O_2 for 6 h. Lamin A-C and porin were used as nuclear and mitochondrial protein loading controls, respectively. (B) *Nrf2*, *HO-1* and *Ucp3* mRNA levels in Scr and siNrf2 HL-1 cells exposed to 300 µM H_2O_2 for 6 h. *HPRT* and *β-actin* were used as housekeeping genes for internal normalization. Histograms show the means ± SEM from 4 independent experiments. C, control untreated cells. $^{*}P < 0.05$, $^{**}P < 0.01$, with respect to Scr C; $^{\#}P < 0.05$, $^{\#\#}P < 0.01$ with respect to Scr H_2O_2 group.

Importantly, the increase in *Ucp3* mRNA and UCP3 protein expression induced by H_2O_2 was not observed in siNrf2 cells (Fig. R12A and B). These results reinforce the conclusion from the above data, all of them indicating that the Nrf2 transcription factor is directly involved in H_2O_2-induced UCP3 upregulation.

1.3. Physiological consequences of UCP3 upregulation induced by H_2O_2

1.3.1. Upregulation of UCP3 via Nrf2 after H_2O_2 treatment increases cell survival

Our previous experiments in which we analysed cell viability showed that the oxidative damage induced by 300 µM H_2O_2 treatment causes cell death in HL-1 cells after a 24 h exposure but not at shorter times (section 1.1.1. of the Results). In order to evaluate the possible protective role of Nrf2 and UCP3 against oxidative damage, we first analysed the effect of *Nrf2* and *Ucp3* silencing on the survival of cells exposed to oxidative damage. For this, we examined H_2O_2-treated HL-1 cells by microscopy. As shown in Fig. R13, H_2O_2 exposure for 6 h did not produce any visible cell death in Scr control cells, in agreement with data in Fig. R3. However, both siNrf2 and siUCP3 cells exhibited increased cell death after 6 h exposure to H_2O_2, which was more evident in siNrf2 cells (Fig. R13).

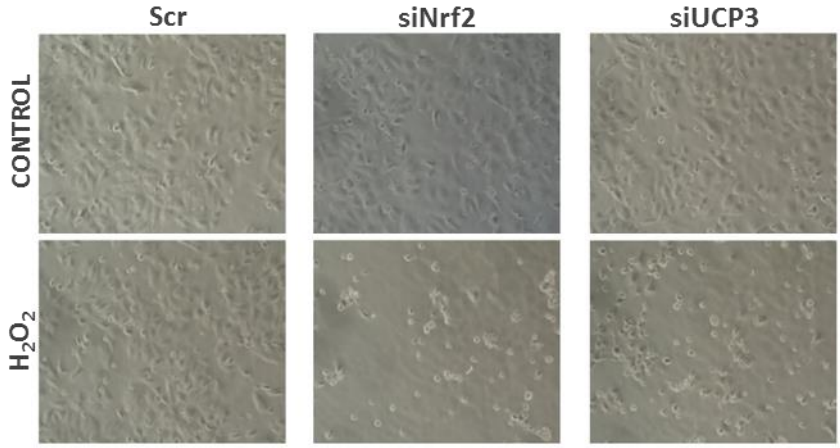

Figure R13. Cell viability in *Nrf2*- and *Ucp3*-silenced cells after H_2O_2. Representative images of Scr, siNrf2 and siUCP3 HL-1 cells treated with 300 µM H_2O_2 for 6 h and untreated cells (control). Note the enhanced cell death in *Nrf2*- and *UCP3*-silenced cells compared with Scr cells after H_2O_2 treatment.

These observations were confirmed by the determination of PI incorporation by flow cytometry in HL-1 cells, which was significantly higher in siNrf2 and siUCP3 cells after H_2O_2 treatment than in Scr cells (Fig. R14).

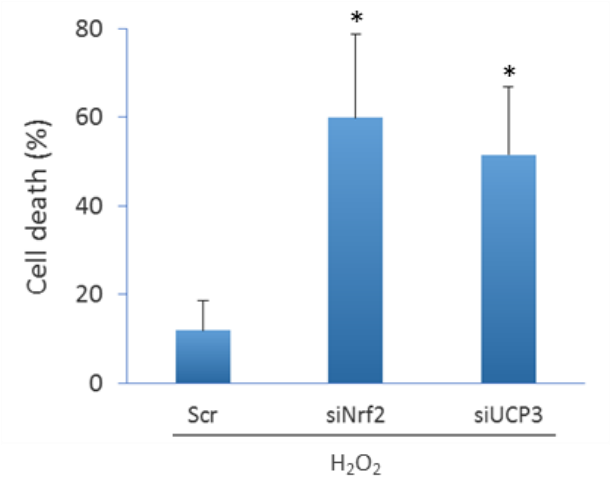

Figure R14. Cell death in *Nrf2*- and *Ucp3*-silenced cells after H_2O_2. Cell death as determined by flow cytometry analysis of PI incorporation in Scr, siNrf2 and siUCP3 HL-1 cells exposed to 300 µM H_2O_2 for 6 h. Histograms show the means ± SEM of the percentage cell death induced by H_2O_2 treatment for 5 independent experiments. *$P < 0.05$ with respect to the Scr group.

Moreover, comparable results were obtained by the estimation of apoptotic HL-1 cells by measuring cleaved caspase 3 expression levels, which clearly increased after a 6 h treatment with H_2O_2 in both siNrf2 and siUCP3 cells in comparison with control Scr cells (Fig. R15).

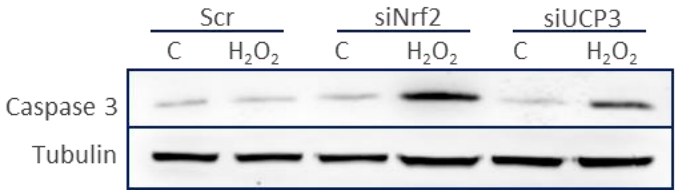

Figure R15. Apoptotic cell death in *Nrf2*- and *Ucp3*-silenced cells after H_2O_2. Representative immunoblot of caspase 3 protein in cytosolic extracts from HL-1 cells exposed to 300 µM H_2O_2 for 6 h. Tubulin was used as protein loading control. C, control untreated cells.

In addition, oxidative stress (as estimated by the DCF-DA fluorescence signal) was markedly higher in HL-1 cells subjected to *Nrf2* or *Ucp3* RNAi after H_2O_2 addition than in control cells (Fig. R16). Taken together, these findings indicate that both UCP3 and Nrf2 promote cell survival under conditions of oxidative stress.

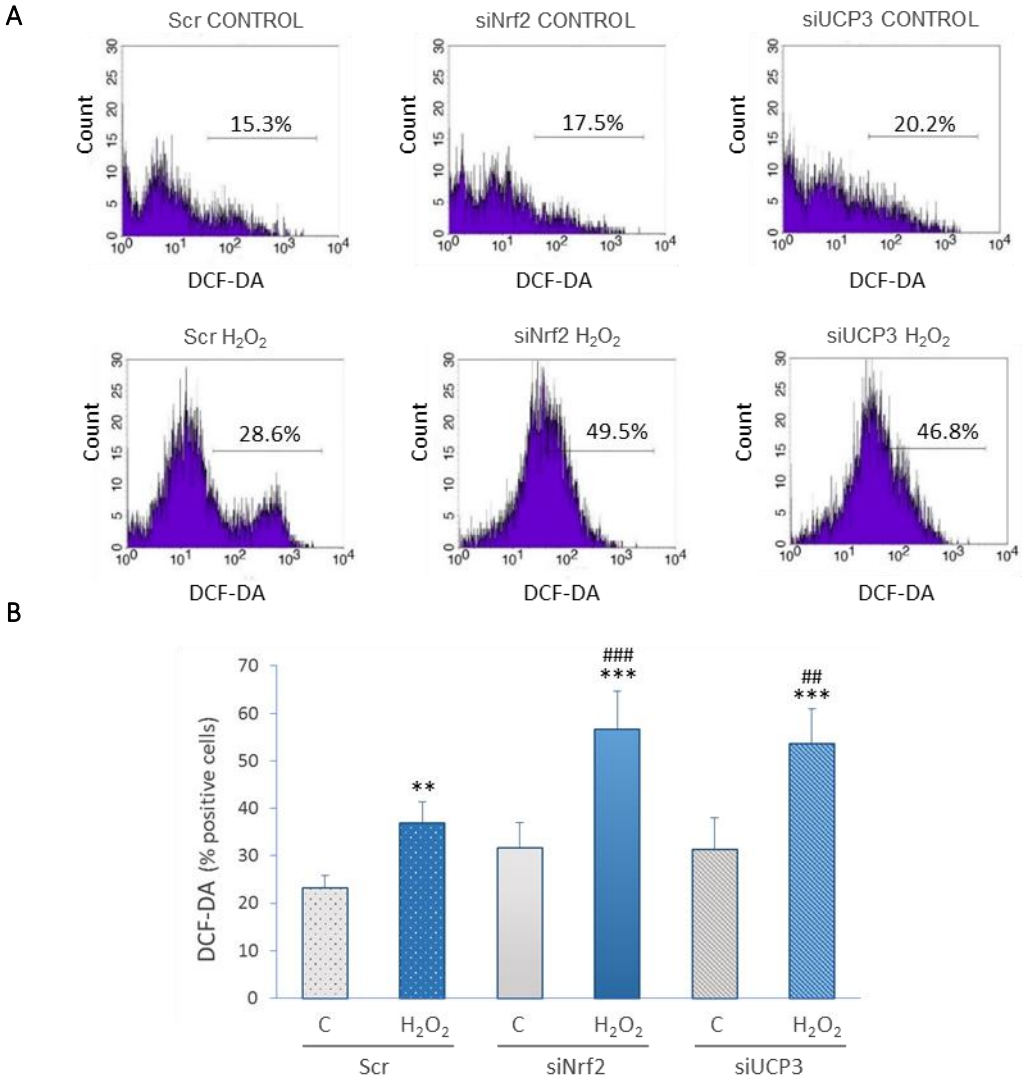

Figure R16. Oxidative stress in *Nrf2*- and *Ucp3*-silenced cells after H_2O_2. (A) Measurement of oxidative stress by flow cytometry as DCF-DA fluorescence in Scr, siNrf2 and siUCP3 HL-1 cells exposed to 300 µM H_2O_2 for 6 h or untreated cells (control). The percentages of positive cells are indicated. (B) Histograms represent the means ± SEM of the ROS levels relative to the basal conditions for 6 independent experiments. C, control untreated cells. $^{**}P < 0.01$, $^{***}P < 0.001$ with respect to Scr C, $^{\#\#}P < 0.01$, $^{\#\#\#}P < 0.001$ with respect to Scr H_2O_2 group.

1.3.2. Effects of H_2O_2-induced UCP3 upregulation on cellular bioenergetics

Next, to study the consequences of UCP3 induction under conditions of oxidative stress on cellular bioenergetics, we performed mitochondrial respiration experiments in HL-1 cells. To this end, we used a XF24 Extracellular Flux Analyser (Seahorse Bioscience). The effect of H_2O_2 treatment for 3 h on respiration in siUCP3 and control Scr cells was determined under several conditions (Fig. R17A): (i) under basal conditions, (ii) after adding oligomycin to inhibit ATP synthesis, (iii) after adding the uncoupler FCCP to determine the maximal respiratory capacity, and (iv) after adding rotenone plus antimycin A to inhibit complexes I and III, respectively, and to determine non-mitochondrial respiration.

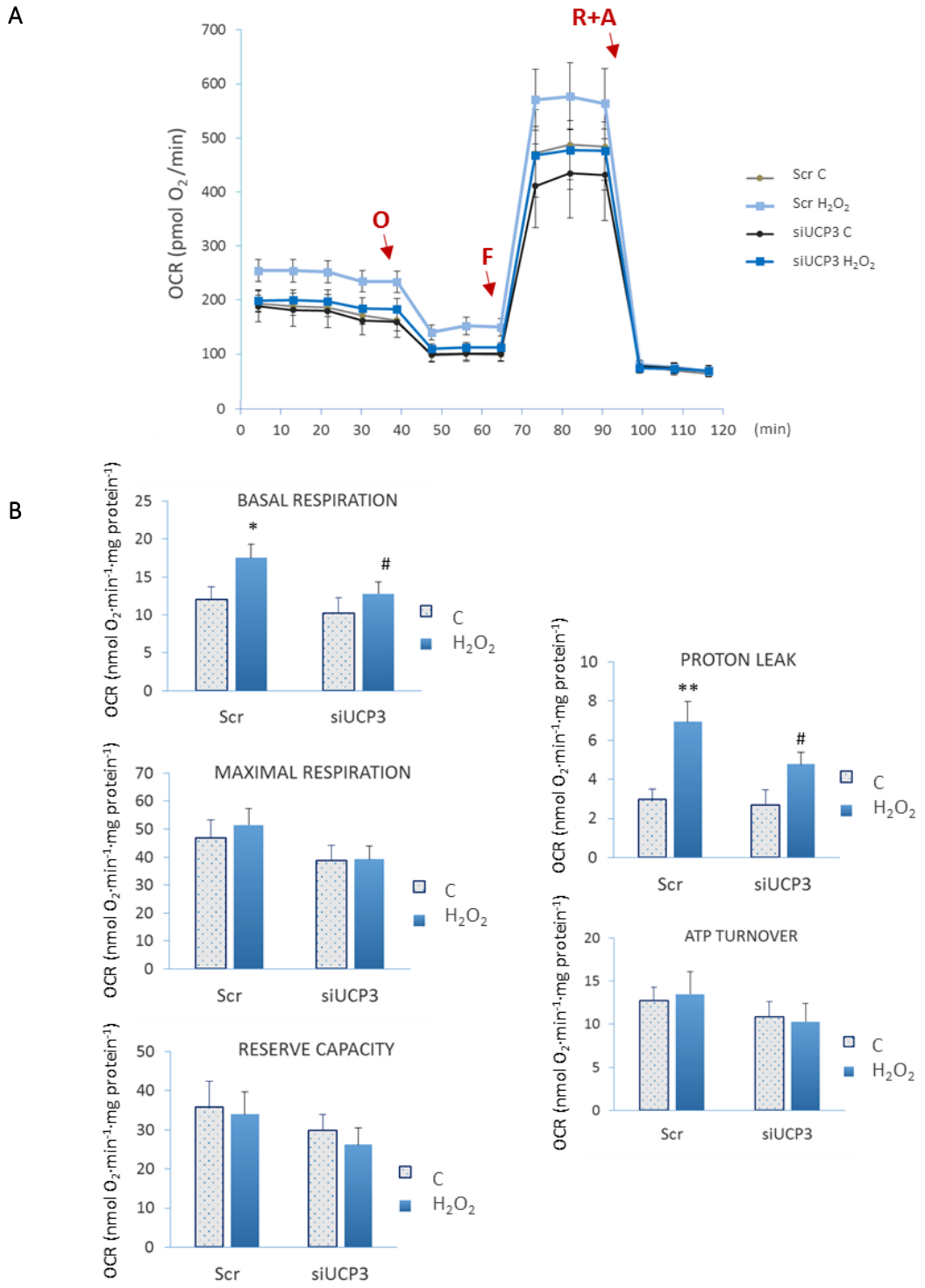

Figure R17. Effects of *Ucp3* interference (siUCP3) on the oxygen consumption rate of HL-1 cells exposed to H_2O_2. (A) The oxygen consumption rate (OCR) was measured in scrambled control (Scr) and *Ucp3*-interfered (siUCP3) HL-1 cells exposed to 300 µM H_2O_2 for 3 h. Sequential additions are indicated with arrows: 5 µg/ml oligomycin (O), 300 nM FCCP (F), 1 µM rotenone plus 1 µM antimycin A (R+A). (B) Quantification of OCR in Scr and siUCP3 HL-1 cells exposed to 300 µM H_2O_2 for 3 h under basal conditions (basal) and after the addition of oligomycin (5 µg/ml; proton leak) and FCCP (300 nM; maximal respiration). Basal minus oligomycin values provides a measure of the OCR due to ATP turnover. FCCP minus basal values represents the reserve capacity. Non-mitochondrial respiration (rotenone plus antimycin A) was subtracted for each condition. Histograms show the means ± SEM from 10 independent experiments. C, control untreated cells. $^{*}P < 0.05$, $^{**}P < 0.01$ with respect to Scr C, $^{\#}P < 0.05$ with respect to Scr H_2O_2 group.

Fig. R17B shows that the H_2O_2 treatment significantly increased basal respiration in cells transfected with Scr siRNA compared to non-treated cells, although no similar increase was observed in siUCP3 cells. The addition of oligomycin allowed *State 4* respiration to be assessed, an indicator of proton leak across the mitochondrial inner membrane. *State 4* respiration increased in Scr cells after H_2O_2 treatment but not in siUCP3 cells (Fig. R17B). Hence, the increase in proton leak and basal respiration observed after H_2O_2 treatment can be partially attributed to UCP3 activation. These results indicate that UCP3 increases the proton conductance across the mitochondrial inner membrane after H_2O_2 treatment in HL-1 cells. Moreover, maximal respiration (FCCP), reserve capacity (FCCP-basal) or ATP turnover (basal-oligomycin) were not significantly modified by H_2O_2 either in Scr or in siUCP3 cells (Fig. R17B).

The same protocol as in the previous experiment was applied to *Nrf2*-silenced cells (Fig. R18). The obtained results indicated that the effects of H_2O_2 on cellular bioenergetics observed in siUCP3 cells were reproduced after the interference of *Nrf2* mRNA. Thus, in control Scr cells, basal respiration and proton leak increased after H_2O_2 treatment, while there was no effect on maximal respiration, reserve capacity or ATP turnover. On the contrary, the H_2O_2 effects on maximal respiration and proton leak were abolished in siNrf2 cells (Fig. R18B). Taken together, these results suggest that H_2O_2-induced UCP3 upregulation increases mitochondrial proton leak and, in turn, basal respiration.

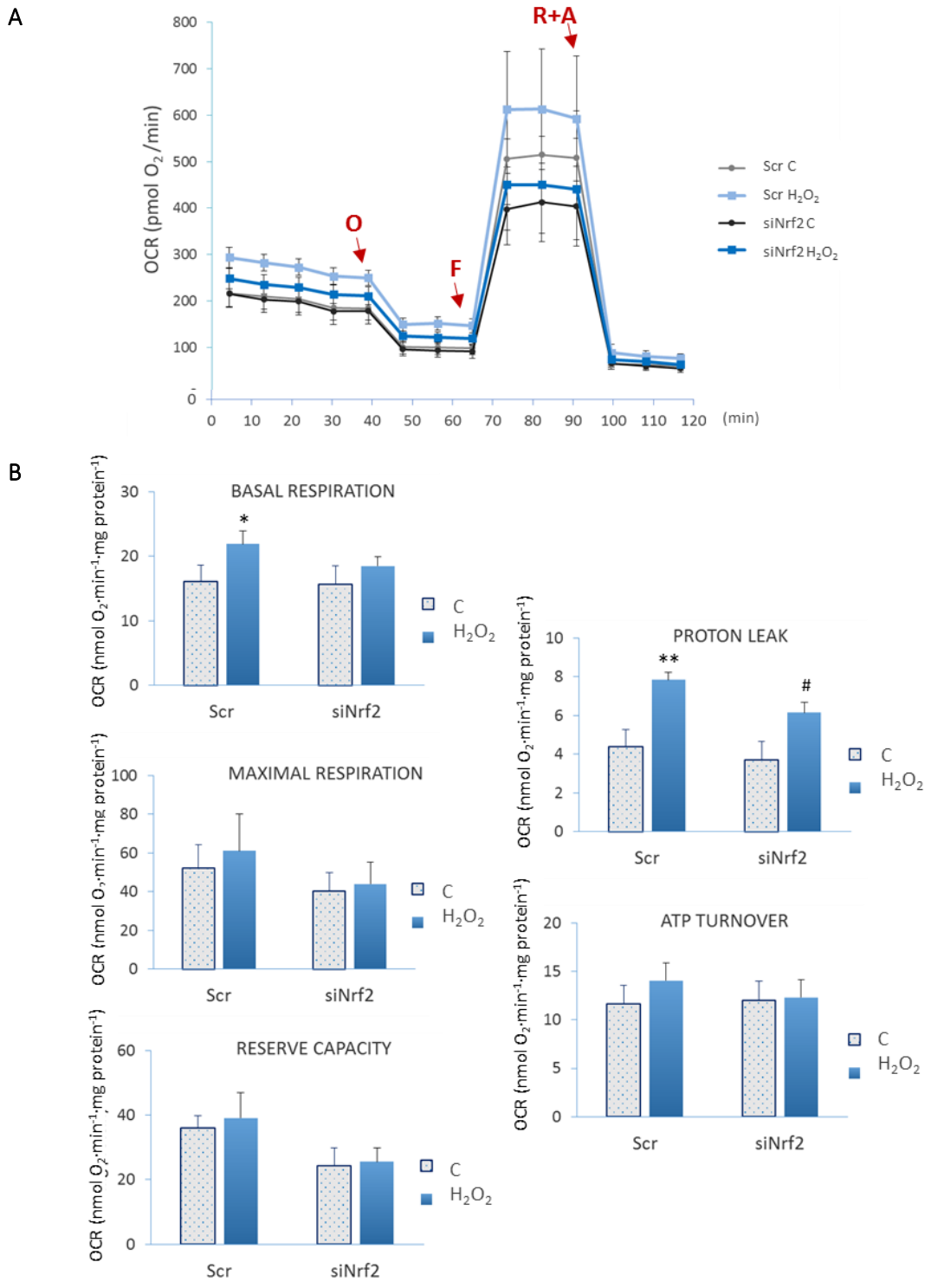

Figure R18. Effects of *Nrf2* interference (siNrf2) on the oxygen consumption rate of HL-1 cells exposed to H_2O_2. (A) The oxygen consumption rate (OCR) was measured in scrambled control (Scr) and *Nrf2*-interfered (siNrf2) HL-1 cells exposed to 300 µM H_2O_2 for 3 h. Sequential additions are indicated with arrows: 5 µg/ml, oligomycin (O), 300 nM FCCP (F), 1 µM rotenone plus 1 µM antimycin A (R+A). (B) Quantification of OCR in Scr and siNrf2 HL-1 cells exposed to 300 µM H_2O_2 for 3 h under basal conditions (basal) and after the addition of oligomycin (5 µg/ml; proton leak) and FCCP (300 nM; maximal respiration). Basal minus oligomycin values provides a measure of the OCR due to ATP turnover. FCCP minus basal values represents the reserve capacity. Non-mitochondrial respiration (rotenone plus antimycin A) was subtracted for each condition. Histograms show the means ± SEM from 10 independent experiments. C, control untreated cells. $^{*}P < 0.05$, $^{**}P < 0.01$ with respect to Scr C, $^{\#}P < 0.05$ with respect to Scr H_2O_2 group.

2. EFFECTS OF 4-HYDROXY-2-NONENAL (HNE) ON UCP3 EXPRESSION AND FUNCTION

2.1. Effects of HNE on UCP3 expression and Nrf2 nuclear accumulation

The lipid peroxidation product 4-hydroxy-2-nonenal (HNE) is involved in the regulation of mitochondrial uncoupling (Echtay et al. 2005, Echtay et al. 2003, Parker et al. 2008a). In addition, HNE has been reported to induce the nuclear translocation of Nrf2 and to enhance the expression of its target genes in cardiomyocytes (Zhang et al. 2010). Following our finding that H_2O_2 upregulates UCP3 via Nrf2, we aimed to investigate whether HNE was also able to induce Nrf2-mediated UCP3 expression.

2.1.1. HNE treatment does not induce cell death at low micromolar doses

First, to establish the appropriate HNE dose to use in subsequent experiments, we estimated cell death in HL-1 cells exposed to three HNE concentrations, by analysing the incorporation of PI by flow cytometry. As shown in Fig. R19, the treatment with 20 or 60 µM HNE for 16 h did not significantly increase cell death, although a slight decrease in cell viability was detected at 60 µM. In contrast, a significant increase in cell death was observed at 100 µM (Fig. R19). We therefore concluded that 20 µM was a non-toxic appropriate dose to study HNE effects on UCP3 expression and Nrf2 nuclear accumulation in HL-1 cells, in accordance with reported data obtained in cardiomyocytes (Zhang et al. 2010).

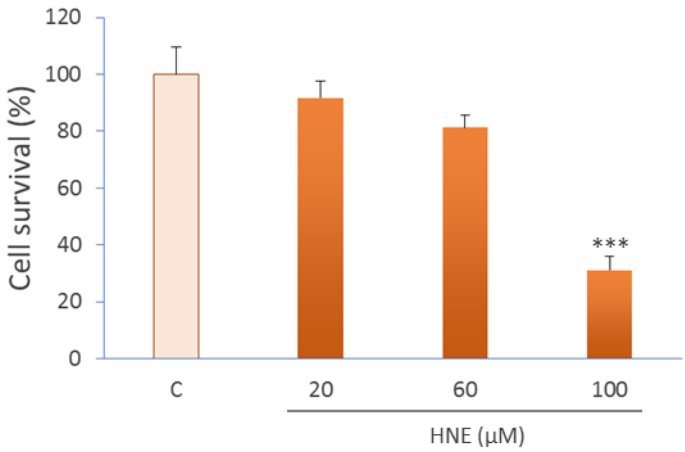

Figure R19. Dose-dependent cell death induced by HNE treatment. Flow cytometry analysis of PI incorporation by HL-1 cells treated with 20, 60, or 100 µM HNE for 16 h. Histograms show the mean ± SEM of cell survival from 4 independent experiments. C, control untreated cells. ***$P < 0.001$.

2.1.2. HNE treatment upregulates UCP3 expression

We then analysed the expression levels of UCP3 after cellular exposure to HNE. Fig. R20 shows that the treatment of HL-1 cells with 20 µM HNE for several hours significantly induced UCP3 expression. As seen in this figure, UCP3 protein levels were significantly increased from 5 h of HNE treatment.

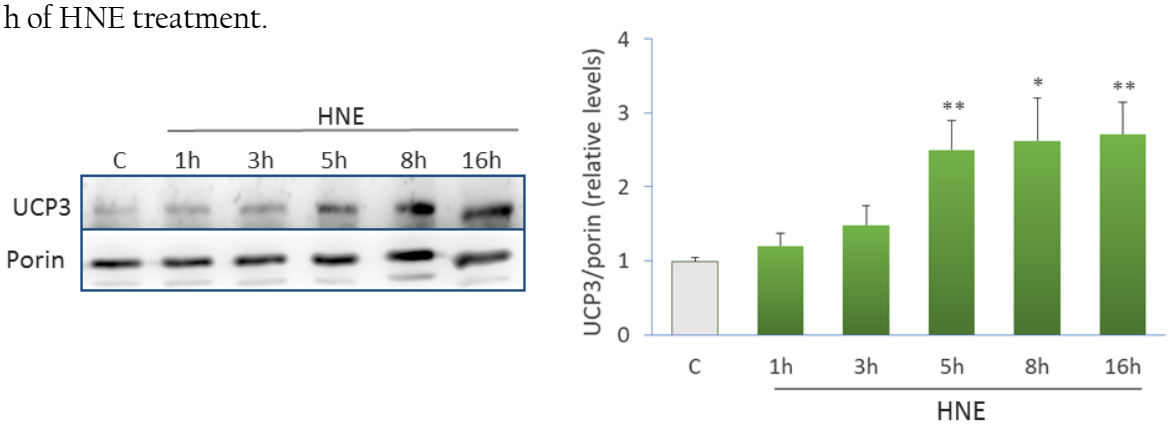

Figure R20. Effects of HNE on UCP3 expression levels. Representative immunoblot of UCP3 protein levels in mitochondrial extracts from HL-1 cells exposed to 20 µM HNE at different exposure times. Porin levels were used as mitochondrial protein loading control. Histograms show the mean ± SEM from 10 independent experiments. C, control untreated cells. *$P < 0.05$, **$P < 0.01$.

In addition, we analysed mRNA levels under the same conditions. Supporting the protein expression data, *Ucp3* mRNA levels were also significantly increased by 20 µM HNE treatment at 3 and 6 h, whereas *Ucp2* mRNA levels remained unaffected (Fig. R21).

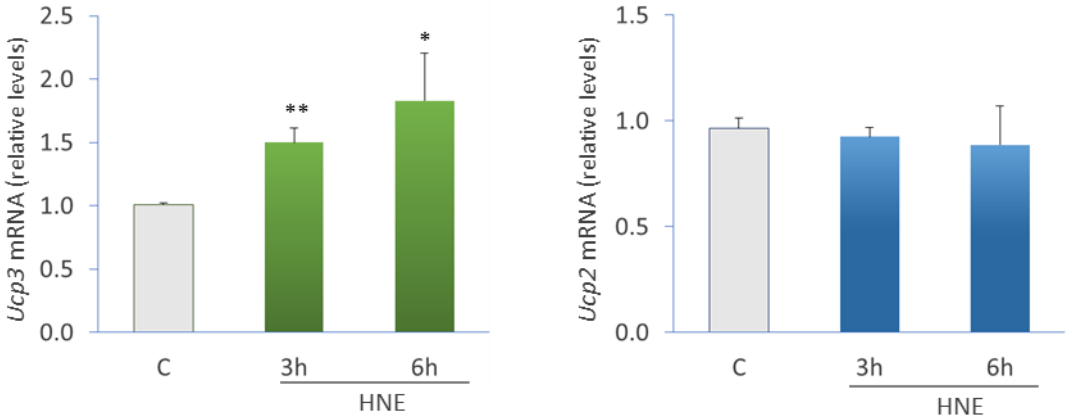

Figure R21. Effects of HNE on *Ucp2* and *Ucp3* mRNA levels. mRNA levels of *Ucp2* and *Ucp3*, in HL-1 cells exposed to 20 µM HNE for 3 or 6 h. *HPRT* and *β-actin* were used as housekeeping genes for internal normalization. Histograms show the mean ± SEM from 5 independent experiments. C, control untreated cells. *$P < 0.05$, **$P < 0.01$.

Next, we tested whether the increase in UCP3 expression was specifically due to the cellular stress conditions originated by the treatment with HNE. To answer this question, HL-1 cells were pre-treated with the antioxidant N-acetylcysteine (NAC; 5 mM) for 1 h before the addition of HNE. Our data indicated that NAC partially abolished the UCP3 increase observed in response to HNE (Fig. R22). NAC modulates the intracellular thiol levels and increases the intracellular levels of glutathione (GSH) (Burgunder et al. 1989), supporting its synthesis when the demand for GSH is increased, as it occurs during an oxidative stress challenge. We conclude that the effects of HNE on UCP3 expression were mediated by enhanced oxidative stress.

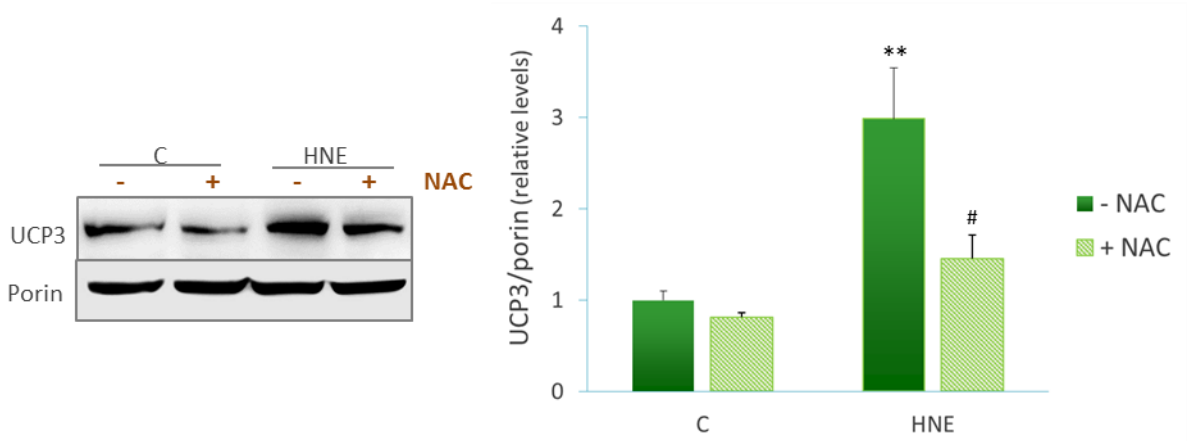

Figure R22. Effects of HNE on UCP3 expression levels. Representative immunoblot of UCP3 protein levels in mitochondrial extracts from HL-1 cells exposed to 20 μM HNE for 5 h with (+) or without (-) previous addition of 5 mM N-acetylcysteine (NAC) for 1 h. Porin was used as mitochondrial protein loading control. Histograms show the mean ± SEM from 5 independent experiments. C, control untreated cells. $^{**}P < 0.01$ with respect to C, $^{\#}P < 0.05$ with respect to HNE group.

2.1.3. HNE treatment induces nuclear accumulation of the transcription factor Nrf2

Since H_2O_2 was able to induce Nrf2 nuclear accumulation (section 1.1.3.), we tested whether Nrf2 also accumulated in the nucleus after HNE treatment in HL-1 cells, as previously reported for mouse cardiomyocytes (Zhang et al. 2010). Nrf2 accumulation was observed in the nuclear fraction of HL-1 cells after 20 μM HNE treatment from 3 h (Fig. R23), an effect that occurred in parallel with increased UCP3 expression (Fig. R20).

Moreover, there was also a significant increase in *Nrf2* mRNA in cells treated with HNE for 3 and 6 h, as well as in the mRNA of its target gene *HO-1* (Fig. R24).

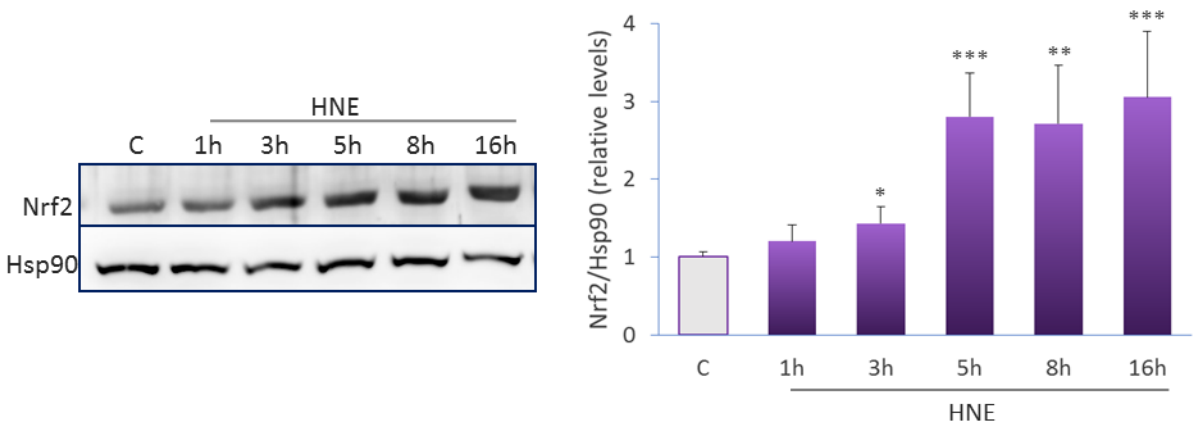

Figure R23. Effects of HNE on Nrf2 expression levels. Representative immunoblots of Nrf2 protein levels in nuclear extracts from HL-1 cells exposed to 20 µM HNE at different exposure times. Hsp90 levels were used as protein loading control. Histograms show the mean ± SEM from 10 independent experiments. C, control untreated cells. *$P < 0.05$, **$P < 0.01$, ***$P < 0.001$.

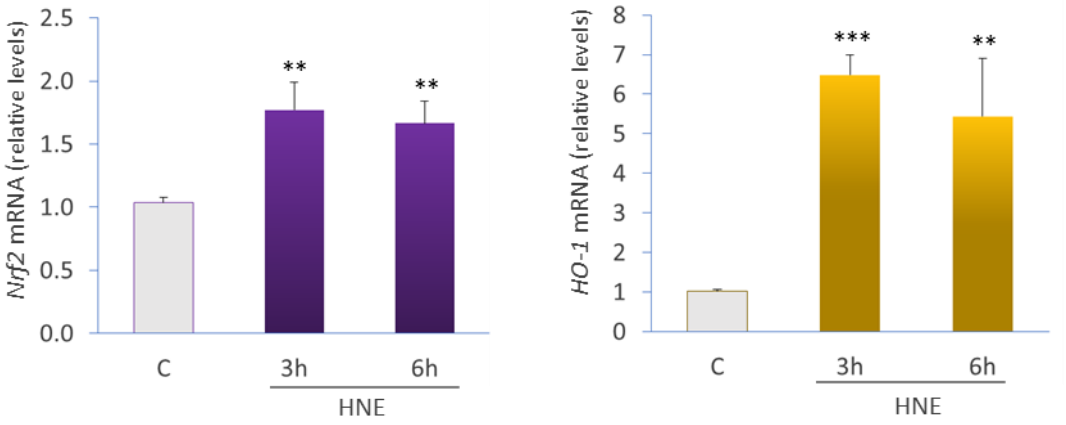

Figure R24. Effects of HNE on *Nrf2* and *HO-1* mRNA levels. mRNA levels of *Nrf2* and *HO-1* in HL-1 cells exposed to 20 µM HNE for 3 or 6 h. *HPRT* and *β-actin* were used as housekeeping genes for internal normalization. Histograms show the mean ± SEM from 5 independent experiments. C, control untreated cells. **$P < 0.01$, ***$P < 0.001$.

In addition, we showed that HNE-induced nuclear accumulation of Nrf2 was prevented by a pre-treatment with NAC (Fig. R25). Therefore, these results indicate that Nrf2 accumulates in the nucleus of HL-1 cells as a consequence of the cellular stress conditions generated by HNE treatment.

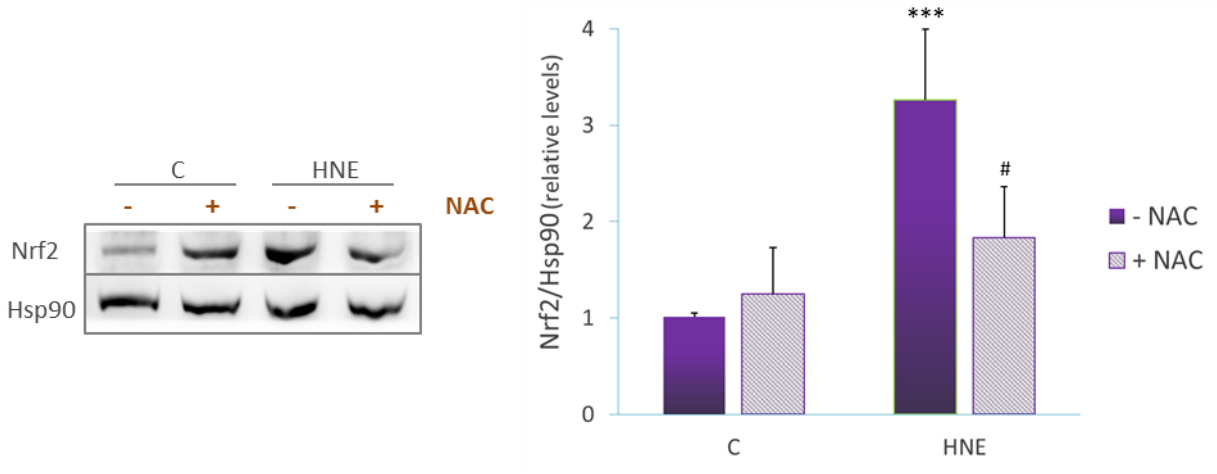

Figure R25. Effects of HNE on Nrf2 expression levels. Representative immunoblot of Nrf2 protein levels in nuclear extracts from HL-1 cells exposed to 20 µM HNE for 5 h with (+) or without (-) previous addition of 5 mM N-acetylcysteine (NAC) for 1 h. Hsp90 levels were used as protein loading control. Histograms show the mean ± SEM from 5 independent experiments. C, control untreated cells. ***$P < 0.001$ with respect to C, $^{\#}P < 0.05$ with respect to HNE group.

2.2. Involvement of Nrf2 in HNE-induced UCP3 upregulation

2.2.1. Nrf2 binds to the *Ucp3* promoter after HNE treatment

Given that the treatment with HNE induces both UCP3 upregulation and Nrf2 nuclear accumulation in HL-1 cells, we wondered whether Nrf2 could induce UCP3 expression in response to HNE, similar to what we found when the cells were exposed to H_2O_2 (section 1.2.). To study the possible binding of Nrf2 to the ARE conserved region of the *Ucp3* promoter (Fig. R8), we performed ChIP analysis following the treatment of HL-1 cells with 5, 10 or 20 µM HNE for 3 or 6 h. As shown in Fig. R26, the results indicated that Nrf2 binds to the ARE region of the *Ucp3* promoter in HL-1 cells after 3 h exposure to 5, 10 or 20 µM HNE.

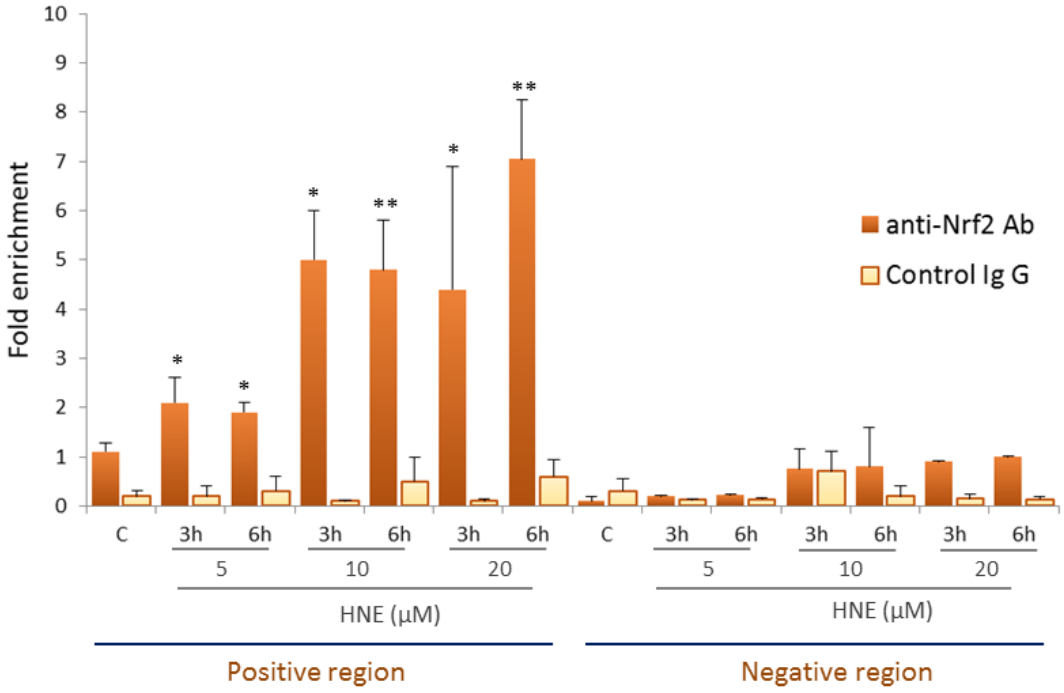

Figure R26. ChIP assay of Nrf2 binding to the *Ucp3* promoter after HNE treatment. ChIP assay of Nrf2 binding to the mouse *Ucp3* promoter in HL-1 cells exposed to 5, 10 and 20 μM HNE for 3 or 6 h. RT-PCR quantification and enrichment of positive and negative regions after immunoprecipitation with Nrf2 or control IgG antibodies are shown. Histograms show the means ± SEM from 3 independent experiments. C, control untreated cells. *$P < 0.05$, **$P < 0.01$.

2.2.2. HNE-induced UCP3 upregulation is mediated by Nrf2

Once we showed that Nrf2 binds to the *Ucp3* promoter at its conserved ARE region after HNE treatment, it was necessary to examine whether this binding promotes the transcription of the gene. To achieve this, we carried out luciferase reporter assays that were conducted in HL-1 cells. These cells were transfected with a plasmid (pGL4.27) containing a 71 bp that included either the ARE or a mutated ARE (mARE) upstream of the luciferase gene (Fig. R10 and section 4.3. of the Materials and Methods,).

HNE treatment (20 μM for 5 h) induced Nrf2 nuclear accumulation, which significantly increased luciferase expression in cells transfected with the ARE but not in those transfected with the mARE (Fig. R27A).

We also performed luciferase reporter experiments in HL-1 cells using another plasmid that contained a much longer fragment of the Ucp3 promoter, also including either the wild-type ARE region (pGL4.27-Prom) or a mutated ARE version (pGL4.27-mProm). This DNA fragment containing the promoter region of Ucp3 was 2205 bp (from -2145 to +60 positions relative to the transcription start site). The data in Fig. R27B show that there was an increased

luciferase expression in cells transfected with the promoter region containing the original ARE, but not in those transfected with the promoter region containing the mutated ARE. Therefore, we conclude that the ARE region is essential for the upregulated transcription of the *Ucp3* gene after HNE treatment.

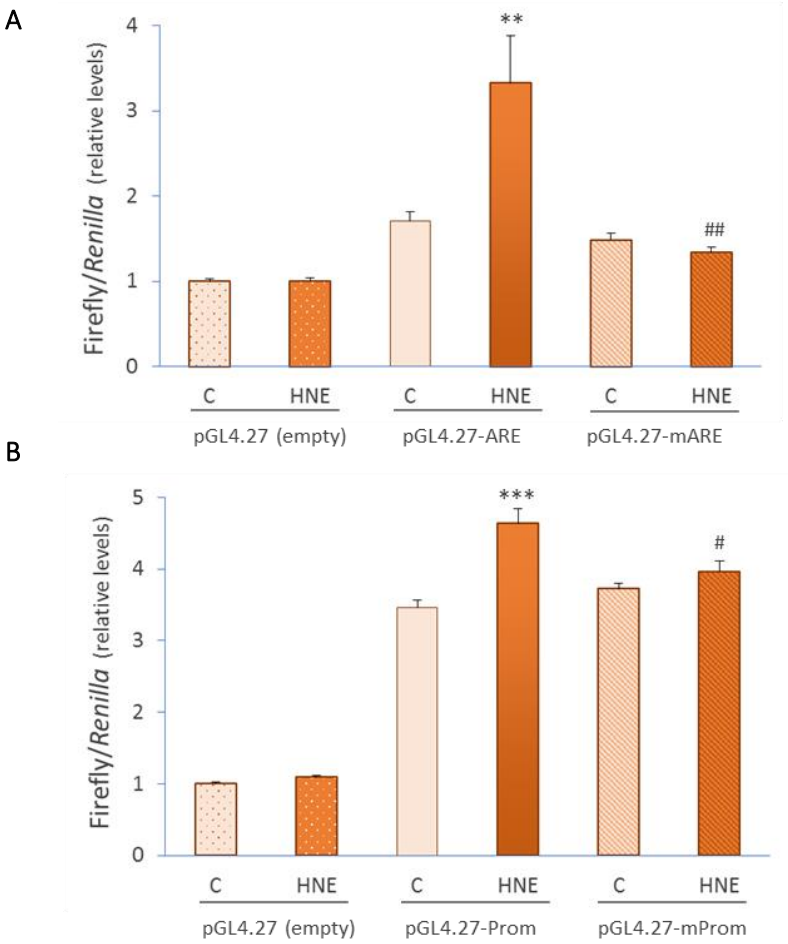

Figure R27. Luciferase reporter assay after HNE-induced Nrf2 activation in HL-1 cells transfected with the ARE-containing *Ucp3* promoter region. Luciferase expression in HL-1 cells transfected with the pGL4.27 plasmid including (A) the 71 bp ARE-containing *Ucp3* promoter region (pGL4.27-ARE) or the mutated ARE (pGL4.27-mARE) and (B) the 2205 bp ARE-containing *Ucp3* promoter region that included the ARE (pGL4.27-Prom) or the mutated ARE (pGL4.27-mProm) and treated with 20 µM HNE for 6 h. Cells transfected with the empty pGL4.27 vector were used as internal control. Histograms show the means ± SEM of normalized firefly/*Renilla* luciferase expression (n = 12 for the 71 bp region, and n = 7 for the 2205 bp region). C, control untreated cells. $^{**}P < 0.01$ with respect to control pGL4.27-ARE, $^{\#\#}P < 0.01$ with respect to HNE pGL4.27-ARE. $^{***}P < 0.001$ with respect to control pGL4.27-Prom, $^{\#}P < 0.05$ with respect to HNE pGL4.27-Prom.

2.2.3. Nrf2 silencing prevents HNE-induced UCP3 upregulation

To confirm that the increase in UCP3 expression after HNE treatment is mediated by Nrf2, we silenced *Nrf2* mRNA using RNA interference (siNrf2) in HL-1 cells and analysed the levels of UCP3 and *Ucp3* mRNA (Fig. R28). As seen in this figure, after silencing *Nrf2*, both the expression of Nrf2 (Fig. R28A) and *Nrf2* mRNA (Fig. R28B), as well as the mRNA of its target

gene *HO-1* (Fig. R28B), were clearly reduced when treated with HNE, in comparison with treated cells previously transfected with Scr RNAi (Fig. R28A and B). Therefore, the silencing of *Nrf2* was efficient. With respect to UCP3, our results show that this protein is not induced in response to HNE treatment when *Nrf2* is silenced (Fig. R28A).

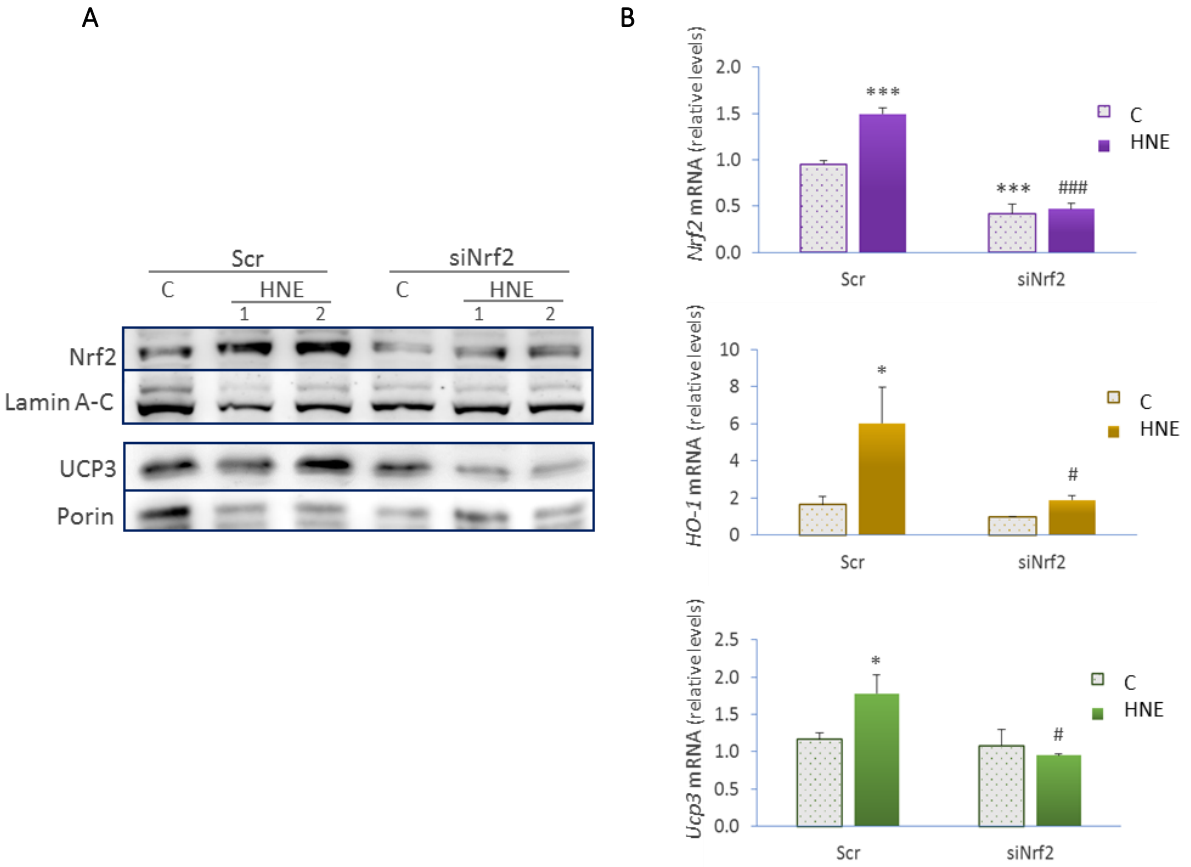

Figure R28. Effects of *Nrf2* RNA interference on UCP3, Nrf2 and HO-1 expression after HNE treatment. (A) Representative immunoblots of Nrf2 and UCP3 protein levels in nuclear and mitochondrial extracts, respectively, from scrambled control (Scr) and *Nrf2*-interfered (siNrf2) HL-1 cells exposed to 20 μM HNE for 6 h. Lamin A-C and porin were used as nuclear and mitochondrial protein loading controls, respectively. Numbers indicate different HNE-treated samples. (B) *Nrf2*, *HO-1* and *Ucp3* mRNA levels in Scr and siNrf2 HL-1 cells exposed to 20 μM HNE for 6 h. *HPRT* and *β-actin* were used as housekeeping genes for internal normalization. Histograms show the means ± SEM from 6 independent experiments. C, control untreated cells. $^{*}P < 0.05$, $^{***}P < 0.001$ with respect to Scr C; $^{\#}P < 0.05$, $^{\#\#\#}P < 0.001$ with respect to Scr HNE group.

Furthermore, the expression of the *Ucp3* gene is not enhanced in siNrf2 cells treated with HNE, as indicated by the absence of increased levels of *Ucp3* mRNA when compared with control Scr cells (Fig. R28B). These results are consistent with the data shown above and indicate that Nrf2 is involved in HNE-induced UCP3 upregulation.

2.3. Physiological consequences of UCP3 upregulation induced by HNE

2.3.1. Upregulation of UCP3 via Nrf2 after HNE treatment increases cell survival

We next examined whether the Nrf2-dependent regulation of UCP3 was important for cell viability under conditions of HNE exposure. As shown in Fig. 19, the treatment with 100 µM HNE for 16 h causes cell death in HL-1 cells, but not the exposure to 20 µM HNE. In agreement with this data, Scr HL-1 cells treated with 20 µM HNE for 5 or 16 h did not show any indications of cell death when examined by microscopy (Fig. R29A and B, left panels).

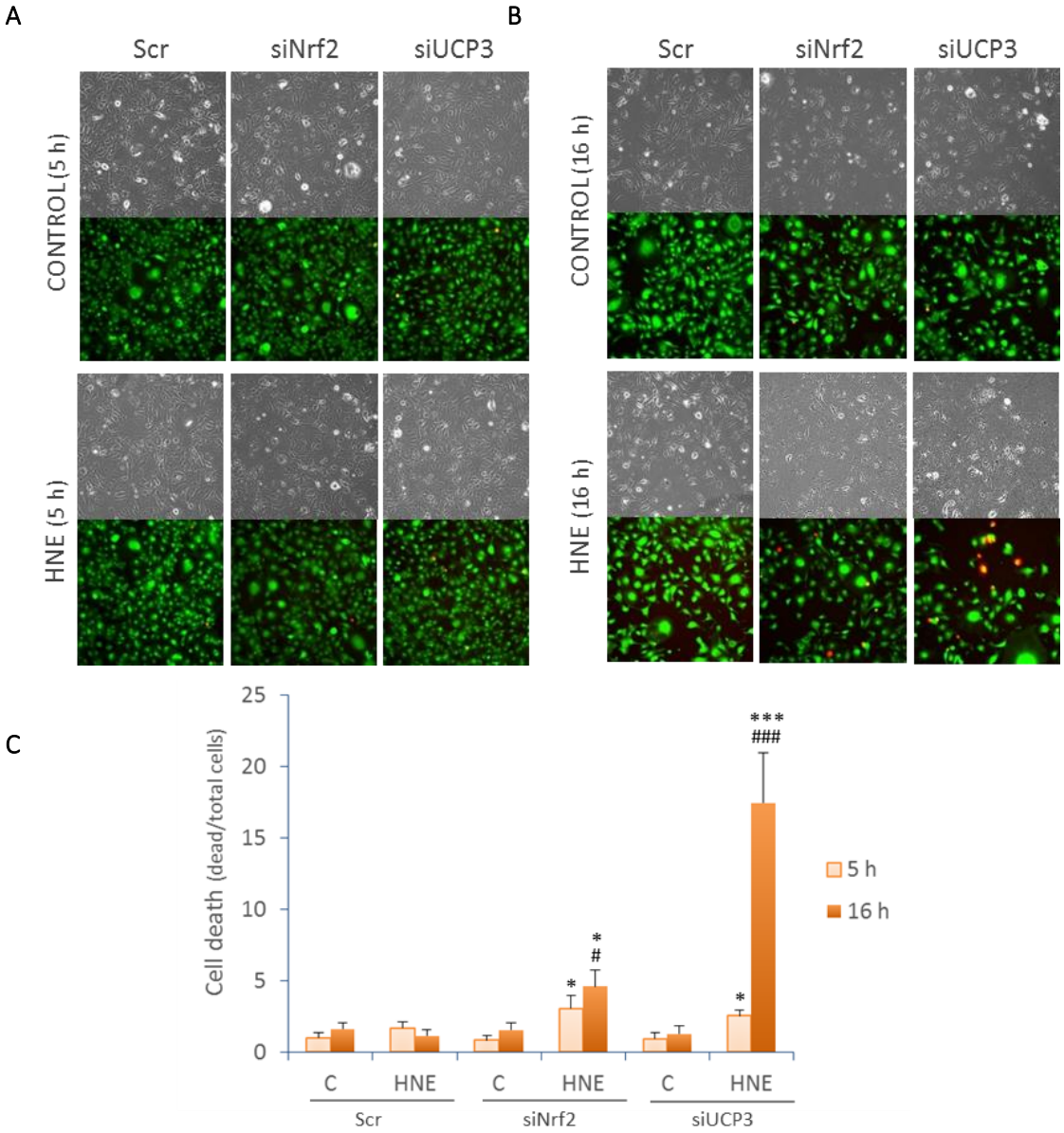

Figure R29. Cell viability in *Nrf2*- and *Ucp3*-silenced cells after HNE treatment. (A, B) Representative images of Scr, siNrf2 and siUCP3 HL-1 cells treated with 20 µM HNE for (A) 5 h and (B) 16 h, or untreated cells (control). Cell death was detected as PI incorporation (red nuclei), and viable cells as calcein incorporation (green cytoplasms). Double positive (PI^+Calc^+) were counted as dead cells. Note the enhanced cell death in *Nrf2*- and *UCP3*- silenced cells compared with Scr cells after 16 h HNE treatment. (C) Histograms show the means ± SEM from 3 independent experiments. $^*P < 0.05$ relative to each correspondent control. C, control untreated cells. $^{\#}P < 0.05$, $^{\#\#\#}P < 0.001$ relative to Scr HNE.

On the contrary, we observed that both siNrf2 and siUCP3 cells exhibited signs of cell death after exposure to the same dose of HNE at 5 h (Fig. R29A) and even clearer signs at 16 h (Fig. R29B).

These observations were confirmed by microscopy examination of PI incorporation, which allows the detection of dead cells (red nuclei), and calcein incorporation, which allows the detection of viable cells (green cytoplasm). The ratio dead/total cells was significantly higher in siNrf2 and siUCP3 cells after 20 μM HNE treatment than in control cells (Fig. R29C), and the effects on cell death were more evident after 16 h. These results indicate that both UCP3 and Nrf2 promote cell survival upon the challenge of HNE treatment.

2.3.2. Effects of HNE-induced UCP3 upregulation on cellular bioenergetics

Previous reports have shown that HNE activates UCP3-mediated proton conductante (Aguirre and Cadenas 2010, Echtay et al. 2005, Echtay et al. 2003, Parker et al. 2008a). To study the consequences of HNE-induced UCP3 upregulation on cellular bioenergetics, we performed mitochondrial respiration experiments in HL-1 cells, using the XF24 Extracellular Flux Analyser (Seahorse Bioscience). HL-1 cells were silenced for *Ucp3* by RNA interference (siUCP3), and the effect of HNE treatment on the oxygen consumption rate (OCR) in siUCP3 and control Scr cells was determined as described in section 1.3.2. Thus, we initially measured OCR under basal conditions, subsequently after adding oligomycin, then after adding the uncoupler FCCP, and finally, after adding rotenone plus antimycin A (Fig. R30A).

Our results indicated that HNE significantly increased basal respiration in cells transfected with both Scr RNAi and siUCP3. *State 4* respiration was assessed by adding oligomycin to the cells, in order to show the leakage of protons across the IMM. Fig. R30B shows that there was a four-fold increase in proton leak in Scr cells after HNE treatment, but this increase was less than two-fold in siUCP3 cells. Notably, maximal respiration (FCCP) was significantly reduced after HNE treatment, both in siUCP3 and in Scr control cells (Fig. R30B). As a result, the reserve capacity (FCCP-basal) was therefore inexistent in HNE-treated cells. Likewise, ATP turnover (basal-oligomycin) was increased after HNE treatment either in Scr or in siUCP3 cells (Fig. R30B).

Taken together, these results suggest that the much higher basal respiration observed in cells after HNE treatment might be due to both increased proton leak and ATP turnover. The increased proton leak could be partially attributed to UCP3 activation, confirming previous reports showing that UCP3 increases the proton conductance across the mitochondrial inner

membrane when activated by HNE (Aguirre and Cadenas 2010, Echtay et al. 2005, Echtay et al. 2003, Parker et al. 2008a).

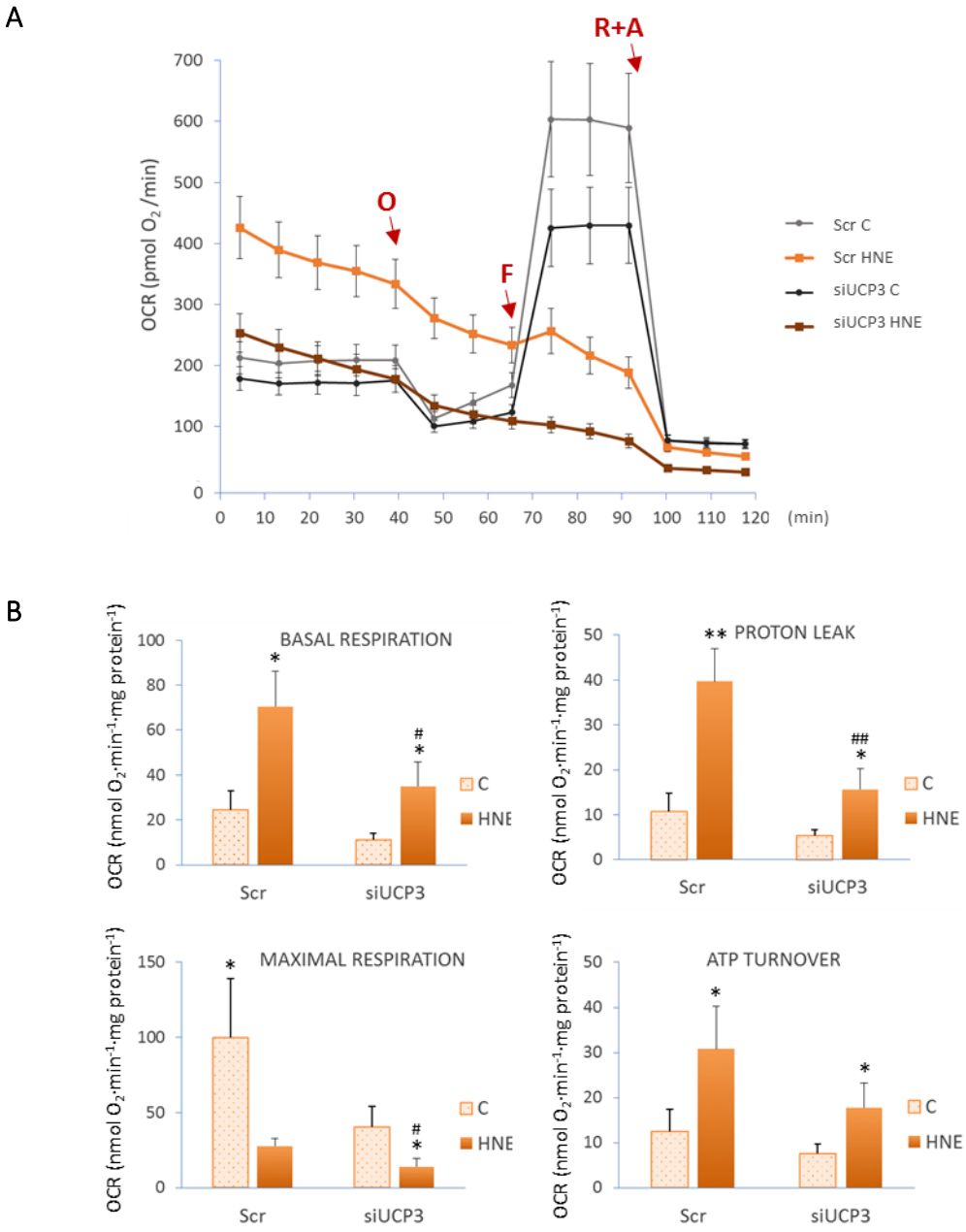

Figure R30. Effects of *Ucp3* interference (siUCP3) on the oxygen consumption rate of HL-1 cells exposed to HNE. (A) The oxygen consumption rate (OCR) was measured in scrambled control (Scr) and *Ucp3*-interfered (siUCP3) HL-1 cells exposed to 20 µM HNE for 5 h. Sequential additions are indicated with arrows: 5 µg/ml oligomycin (O), 300 nM FCCP (F), 1 µM rotenone plus 1 µM antimycin A (R+A). (B) Quantification of OCR in Scr and siUCP3 HL-1 cells exposed to 20 µM HNE for 5 h under basal conditions (basal) and after the addition of oligomycin (5 µg/ml; proton leak) and FCCP (300 nM; maximal respiration). Basal minus oligomycin values provides a measure of the OCR due to ATP turnover. FCCP minus basal values represent the reserve capacity. Non-mitochondrial respiration (rotenone plus antimycin A) was subtracted for each condition. Histograms show the means ± SEM from 5 independent experiments. C, control untreated cells. $^{*}P < 0.05$, $^{**}P < 0.01$, $^{***}P < 0.001$ with respect to Scr C; $^{\#}P < 0.05$, $^{\#\#}P < 0.01$ with respect to Scr HNE group.

PART II. ANALYSIS OF THE CARDIOPROTECTIVE ROLE OF UCP3 AGAINST ISCHEMIA-REPERFUSION INJURY: INVOLVEMENT OF THE TRANSCRIPTION FACTOR NRF2

1. STUDY OF NRF2-MEDIATED UCP3 INDUCTION AND ITS CARDIOPROTECTIVE ROLE IN THE ISOLATED MOUSE HEART AFTER ISCHEMIA-REPERFUSION

1.1. Ischemia-reperfusion (IR) increases UCP3 expression and Nrf2 nuclear accumulation in the isolated mouse heart

To investigate whether the Nrf2-mediated UCP3 induction that we described in cells subjected to H_2O_2 or HNE treatment could have pathophysiological relevance, we studied isolated mouse hearts subjected to ischemia-reperfusion (IR), a condition known to increase ROS production and oxidative damage (Zweier and Talukder 2006). For this, we started by analysing UCP3 expression and Nrf2 nuclear accumulation in this multicellular system (Fig. R31).

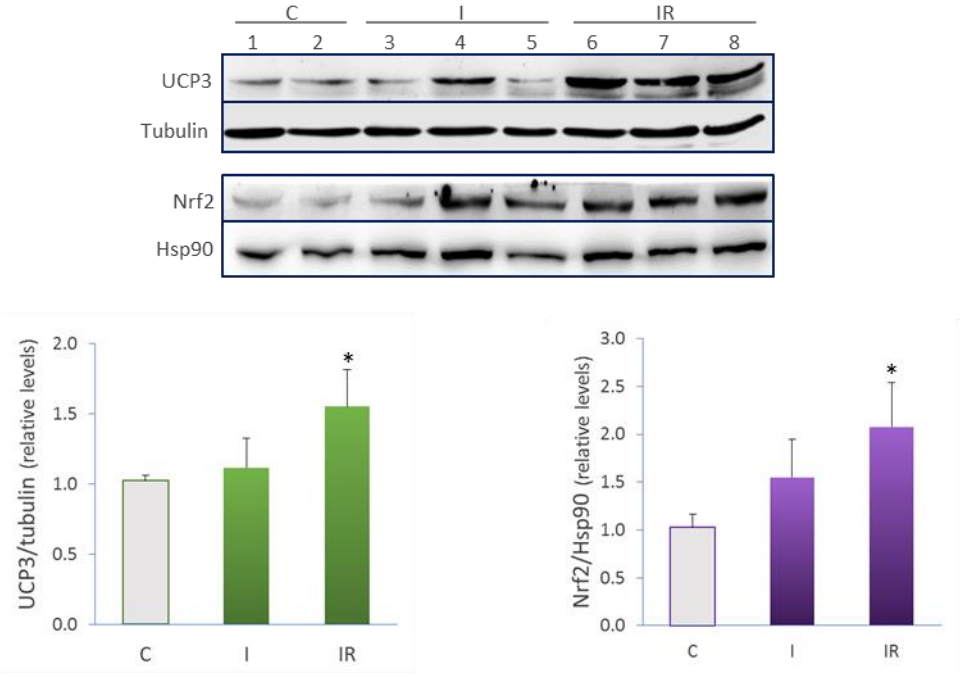

Figure R31. UCP3 and Nrf2 expression levels in mouse heart after ischemia (I) and ischemia-reperfusion (IR). Representative immunoblot of UCP3 in total extracts and Nrf2 in nuclear extracts from control (C) hearts, and hearts subjected to ischemia (I) or ischemia-reperfusion (IR). Numbers 1-8 indicate different mice. Tubulin and Hsp90 were used as protein loading controls in total and nuclear fractions, respectively. Histograms show the means ± SEM relative to control from 4 hearts per group. *$P < 0.05$.

Hearts were perfused *ex vivo* using the Langendorff perfusion system to apply protocols of ischemia (I) and IR (Fig. M6 and section 8.2. of the Materials and Methods). They were allowed to stabilize for 20 min before the flow was completely stopped to generate global normothermic ischemia for 40 min. The flow was then restored, and the hearts were reperfused for 60 min. In agreement with the results we obtained in cells, Nrf2 and UCP3 expression levels increased significantly after IR in the nuclear and total tissue extracts, respectively (Fig. R31), suggesting that Nrf2-mediated UCP3 upregulation might also take place during cardiac IR.

1.2. Infarct size after IR increases in hearts from UCP3-KO compared to WT mice: cardioprotective role of UCP3 against IR injury

Since UCP3 has been reported to decrease ROS production and oxidative damage (Brand and Esteves 2005, Mailloux and Harper 2011, Toime and Brand 2010), and given that this protein is upregulated via Nrf2 in response to oxidative stress (sections 1.2. and 2.2. of the Results, *Part I*) to promote cell survival (sections 1.3.1. and 2.3.1. of the Results, *Part I*), we hypothesized that UCP3 could play a protective role against IR damage in the heart.

To test this hypothesis, we investigated whether hearts lacking UCP3 have increased tissue damage after an ischemic insult compared to wild-type hearts. For this, hearts from UCP3-knockout (UCP3-KO) and wild-type (WT) mice were subjected to IR using the Langendorff system (Fig. R32).

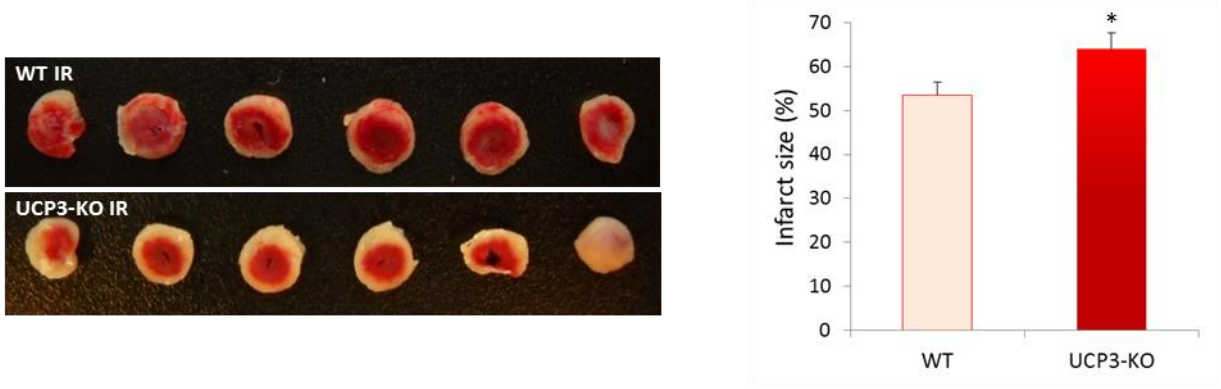

Figure R32. Infarct size in hearts from WT and UCP3-KO mice subjected to IR. Representative images of heart slices from WT and UCP3-KO mice subjected to IR and stained with tetrazolium chloride (TTC), which results in white necrotic tissue and red viable tissue. Histograms show the means ± SEM of the percentage of infarct as necrotic area related to risk area (total) (n = 7-8 hearts per group). *$P < 0.05$.

After 20 min stabilization, the flow was completely stopped to generate global normothermic ischemia for 40 min, and then restored for 60 min. At the end of the IR protocol, the hearts were stained with tetrazolium chloride (TTC), and the infarct size was analysed to determine tissue damage (necrosis) (section 8.4. of the Materials and Methods). The analysis

of the percentage of the necrotic area (white) in relation to the risk area (total), showed a significantly larger infarction after IR in hearts from UCP3-KO (64.1%) mice compared to WT (53.5%) (Fig. R32), suggesting that UCP3 plays a cardioprotective role against IR injury.

1.3. Creatine kinase release after IR is higher in hearts from UCP3-KO mice than in those from WT mice

Creatine kinase (CK) levels are elevated when myocardial cellular damage occurs (Blanke et al. 1984, Ellis 1991). Hence, CK activity is normally used in the diagnosis of myocardial infarction as a biomarker to assess damage. To determine IR injury in the hearts from UCP3-KO and WT mice, we measured CK activity levels in the coronary effluent during the perfusion experiments.

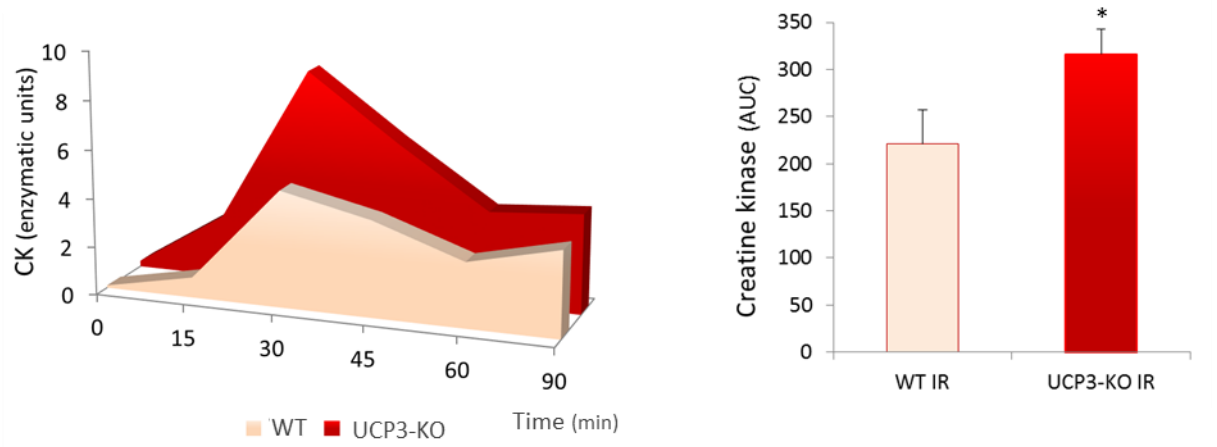

Figure R33. Creatine kinase release during reperfusion of hearts from WT and UCP3-KO mice. Enzymatic units of creatine kinase (CK) measured in the coronary effluent over time during the reperfusion of WT and UCP3-KO hearts. Histograms show the means ± SEM of the area under the curve (AUC) (n = 6-8 hearts per group) *$P < 0.05$.

Thus, after 20 min stabilization, the hearts were subjected to global normothermic ischemia for 40 min, and then to reperfusion for 60 min. Afterwards we analysed total units of CK released in the coronary effluent throughout the experiment, and compared the results obtained in WT and UCP3-KO hearts (Fig. R33). Our results showed that hearts lacking UCP3 presented a significant increment in the total CK release after IR compared to WT hearts, thereby indicating that UCP3-KO hearts suffer more damage than WT hearts (Fig. R33). CK enzymatic units are represented over time throughout the experiment, usually showing a peak 30 min after ischemia (Fig. R33). This is later than expected due to the delayed release of effluent caused by the perfusion chamber dead volume (see section 8.5 of the Materials and

Methods). The peak reflects the highest CK levels, which are being released at the beginning of reperfusion, precisely during a time period between 10 and 20 min into reperfusion.

We also analysed whether there was a basal damage in the UCP3-KO hearts. For this, we measured the CK pre-ischemic units. As shown in Fig. R34, the results obtained proved that the basal damage, as determined by CK activity, was not significantly different in UCP3-KO and WT hearts.

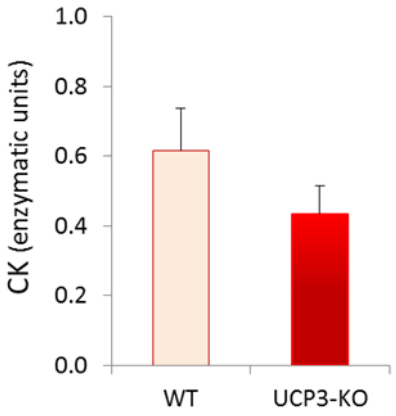

Figure R34. Creatine kinase basal levels of hearts from WT and UCP3-KO mice. Enzymatic units of creatine kinase (CK) measured in the coronary effluent after stabilization and before ischemia in WT and UCP3-KO hearts. Histograms show the means ± SEM of enzymatic units (n = 6-8 hearts per group).

Taken together, these results indicate that the hearts that express UCP3 are significantly less damaged than the UCP3-KO hearts after IR, despite similar levels of damage occurring in basal conditions. Therefore, we conclude that UCP3 positively influences the outcome of an ischemic insult followed by reperfusion.

1.4. Infarct size after IR increases in hearts from Nrf2-KO compared to WT mice: cardioprotective role of Nrf2 against IR injury

Our data above show that UCP3 is upregulated in parallel with Nrf2 nuclear accumulation in the heart after IR, and that UCP3 provides cardioprotection against IR damage. Moreover, we found that UCP3 is induced via Nrf2 in cells (sections 1.2. and 2.2. of the Results, *Part I*) to confer protection against oxidative stress (sections 1.3.1. and 2.3.1. of the Results, *Part I*). Therefore, we wondered whether Nrf2 could also have a protective role against IR injury. To test this possibility, we analysed the infarct size of hearts from Nrf2-KO mice subjected to IR, using the Langendorff system (Fig. R35). Thus, the hearts were allowed to stabilize for 20 min, and then subjected to 40 min global normothermic ischemia followed by 60 min reperfusion. At the end of the IR protocol, the hearts were stained with TTC, and the infarct size was determined to observe tissue damage (section 8.4. of the Materials and Methods). The

percentage of the necrotic area (white) in relation to the risk area (total) showed a significantly larger infarction in hearts from Nrf2-KO mice compared to WT mice (Fig. R35). Importantly, the percentage of infarct size in Nrf2-KO hearts was very similar to that of the UCP3-KO hearts (63.3% and 64.1%, respectively, compared to 53.5% of WT hearts), strongly suggesting that, like UCP3, Nrf2 plays a cardioprotective role against IR injury.

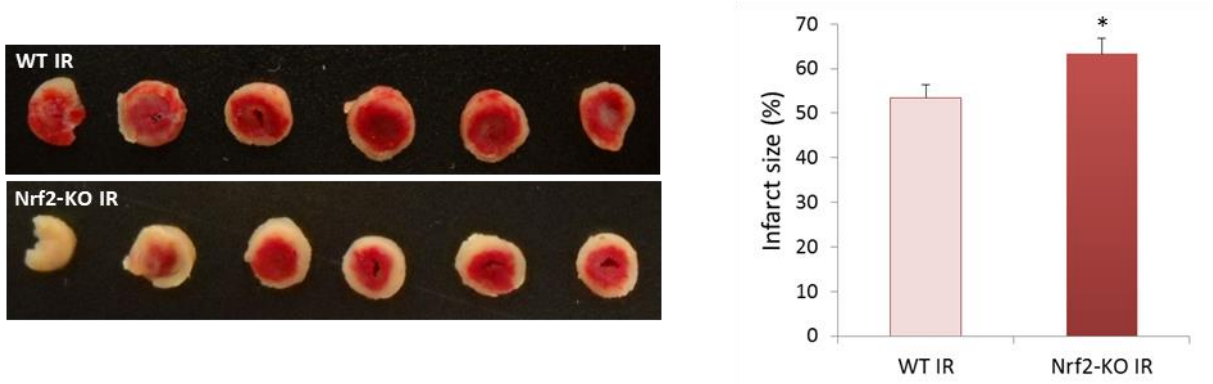

Figure R35. Infarct size in hearts from WT and Nrf2-KO mice subjected to IR. Representative images of heart slices from WT and Nrf2-KO mice subjected to IR and stained with tetrazolium chloride (TTC), which results in white necrotic tissue and red viable tissue. (B) Histograms show the means ± SEM of the percentage of infarct as necrotic area related to risk area (total) (n = 5-7 hearts per group). *$P < 0.05$.

1.5. Creatine kinase release after IR is higher in hearts from Nrf2-KO mice than in those from WT mice

As we did for UCP3-KO mice, we also determined CK levels in the coronary effluent of Nrf2-KO mice during the perfusion experiments, which allows an estimation of IR damage (Fig. R36). For this, after 20 min stabilization, the hearts were subjected to global normothermic ischemia for 40 min, and then to reperfusion for 60 min. We then analysed total units of CK released in the coronary effluent throughout the IR experiment, and compared the results between the WT and the Nrf2-KO hearts. As shown in Fig. R36, the hearts lacking Nrf2 exhibited a significant increment in the total CK release after IR compared to the WT hearts, indicating that Nrf2-KO hearts suffer more damage after IR, and therefore suggesting that Nrf2 plays a cardioprotective role against IR injury. The increase in cardiac damage shown by Nrf2-KO hearts after IR injury compared to WT hearts indicates that those are less protected and therefore more vulnerable to IR damage, a result similar to that found in UCP3-KO mice.

The CK released during reperfusion in Nrf2-KO mice, measured as the area under the curve, was very similar to that in UCP3-KO hearts (331 and 316 AUC, respectively, compared to 221 AUC in WT hearts) (section 1.3.).

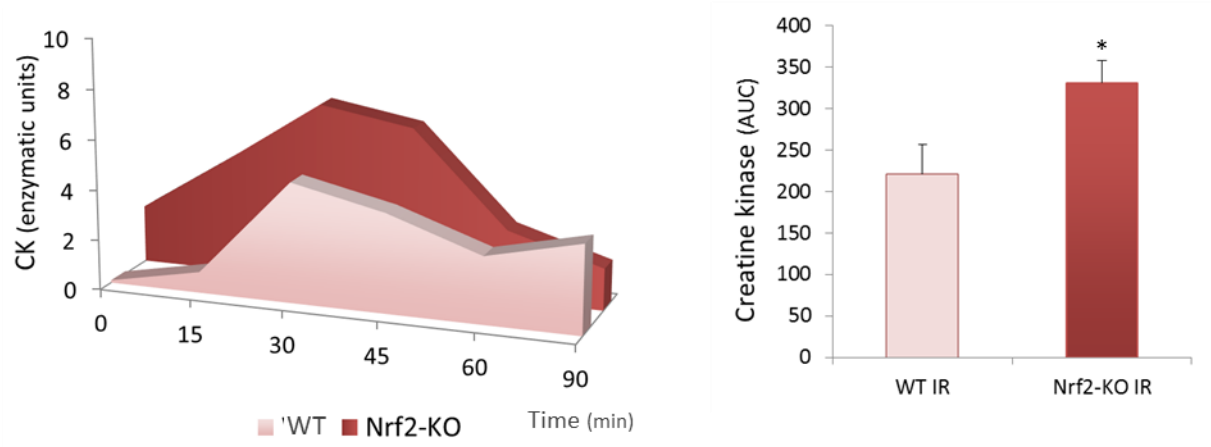

Figure R36. Creatine kinase release during reperfusion of hearts from WT and Nrf2-KO mice. Enzymatic units of creatine kinase (CK) measured in the coronary effluent over time during the reperfusion of WT and Nrf2-KO hearts. Histograms show the means ± SEM of the area under the curve (AUC) (n = 4-6 hearts per group). **P* < 0.05.

Interestingly, we found that, in contrast to UCP3-KO hearts (Fig. R34), there was a basal damage in the Nrf2-KO hearts, as indicated by the elevated pre-ischemic CK units, which were two-fold higher than in the WT hearts (Fig. R37).

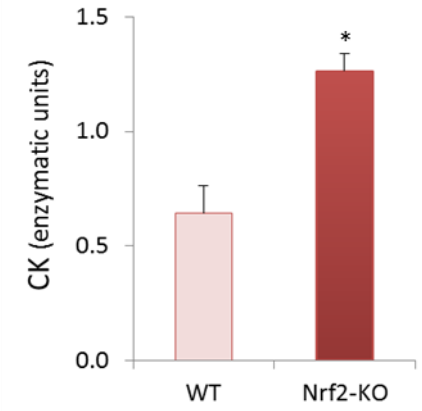

Figure R37. Creatine kinase basal levels of hearts from WT and Nrf2-KO mice. Enzymatic units of creatine kinase (CK) measured in the coronary effluent after stabilization and before ischemia in WT and Nrf2-KO hearts. Histograms show the means ± SEM of enzymatic units (n = 4-6 hearts per group).

2. STUDY OF THE INVOLVEMENT OF NRF2-MEDIATED UCP3 INDUCTION IN ISCHEMIC PRECONDITIONING IN THE ISOLATED MOUSE HEART

2.1. Cardiac ischemic preconditioning (IPC) increases UCP3 expression levels and Nrf2 nuclear accumulation

The results shown above, together with those obtained in cells (*Part I* of the Results), suggest that Nrf2-mediated UCP3 induction could be involved in protecting the heart against the damaging effects of IR. Ischemic preconditioning (IPC) is an endogenous adaptive mechanism that consists of a series of repetitive short periods of sub-lethal myocardial ischemia followed by reperfusion which protects the heart from a subsequent prolonged ischemic insult (Yellon and Downey 2003). As ROS may be one of the several triggers proposed for IPC (Cai et al. 2008, Halestrap et al. 2007, Murphy and Steenbergen 2008) we studied whether Nrf2-mediated UCP3 induction could be involved in this phenomenon.

We first examined the effects of IPC on UCP3 expression. Hearts were perfused using the Langendorff perfusion system. We applied a protocol for IPC, consisting of 2 cycles of 5 min ischemia plus 5 min reperfusion, before IR (40 min global normothermic ischemia followed by 60 min reperfusion), and then evaluated UCP3 protein expression levels in total extracts. As shown in Fig. R38, we found that UCP3 was upregulated in hearts subjected to IPC, even to a higher extent than after IR, which strongly suggests the involvement of UCP3 in IPC.

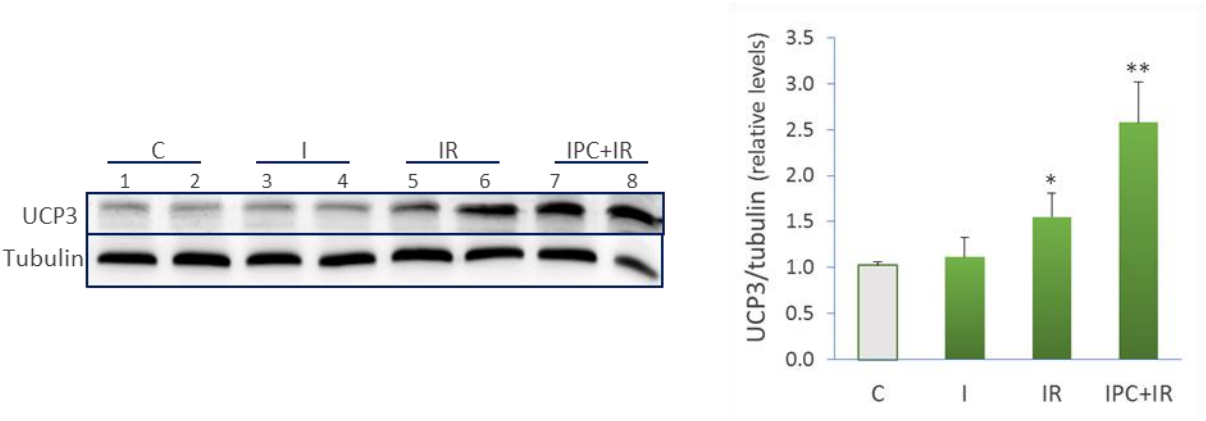

Figure R38. UCP3 expression levels in mouse hearts after I, IR or ischemic preconditioning (IPC). Representative immunoblot of UCP3 in total extracts from control (C) hearts and hearts subjected to I, IR, or IPC prior to IR (IPC+IR). Numbers 1-8 indicate different mice. Tubulin was used as protein loading control. Histograms show the means ± SEM relative to control from 4 hearts per group. **P* < 0.05, ***P* < 0.01.

To determine the precise moment at which UCP3 induction occurred, we examined UCP3 expression levels after IPC+C, IPC+I and IPC+IR (Fig. R39). The increase in UCP3 expression induced by IPC was only observed when the IPC protocol was applied before an injury-inducing IR event, but not when the IPC was followed solely by normal perfusion or by ischemia (Fig. R39). This indicates that IPC alone is not sufficient to upregulate UCP3, but a damaging IR event following IPC is necessary for UCP3 upregulation.

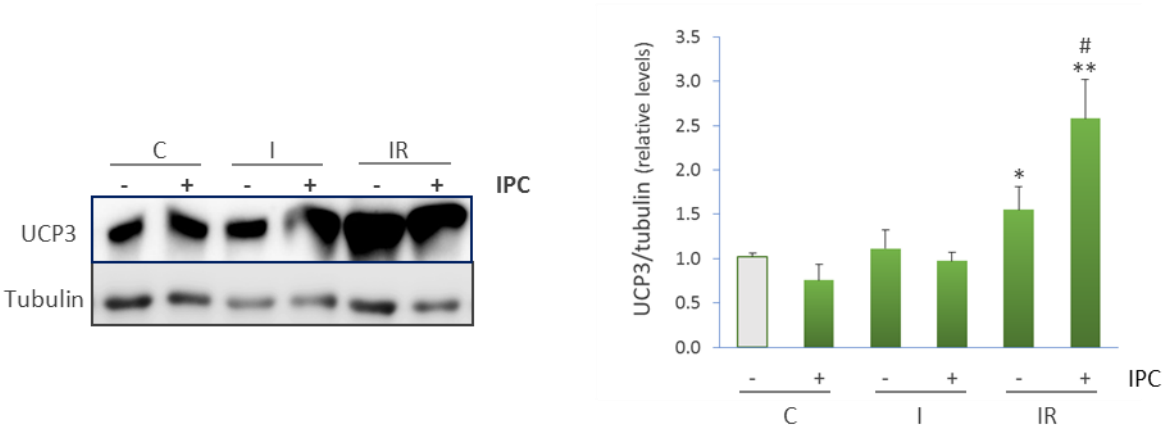

Figure R39. Effects of IPC on UCP3 expression levels in mouse hearts subjected to I or IR. Representative immunoblot of UCP3 in total extracts from control (C), I and IR hearts subjected (+) or not (-) to IPC. Tubulin was used as protein loading control. Histograms show the means ± SEM relative to control from 4 hearts per group. $*P < 0.05$, $**P < 0.01$ with respect to C; $^{\#}P = 0.062$ with respect to IR(-).

We next analysed the Nrf2 levels in the nuclear extracts of the myocardial tissue after the same IPC perfusion protocols described above. Our results indicated that Nrf2 significantly accumulated in IPC+IR hearts, even to a higher degree than in IR hearts (Fig. R40). Interestingly, Nrf2 accumulated in the nucleus in parallel with increased mitochondrial UCP3 expression (Fig. R38).

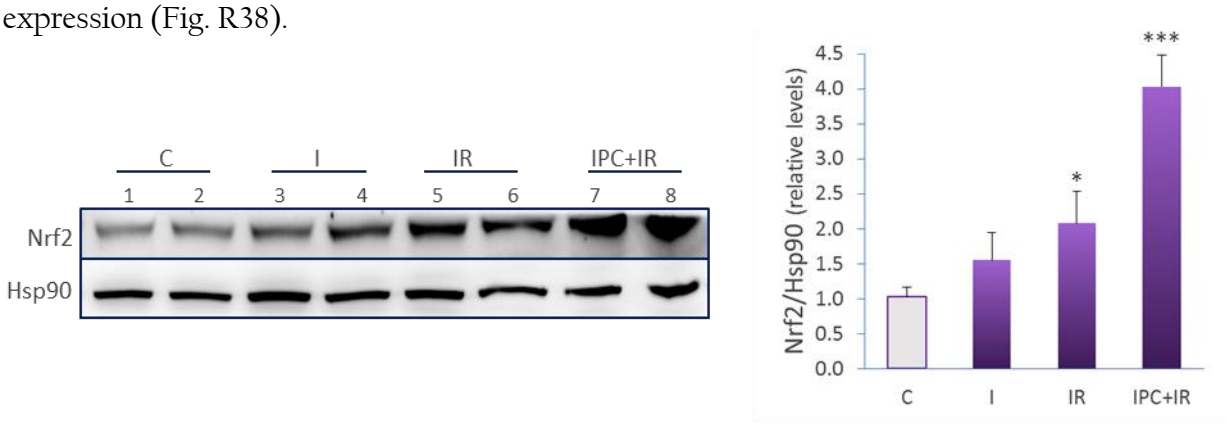

Figure R40. Nrf2 expression levels in mouse hearts after I, IR or IPC. Representative immunoblot of Nrf2 in nuclear extracts from control (C) hearts and hearts subjected to I, IR or IPC prior to IR (IPC+IR). Numbers 1-8 indicate different mice. Hsp90 was used as protein loading control. Histograms show the means ± SEM relative to control from 4 hearts per group. $*P < 0.05$, $***P < 0.001$.

As in the case of UCP3 regulation (Fig. R39), the nuclear accumulation in Nrf2 induced by IPC occurred only when the IPC protocol was applied before an injury-inducing IR event, but not when the IPC was followed solely by normal perfusion or by ischemia (Fig. R41). This result indicates that, as for UCP3 expression, IPC alone is not sufficient to increase Nrf2 expression, but a prolonged IR event following IPC is necessary for Nrf2 induction.

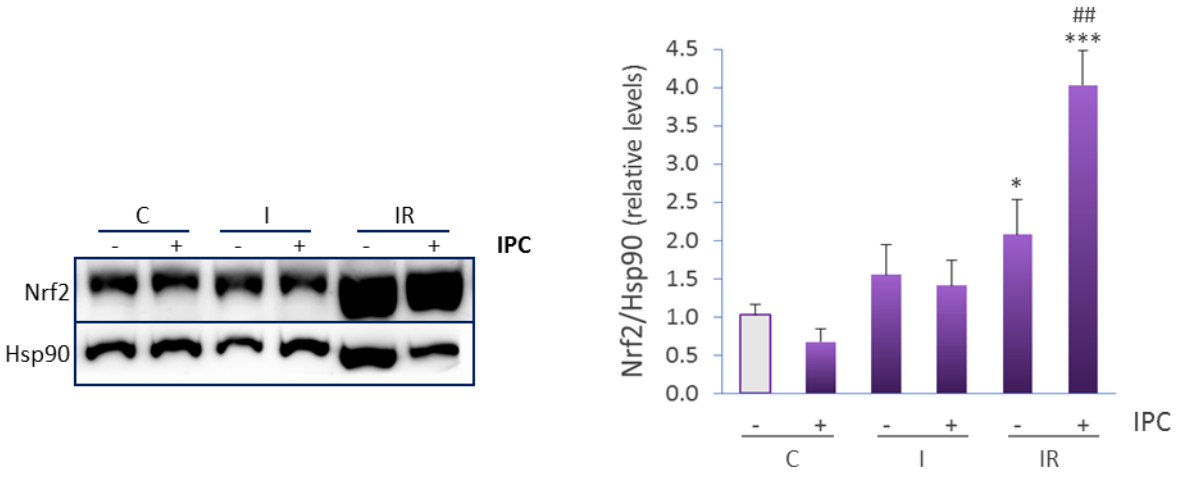

Figure R41. Effects of IPC on Nrf2 expression levels in mouse hearts subjected to I or IR. Representative immunoblot of Nrf2 in nuclear extracts from control (C), I and IR hearts subjected (+) or not (-) to IPC. Hsp90 was used as protein loading control. Histograms show the means ± SEM relative to control from 4 hearts per group. $^{*}P < 0.05$, $^{***}P < 0.001$ with respect to C; $^{\#\#}P < 0.01$ with respect to IR (-).

Taken together, these results suggest that the Nrf2-mediated induction of UCP3, which we showed in cells treated with H_2O_2 or HNE, could be conferring protection to the heart under oxidative stress induced by IR, and that this event might also be involved in IPC.

2.2. IPC does not reduce infarct size after IR in hearts from UCP3-KO mice: involvement of UCP3 in IPC

Next, to study whether UCP3 is involved in the protective mechanism of IPC as suggested by the data above, we determined the infarct size in hearts obtained from preconditioned UCP3-KO and WT mice.

For these experiments, an IPC protocol (2 cycles of 5 min ischemia plus 5 min reperfusion) was performed before IR (40 min global normothermic ischemia followed by 60 min reperfusion) to determine whether cardiac tissue damage would be reduced in UCP3-KO hearts, as reported for wild-type hearts (Murry et al. 1986). Our results showed that, as expected, preconditioned hearts from WT mice exhibited a significantly reduced infarct size after IR compared to non-preconditioned WT hearts (Fig. R42). By contrast, the hearts from

UCP3-KO mice subjected to IPC exhibited no differences in infarct size after IR compared to the hearts from UCP3-KO mice subjected to IR only (Fig. R42), thus showing that the IPC protocol was not effective in mice lacking UCP3. Moreover, the infarct size after IR in UCP3-KO mice was larger than in WT mice, both in the presence and absence of IPC (Fig. R42). On the whole, these results indicate a clear implication of UCP3 in the IPC phenomenon and its protective effect against IR injury.

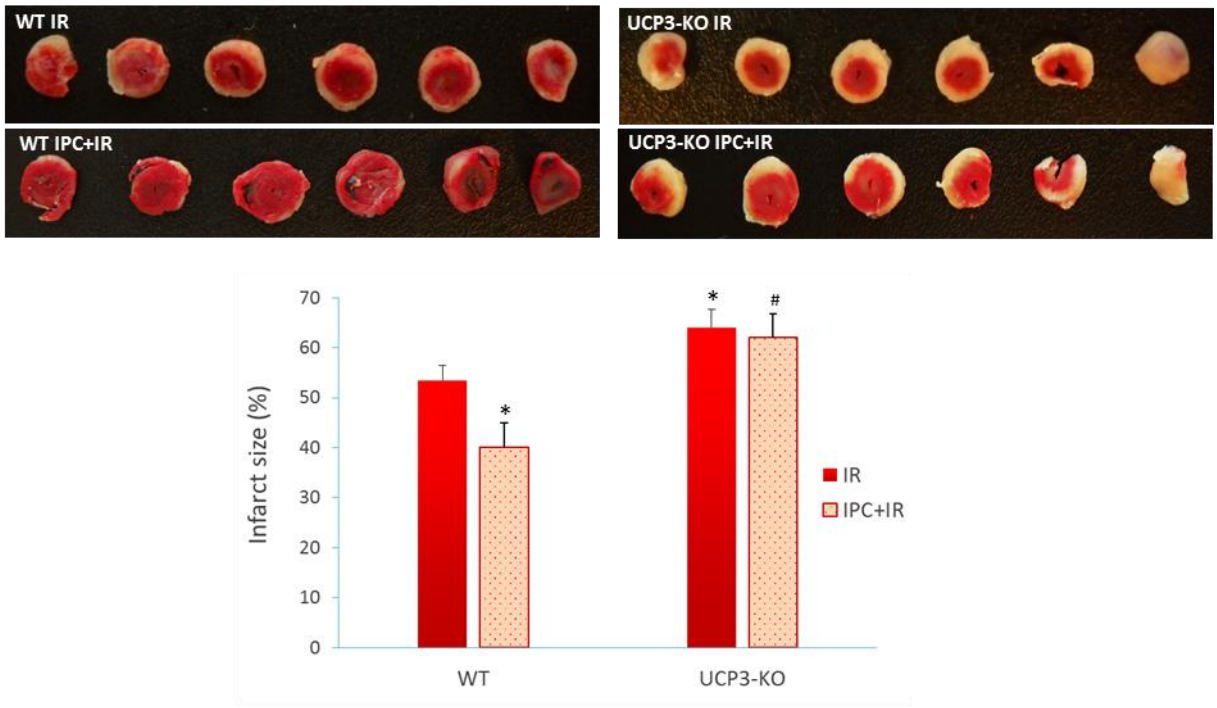

Figure R42. Infarct size in hearts from WT and UCP3-KO mice subjected to IR and IPC. Representative images of heart slices from WT and UCP3-KO mice subjected to IR, or IPC prior to IR (IPC+IR) and stained with tetrazolium chloride (TTC), which results in white necrotic tissue and red viable tissue. Histograms show the means ± SEM of the percentage of infarct as necrotic area (white) related to risk area (total) (n = 6-8 hearts per group). *$P < 0.05$ with respect to WT IR; #$P < 0.05$ with respect to UCP3-KO IR group.

2.3. Creatine kinase release after IR is higher in preconditioned hearts from UCP3-KO mice than in those from WT mice

As in the IR experiments (section 1.3.), we also analysed CK enzymatic units released in the coronary effluent throughout the IPC+IR experiment, and compared the results between WT and UCP3-KO hearts. UCP3-KO hearts displayed increased CK release with respect to WT hearts after IPC+IR (324 to 218 AUC, respectively) (Fig. R43), which confirmed that IR caused more damage to UCP3-KO than to WT hearts, even after IPC.

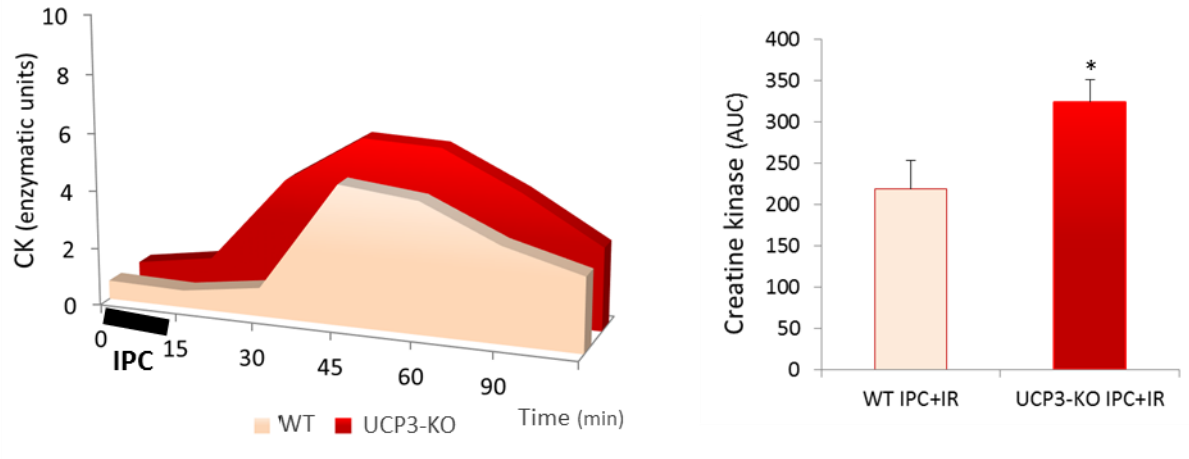

Figure R43. Effects of IPC on creatine kinase release during reperfusion of hearts from WT and UCP3-KO mice. Enzymatic units of creatine kinase (CK) measured in the coronary effluent over time during reperfusion of WT and UCP3-KO mice subjected (+) or not (-) to IPC. Histograms show the means ± SEM of the area under the curve (AUC) (n = 6 mice per group). *$P < 0.05$.

Regarding the analysis of CK release, the comparison between preconditioned and non-preconditioned hearts subjected to IR cannot be performed due to a methodological problem. The IPC+IR protocols are 20 min longer than the IR experiments (Fig. M6 and section 8.2. of the Materials and Methods). During these 20 min, there are two 5-min periods of reperfusion releasing effluent that are absent in IR protocols and make the comparison meaningless. Therefore, we grouped only comparable experiments, and thus Fig. R43 shows the results of CK activity levels of IPC+IR perfused hearts from WT and UCP3-KO mice.

vi. DISCUSSION

Mitochondria are a major source of ROS in cells, and mitochondrial superoxide ($O_2^{\cdot-}$) production is highly sensitive to the protonmotive force (Δp) created across the IMM by the electron transport chain (ETC) (Korshunov et al. 1997). The activation of uncoupling proteins (UCPs) and the subsequent mitochondrial depolarization have been proposed as a mechanism to decrease mitochondrial $O_2^{\cdot-}$ generation (Brand and Esteves 2005, Mailloux and Harper 2011, Negre-Salvayre et al. 1997). This hypothesis, however, remains controversial (Nabben et al. 2011, Shabalina and Nedergaard 2011). It has been demonstrated that UCPs can be activated by endogenous (Talbot et al. 2003) and exogenous (Echtay et al. 2002) $O_2^{\cdot-}$, as well as by lipid peroxidation products such as 4-hydroxy-2-nonenal (HNE) (Aguirre and Cadenas 2010, Murphy et al. 2003, Parker et al. 2008a), suggesting that UCPs are central to the mitochondrial response to ROS. It is unclear, however, whether UCP expression is regulated by oxidative stress and, if this is the case, what are the physiological consequences of such regulation.

1. UCP3 EXPRESSION INCREASES IN RESPONSE TO OXIDATIVE STRESS, AN EFFECT MEDIATED BY THE TRANSCRIPTION FACTOR NRF2

The results described in this thesis show that the treatment with sub-toxic concentrations of the oxidant H_2O_2 or the lipid electrophile HNE, induces the upregulation of UCP3 in both C2C12 and HL-1 mouse cell lines. We used doses of these compounds that cause cellular stress but not cell death. H_2O_2 is relatively unreactive compared to $O_2^{\cdot-}$ but, in the presence of ferrous iron (Fe^{2+}), it can induce the generation of highly reactive hydroxyl radicals ($OH^{\cdot}$) via the Fenton reaction. Then, $OH^{\cdot}$ can initiate lipid peroxidation cascades in phospholipid membranes. Moreover, the products of sugar, protein, and lipid oxidation can cause secondary damage to proteins, which may lose their catalytic function and undergo selective degradation. One of the most abundant lipid peroxidation products, HNE, has been described as an activator of UCPs, and it has been proposed that the activation of UCPs by HNE would induce mild uncoupling, therefore decreasing IMM potential and subsequently superoxide generation by the ETC (Echtay et al. 2003). Thus, HNE would act as a biological signal to decrease mitochondrial ROS production.

The effects of H_2O_2 and HNE on protein induction are specific for UCP3, as the expression of UCP2, the other UCP present in skeletal muscle and heart, is not affected by these treatments. UCP3 upregulation occurs after short exposure times (3-5 h) to these stressors, which is compatible with the exceptionally short half-life of UCP3 (0.5–4 h) compared to that

of other mitochondrial proteins such as ANT or UCP1, which have longer half-lives (Azzu et al. 2010a, Azzu et al. 2010b). The degradation of UCP3 occurs through ubiquitylation via 26S proteasome and requires a specific mitochondrial status consisting of high matrix ATP concentration and a high $\Delta\Psi_m$ (Mookerjee and Brand 2011). This rapid turnover has been suggested to represent a means of dynamically regulating this protein in various physiological contexts including the adaptation to fasting and protection from oxidative damage (Azzu et al. 2010a).

The increase in UCP3 expression in response to H_2O_2 or HNE treatment that we found in this work, together with its proposed function in the control of mitochondrial ROS production, led us to investigate the potential implication of the redox-sensitive transcription factor Nrf2 in UCP3 upregulation under oxidative stress conditions. Thus, the treatment with sub-toxic concentrations of H_2O_2 or HNE induced the nuclear accumulation of Nrf2 in C2C12 and HL-1 cells. Our results are consistent with previous reports showing that Nrf2 signalling plays an important role in H_2O_2-induced protection against oxidative injury in cardiomyocytes (Purdom-Dickinson et al. 2007). They also agree with the notion that Nrf2 is a key transcriptional regulator for the HNE-mediated induction of antioxidant defences in the same cell type and in isolated perfused hearts (Zhang et al. 2010). However, the mechanism by which HNE induces the nuclear accumulation of Nrf2 in our experiments remains to be clarified. It is well-known that specific cysteine residues (Cys151, Cys273 and Cys288) in Keap1 (the cytosolic repressor of Nrf2) act as a sensor for oxidative stress, and modification of these residues leads to a conformational change in Keap1, with the subsequent release of Nrf2 (Kobayashi et al. 2006). Our experiments using N-acetylcysteine (NAC) indicate that Nrf2 nuclear accumulation and UCP3 upregulation are prevented in the presence of this antioxidant, probably due to the ability of NAC to reduce the oxidized cysteines in Keap1. This would prevent Nrf2 activation and therefore its effect on UCP3 expression.

We observed increases in *Nrf2* mRNA levels after H_2O_2 or HNE treatment that were accompanied by enhanced protein expression in the nuclear fraction. Importantly, Nrf2 nuclear accumulation correlated with increased transcriptional activity, since the expression levels of its target gene *HO-1* were also increased, demonstrating Nrf2 activation under H_2O_2 or HNE treatment. Under these conditions, the degradation of Nrf2 by the proteasome system is inhibited and its nuclear translocation allows the binding of the protein to the ARE sequences of its target genes, which leads to the activation of a variety of antioxidant defences, including HO-1 and, as found in this work, UCP3.

There are several potential sites for Nrf2 binding in the *Ucp3* promoter. One of them consists of a region containing an ARE sequence highly conserved between mammalian species. Our ChIP experiments revealed the specific binding of Nrf2 to this conserved ARE region after H_2O_2 or HNE treatment. Moreover, luciferase reporter experiments demonstrated that Nrf2 binding to the *Ucp3* promoter induces downstream gene transcription. Importantly, we showed that the ARE sequence is absolutely necessary for oxidative stress-induced transcription, as the mutated form of the ARE did not result in increased transcription.

It is worth noting that the basal levels of luciferase expression in cells transfected with the plasmid containing the longer *Ucp3* promoter sequence were higher than those detected in cells transfected with the plasmid containing the shorter sequence of the *Ucp3* promoter. This could reflect the fact that other factors could bind the promoter at specific sites and increase the basal transcription of the gene. Indeed, the transcriptional regulation of *Ucp3* by factors such as PPARs and the myogenic regulatory factor MyoD (Solanes et al. 2003), thyroid hormones (Solanes et al. 2005) and glucocorticoids (Amat et al. 2007), have been described.

The involvement of Nrf2 on UCP3 upregulation under oxidative stress was confirmed by *Nrf2* mRNA interference experiments. The results showed that UCP3 was not induced in the absence of Nrf2 under conditions of oxidative stress. Therefore, the absence of Nrf2 via RNA interference, prevents the H_2O_2 or HNE-induced increase in UCP3 expression, confirming the involvement of Nrf2 in this process. However, the possibility that H_2O_2 or HNE are also acting on UCP3 stability cannot be excluded.

Our results provide direct biochemical evidence that, in response to oxidative stress, Nrf2 interacts with and activates a specific antioxidant response element (ARE) in the *Ucp3* promoter, demonstrating that UCP3 is induced via Nrf2 under oxidative stress conditions.

2. UCP3 UPREGULATION MEDIATED BY NRF2 PROTECTS AGAINST OXIDATIVE DAMAGE AND INCREASES CELL SURVIVAL

The results obtained using *Ucp3*-silenced HL-1 cells treated with H_2O_2, showed that these cells have enhanced levels of oxidative stress compared to control cells. In accordance with this, the absence of UCP3 led to an increase in cell death after H_2O_2 or HNE treatment. These findings support a protective role for the protein against oxidative stress.

Our bioenergetic analysis of siUCP3 and scrambled (Scr) control HL-1 cells in the absence of treatment, revealed comparable levels of both basal respiration and proton leak in the absence or presence of UCP3. This is consistent with the similar proton leak reported for UCP3-KO and wild-type (WT) mice under basal conditions (Cadenas et al. 2002, Nabben et al. 2011), and supports the accepted view that UCP3 does not catalyse the basal proton conductance unless appropriately activated (Brand and Esteves 2005). Indeed, the physiologically-induced upregulation of UCP3 often fails to increase mitochondrial basal uncoupling (Bugger et al. 2008, Cadenas et al. 1999, Crescenzo et al. 2003).

After the treatment with H_2O_2 or HNE, the increment in UCP3 levels was accompanied by enhanced basal respiration and proton conductance in Scr control cells. However, the addition of H_2O_2 did not significantly increase basal respiration or proton leak in siUCP3 cells, indicating that the enhanced respiration observed in control cells was specifically mediated by UCP3. The bioenergetic analysis of *Nrf2*-silenced HL-1 cells under H_2O_2 exposure reproduced similar results, since UCP3 was not induced in the absence of Nrf2 under conditions of oxidative stress. In contrast to H_2O_2 treatment, basal respiration and proton leak after HNE exposure were still elevated in siUCP3 cells, although the increase in proton leak was significantly reduced compared to Scr cells. Therefore, the elevated proton leak after HNE addition can be partially attributed to UCP3. According to our data, the contribution of UCP3 to HNE-induced proton leak is around 21%. This observation is similar to the reported contribution of UCP3 to HNE-induced proton leak in mouse skeletal muscle mitochondria (Aguirre and Cadenas 2010, Echtay et al. 2003, Parker et al. 2008a).

The effects of UCP3 upregulation on ATP turnover, maximal respiration and respiratory reserve capacity of HL-1 cells, also showed some differences depending on the treatment. The induction of UCP3 after H_2O_2 exposure did not significantly modify ATP turnover, maximal respiration or respiratory reserve capacity. By contrast, after HNE addition, the maximal respiration was dramatically decreased, even more so in siUCP3 cells, and therefore the reserve

capacity of the cells was inexistent. This exhaustion of the reserve capacity by HNE treatment does not depend on UCP3, as it occurs in both Scr and siUCP3 cells, and it is in agreement with reported data in rat neonatal cardiomyocytes (Hill et al. 2009a). Surprisingly, in both Scr and *Ucp3*-silenced cells, ATP turnover was significantly elevated after HNE addition, also in agreement with the mentioned report (Hill et al., 2009), although this result was independent of the presence of UCP3 as well. HNE levels are increased in several myocardial pathologies (Eaton et al. 1999, Hill et al. 2009b, Mak et al. 2000, Nakamura et al. 2002, Srivastava et al. 2007), and the activation of critical enzymes for HNE detoxification protects the heart from ischemic injury (Chen et al. 2008, Churchill et al. 2009). Our data suggest that the decrease in respiratory reserve capacity promoted by HNE could contribute to tissue damage and dysfunction.

Our results support the hypothesis that, in the presence of activators, UCP3 enhances proton conductance slightly lowering $\Delta\Psi_m$ (mild uncoupling), which could led in turn to decreased mitochondrial ROS production and enhanced cell survival (Brand and Esteves 2005, Mailloux and Harper 2011). In fact, the observation of the cells by microscopy after treatment with H_2O_2 or HNE clearly showed augmented cell death in *Ucp3*- or *Nrf2*-silenced cells, confirming the role of this protein in the protection against oxidative stress.

3. UCP3 EXPRESSION AND NRF2 NUCLEAR ACCUMULATION INCREASE AFTER ISCHEMIA-REPERFUSION IN THE ISOLATED PERFUSED MOUSE HEART: CARDIOPROTECTIVE ROLE OF UCP3 AND NRF2

We confirmed the physiological relevance of our findings by studying a condition known to increase ROS generation, ischemia-reperfusion (IR), in the isolated perfused mouse heart. Our results show that IR increases both Nrf2 nuclear accumulation and UCP3 expression, suggesting that Nrf2-mediated UCP3 upregulation might play an important role in the protection against oxidative damage during IR.

Several studies have demonstrated that the Nrf2/ARE pathway is activated by oxidative stress, and that this activation protects against cell death. Indeed, mild oxidative stress, including sub-toxic H_2O_2, strongly activates astrocytic Nrf2/ARE-dependent gene expression, which in turn contributes to neuroprotective ischemic preconditioning (IPC) (Bell et al. 2011a, Bell et al. 2011b). Moreover, there is evidence that high concentrations of reactive aldehydes

such as HNE are responsible for much of the damage elicited by cardiac IR injury (Conklin et al. 2007), while sub-lethal concentrations of aldehydes stimulate stress resistance pathways to achieve cardioprotection (Zhang et al. 2010). Thus, the pre-treatment with an activator of an aldehyde-detoxifying enzyme, aldehyde dehydrogenase-2 (ALDH2), reduced infarct size by 60% in a rat model of IR injury (Chen et al. 2008). Moreover, Nrf2 activation and Nrf2-dependent antioxidant gene expression were demonstrated in an *in vivo* model of IR damage, providing evidence for the involvement of ROS in the reoxygenation-specific activation of Nrf2 (Leonard et al. 2006). Furthermore, sub-lethal concentrations (5 µM) of HNE prime cardiomyocytes to become resistant to cytotoxic concentrations of HNE via Nrf2-mediated gene expression and GSH biosynthesis, thereby conferring protection against IR injury (Zhang et al. 2010).

We observed an upregulation of UCP3 after IR. Recently, UCP2 and UCP3 have been reported to increase in rat hearts subjected to IR (Safari et al. 2014). In this paper, the authors show that, whereas the effect of IR on UCP2 protein is a local process, UCP3 protein increases in the whole heart. The expression of UCP3 has also been studied in human failing hearts, but in this case the conclusion is unclear. Although there is evidence of increased levels of cardiac UCP3 in patients with heart failure (Murray et al. 2004), other data showed unchanged *UCP3* gene expression in human failing hearts compared to non-failing hearts (Razeghi et al. 2001). This disagreement might be caused by the measurement of protein levels versus *Ucp3* mRNA or by the differences in the type of samples obtained from the patients.

Our description of a novel signalling pathway mediated by Nrf2 and involving the mitochondrial protein UCP3, which is implicated in the control of $O_2^{\cdot-}$ production, is highly relevant to IR, a situation in which there is a burst of ROS generation. The activation of UCPs and the subsequent modest mitochondrial depolarization could diminish $O_2^{\cdot-}$ production in cardiac ischemia, thus conferring ischemia tolerance (Cadenas et al. 2010, Sack 2006). Indeed, there are some reports suggesting a protective role of UCP-mediated uncoupling against IR injury. Thus, mitochondrial UCP1 protects against IR injury when expressed ectopically in cardiac-derived H9c2 cells (Bienengraeber et al. 2003) and in the hearts of transgenic mice (Hoerter et al. 2004). In rat neonatal cardiomyocytes, UCP2 overexpression does not have intrinsic uncoupling activity but it confers tolerance to oxidative stress by diminishing mitochondrial Ca^{2+} overload and reducing ROS generation (Teshima et al. 2003). Additionally, there is an inverse relationship between ROS and UCP3 levels in cardiomyocytes, and proper UCP3 expression protects against restrain stress-induced myocardial injury in rats (Wang et al. 2010).

Our results show a significantly greater infarct size after IR in UCP3-KO than in WT hearts, which suggest that hearts lacking UCP3 are less protected and, therefore, result more damaged than those in which the protein is present. Taking into account that UCP3 was upregulated in the hearts of WT mice after IR, these results strongly suggest that UCP3 plays a protective role against IR injury. This conclusion was confirmed using another indicator of cardiac tissue damage, the activity levels of creatine kinase (CK) released in the coronary effluent during reperfusion. This parameter showed the same pattern, confirming that UCP3-KO mice present greater damage than their WT counterparts. The basal measurement of CK (previous to ischemia) was comparable in both groups, discarding basal damage in UCP3-KO hearts, and reinforcing the idea that the increased cardiac damage observed in these hearts is caused by IR.

During the performance of these experiments, an article was published to show that UCP3 plays a critical role in cardioprotection against IR injury (Ozcan et al. 2013). The authors analysed physiological parameters such as contractile function, and reported that hearts from UCP3-KO mice have poorer recovery of left-ventricular function compared to WT hearts after *ex vivo* IR. Likewise, *in vivo* occlusion of the left coronary artery resulted in two-fold larger infarcts in UCP3-KO compared to WT mice, in agreement with our findings in isotated perfused hearts.

We performed *ex vivo* experiments in hearts of Nrf2-KO mice and obtained similar results. These hearts showed a significantly greater infarction after IR than the WT hearts. The increased cardiac damage was confirmed by the measurement of CK released in the coronary effluent during reperfusion, which was elevated in Nrf2-KO compared to WT hearts. Importantly, the basal measurement of CK (previous to ischemia) was higher in Nrf2-KO hearts, contrarily to the case of UCP3-KO hearts, indicating that there is some degree of basal damage in these hearts. To confirm this result, however, the infarct size of the hearts after control perfusion only, would have to be determine in both WT and Nrf2-KO mice, and therefore the conclusion that the basal cardiac damage is increased in these mice should be taken with caution.

On the whole, these results appear to be in agreement with the proposed role for UCP3 in cardioprotection, although they bring some discrepancy with reported work in which the worse outcome for the Nrf2-KO compared to the WT hearts is not evident as determined by ventricular recovery function and lactate dehydrogenase (LDH) release (Zhang et al. 2010). In this paper, the authors manifest confusion by their findings and, considering all their results

together, they conclude nonetheless that Nrf2 is essential for cardioprotection mediated by HNE.

4. UCP3 IS INVOLVED IN THE CARDIOPROTECTIVE PHENOMENON OF ISCHEMIC PRECONDITIONING

Ischemic preconditioning (IPC) is a protective phenomenon evoked by transient non-lethal tissue ischemia prior to a prolonged ischemic insult (Murry et al., 1986). Although IPC protection has been well documented since its discovery, the specific mechanisms involved are not completely understood despite intense investigation (Bell and Yellon 2012, Hausenloy and Yellon 2011, Semenza 2011, Shi and Vinten-Johansen 2012). Several protective pathways have been described (Hausenloy et al. 2005, Suleman et al. 2008). In addition, upregulation of UCP2 and UCP3 has been observed in the delayed preconditioned heart (McLeod et al. 2005), suggesting a role for these proteins in this phenomenon.

Our experiments in isolated preconditioned hearts show that IPC strongly induces UCP3 expression and Nrf2 nuclear accumulation. The induction is higher than that observed after IR in non-preconditioned hearts, and clearly implicates these proteins in the IPC phenomenon. UCP3 and Nrf2 upregulation was detected after the complete IPC plus IR protocol, and not after IPC followed solely by reperfusion or by ischemia. Since the former protocol was 1 h longer than the others, we cannot discard that this extra time is required for new protein synthesis.

Our results show that IPC decreases the infarct size after IR in WT hearts, as expected. However, mice lacking UCP3 do not show this protective effect, which clearly demonstrates the involvement of UCP3 in IPC. These results agree with those recently published by Ozcan and col. (Ozcan et al. 2013). However, the precise mechanism by which UCP3 confers protection remains to be determined.

In summary, in this thesis we present evidence of a novel antioxidant pathway mediated by the redox-sensitive transcription factor Nrf2 and involving the mitochondrial protein UCP3. Our data support a model in which the addition of oxidants or lipid peroxidation products, or conditions leading to ROS formation such as IR, activates Nrf2, which translocates to the nucleus and binds to the *Ucp3* promoter, thereby enhancing its expression. The increase in UCP3 expression, together with UCP3 protein activation by $O_2^{\cdot-}$ and HNE, enhances proton conductance, lowering the membrane potential and decreasing mitochondrial superoxide generation. This effect is reflected into increased cell survival under conditions of oxidative stress, and cardioprotection against IR injury in the isolated perfused mouse heart. Likewise, this protective pathway might be involved in IPC. Therefore, this novel pathway is a plausible therapeutic target for novel strategies aimed at preventing oxidative damage.

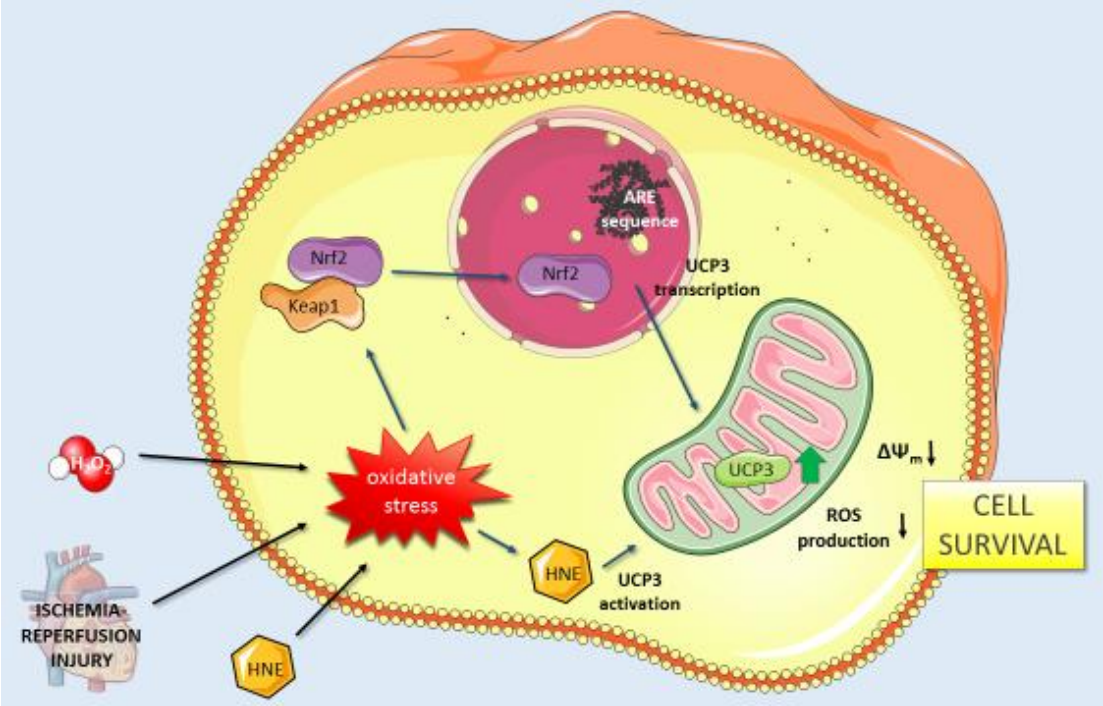

Figure D1. The treatment with H_2O_2, HNE, or conditions leading to ROS formation such as IR, increases UCP3 expression via Nrf2, promoting cell survival under conditions of oxidative stress. Model showing the activation and nuclear translocation of Nrf2 induced by oxidative stress. The binding of Nrf2 to an ARE within the *Ucp3* promoter increases UCP3 expression, whereas HNE also increases directly UCP3 activity. Increased UCP3 expression together with protein activation induces a slight decrease in the membrane potential (mild uncoupling) and an ensuing decrease in $O_2^{\cdot-}$ production. This mechanism promotes cell survival under conditions of oxidative stress.

vii. CONCLUSIONS

1. UCP3 expression is regulated in response to oxidative stress. Thus, both mRNA and protein levels are upregulated after the treatment with hydrogen peroxide (H_2O_2) or 4-hydroxy-2-nonenal (HNE) in cell lines from mouse heart and skeletal muscle.

2. The transcription factor Nrf2 is involved in the upregulation of UCP3 under oxidative stress conditions. Nrf2 binds to a specific ARE sequence conserved in the *Ucp3* promoter to activate *Ucp3* transcription in response to oxidative stress.

3. Nrf2-mediated UCP3 upregulation, as well as its activation by superoxide and HNE, enhance mitochondrial proton leak diminishing ROS generation and promoting cell survival.

4. Myocardial ischemia-reperfusion (IR) in isolated perfused mouse hearts increases UCP3 expression and Nrf2 nuclear accumulation, effects that are potentiated in ischemic preconditioned hearts.

5. Both UCP3 and Nrf2 protect the heart from the damaging effects of IR, since hearts from mice lacking any of these proteins exhibit more damage than those from wild-type mice.

6. UCP3 takes part in the protective programme of ischemic preconditioning (IPC) in isolated perfused mouse hearts, since both preconditioned and non-preconditioned hearts from UCP3-KO mice have similar damage after IR.

CONCLUSIONES

1. La expresión de UCP3 está regulada en respuesta al estrés oxidativo. Así, tanto el mRNA como la proteína se encuentran incrementados tras el tratamiento con peróxido de hidrógeno (H_2O_2) o 4-hidroxi-2-nonenal (HNE) en líneas celulares de corazón y músculo esquelético de ratón.

2. El factor de transcripción Nrf2 está involucrado en la inducción de UCP3 en condiciones de estrés oxidativo. Nrf2 se une a una secuencia específica ARE conservada en el promotor de *Ucp3* para activar la transcripción del gen en respuesta al estrés oxidativo.

3. La inducción de UCP3 mediada por Nrf2, así como su activación por superóxido y HNE, aumentan la fuga de protones ('proton leak') mitocondrial, disminuyendo así la generación de ROS y promoviendo la supervivencia celular.

4. La isquemia-reperfusión cardíaca (IR) en corazones aislados perfundidos de ratón aumenta la expresión de UCP3 y la acumulación nuclear de Nrf2, efectos que están potenciados en los corazones precondicionados.

5. Tanto UCP3 como Nrf2 protegen al corazón frente a los efectos perjudiciales de la IR, ya que los corazones de ratones que carecen de alguna de estas proteínas muestran más daño quelos de ratones de tipo silvestre.

6. UCP3 participa en el programa protector del precondicionamiento isquémico (IPC) en corazones aislados perfundidos de ratón, ya que los corazones de ratones UCP3-KO precondicionados y no precondicionados presentan un daño similar tras IR.

REFERENCES

Abdul-Ghani S, Heesom KJ, Angelini GD, Suleiman MS. 2014. Cardiac phosphoproteomics during remote ischemic preconditioning: a role for the sarcomeric Z-disk proteins. Biomed Res Int 2014: 767812.

Affourtit C, Brand MD. 2008. Uncoupling protein-2 contributes significantly to high mitochondrial proton leak in INS-1E insulinoma cells and attenuates glucose-stimulated insulin secretion. Biochem J 409: 199-204.

Aguirre E, Cadenas S. 2010. GDP and carboxyatractylate inhibit 4-hydroxynonenal-activated proton conductance to differing degrees in mitochondria from skeletal muscle and heart. Biochim Biophys Acta 1797: 1716-1726.

Alary J, Gueraud F, Cravedi JP. 2003. Fate of 4-hydroxynonenal in vivo: disposition and metabolic pathways. Mol Aspects Med 24: 177-187.

Amat R, Solanes G, Giralt M, Villarroya F. 2007. SIRT1 is involved in glucocorticoid-mediated control of uncoupling protein-3 gene transcription. J Biol Chem 282: 34066-34076.

Andreyev AY, Kushnareva YE, Starkov AA. 2005. Mitochondrial metabolism of reactive oxygen species. Biochemistry (Mosc) 70: 200-214.

Arsenijevic D, et al. 2000. Disruption of the uncoupling protein-2 gene in mice reveals a role in immunity and reactive oxygen species production. Nat Genet 26: 435-439.

Azzu V, Brand MD. 2010. The on-off switches of the mitochondrial uncoupling proteins. Trends Biochem Sci 35: 298-307.

Azzu V, Mookerjee SA, Brand MD. 2010a. Rapid turnover of mitochondrial uncoupling protein 3. Biochem J 426: 13-17.

Azzu V, Jastroch M, Divakaruni AS, Brand MD. 2010b. The regulation and turnover of mitochondrial uncoupling proteins. Biochim Biophys Acta 1797: 785-791.

Balaban RS, Nemoto S, Finkel T. 2005. Mitochondria, oxidants, and aging. Cell 120: 483-495.

Balogh LM, Atkins WM. 2011. Interactions of glutathione transferases with 4-hydroxynonenal. Drug Metab Rev 43: 165-178.

Banerjee A, Locke-Winter C, Rogers KB, Mitchell MB, Brew EC, Cairns CB, Bensard DD, Harken AH. 1993. Preconditioning against myocardial dysfunction after ischemia and reperfusion by an alpha 1-adrenergic mechanism. Circ Res 73: 656-670.

Barreiro E, Garcia-Martinez C, Mas S, Ametller E, Gea J, Argiles JM, Busquets S, Lopez-Soriano FJ. 2009. UCP3 overexpression neutralizes oxidative stress rather than nitrosative stress in mouse myotubes. FEBS Lett 583: 350-356.

Bell KF, Fowler JH, Al-Mubarak B, Horsburgh K, Hardingham GE. 2011a. Activation of Nrf2-regulated glutathione pathway genes by ischemic preconditioning. Oxid Med Cell Longev 2011: 689524.

Bell KF, et al. 2011b. Mild oxidative stress activates Nrf2 in astrocytes, which contributes to neuroprotective ischemic preconditioning. Proc Natl Acad Sci U S A 108: E1-2; author reply E3-4.

Bell RM, Yellon DM. 2012. Conditioning the whole heart—not just the cardiomyocyte. J Mol Cell Cardiol 53: 24-32.

Bell RM, Mocanu MM, Yellon DM. 2011c. Retrograde heart perfusion: the Langendorff technique of isolated heart perfusion. J Mol Cell Cardiol 50: 940-950.

Benedetti A, Comporti M, Fulceri R, Esterbauer H. 1984. Cytotoxic aldehydes originating from the peroxidation of liver microsomal lipids. Identification of 4,5-dihydroxydecenal. Biochim Biophys Acta 792: 172-181.

Bezaire V, Seifert EL, Harper ME. 2007. Uncoupling protein-3: clues in an ongoing mitochondrial mystery. FASEB J 21: 312-324.

Bezaire V, Spriet LL, Campbell S, Sabet N, Gerrits M, Bonen A, Harper ME. 2005. Constitutive UCP3 overexpression at physiological levels increases mouse skeletal muscle capacity for fatty acid transport and oxidation. FASEB J 19: 977-979.

Bienengraeber M, Ozcan C, Terzic A. 2003. Stable transfection of UCP1 confers resistance to hypoxia/reoxygenation in a heart-derived cell line. J Mol Cell Cardiol 35: 861-865.

Blanc J, Alves-Guerra MC, Esposito B, Rousset S, Gourdy P, Ricquier D, Tedgui A, Miroux B, Mallat Z. 2003. Protective role of uncoupling protein 2 in atherosclerosis. Circulation 107: 388-390.

Blanke H, von Hardenberg D, Cohen M, Kaiser H, Karsch KR, Holt J, Smith H, Jr., Rentrop P. 1984. Patterns of creatine kinase release during acute myocardial infarction after nonsurgical reperfusion: comparison with conventional treatment and correlation with infarct size. J Am Coll Cardiol 3: 675-680.

Bolli R, Marban E. 1999. Molecular and cellular mechanisms of myocardial stunning. Physiol Rev 79: 609-634.

Bolli R, Bhatti ZA, Tang XL, Qiu Y, Zhang Q, Guo Y, Jadoon AK. 1997. Evidence that late preconditioning against myocardial stunning in conscious rabbits is triggered by the generation of nitric oxide. Circ Res 81: 42-52.

Bordone L, et al. 2006. Sirt1 regulates insulin secretion by repressing UCP2 in pancreatic beta cells. PLoS Biol 4: e31.

Boss O, Samec S, Paoloni-Giacobino A, Rossier C, Dulloo A, Seydoux J, Muzzin P, Giacobino JP. 1997. Uncoupling protein-3: a new member of the mitochondrial carrier family with tissue-specific expression. FEBS Lett 408: 39-42.

Bouillaud F, Ricquier D, Thibault J, Weissenbach J. 1985. Molecular approach to thermogenesis in brown adipose tissue: cDNA cloning of the mitochondrial uncoupling protein. Proc Natl Acad Sci U S A 82: 445-448.

Brand MD. 1990. The proton leak across the mitochondrial inner membrane. Biochim Biophys Acta 1018: 128-133.

Brand MD. 2000. Uncoupling to survive? The role of mitochondrial inefficiency in ageing. Exp Gerontol 35: 811-820.

Brand MD. 2010. The sites and topology of mitochondrial superoxide production. Exp Gerontol 45: 466-472.

Brand MD, Esteves TC. 2005. Physiological functions of the mitochondrial uncoupling proteins UCP2 and UCP3. Cell Metab 2: 85-93.

Brand MD, Pakay JL, Ocloo A, Kokoszka J, Wallace DC, Brookes PS, Cornwall EJ. 2005. The basal proton conductance of mitochondria depends on adenine nucleotide translocase content. Biochem J 392: 353-362.

Brand MD, Pamplona R, Portero-Otin M, Requena JR, Roebuck SJ, Buckingham JA, Clapham JC, Cadenas S. 2002. Oxidative damage and phospholipid fatty acyl composition in skeletal muscle mitochondria from mice underexpressing or overexpressing uncoupling protein 3. Biochem J 368: 597-603.

Brand MD, Affourtit C, Esteves TC, Green K, Lambert AJ, Miwa S, Pakay JL, Parker N. 2004. Mitochondrial superoxide: production, biological effects, and activation of uncoupling proteins. Free Radic Biol Med 37: 755-767.

Breen EP, Gouin SG, Murphy AF, Haines LR, Jackson AM, Pearson TW, Murphy PV, Porter RK. 2006. On the mechanism of mitochondrial uncoupling protein 1 function. J Biol Chem 281: 2114-2119.

Brookes PS, Rolfe DF, Brand MD. 1997. The proton permeability of liposomes made from mitochondrial inner membrane phospholipids: comparison with isolated mitochondria. J Membr Biol 155: 167-174.

Brookes PS, Buckingham JA, Tenreiro AM, Hulbert AJ, Brand MD. 1998. The proton permeability of the inner membrane of liver mitochondria from ectothermic and endothermic vertebrates and from obese rats: correlations with standard metabolic rate and phospholipid fatty acid composition. Comp Biochem Physiol B Biochem Mol Biol 119: 325-334.

Brunelle JK, Bell EL, Quesada NM, Vercauteren K, Tiranti V, Zeviani M, Scarpulla RC, Chandel NS. 2005. Oxygen sensing requires mitochondrial ROS but not oxidative phosphorylation. Cell Metab 1: 409-414.

Bryan HK, Olayanju A, Goldring CE, Park BK. 2013. The Nrf2 cell defence pathway: Keap1-dependent and -independent mechanisms of regulation. Biochemical Pharmacology 85: 705-717.

Bugger H, et al. 2008. Type 1 diabetic akita mouse hearts are insulin sensitive but manifest structurally abnormal mitochondria that remain coupled despite increased uncoupling protein 3. Diabetes 57: 2924-2932.

Busquets S, Sanchis D, Alvarez B, Ricquier D, Lopez-Soriano FJ, Argiles JM. 1998. In the rat, tumor necrosis factor alpha administration results in an increase in both UCP2 and UCP3 mRNAs in skeletal muscle: a possible mechanism for cytokine-induced thermogenesis? FEBS Lett 440: 348-350.

Cadenas E, Davies KJ. 2000. Mitochondrial free radical generation, oxidative stress, and aging. Free Radic Biol Med 29: 222-230.

Cadenas S, Aragones J, Landazuri MO. 2010. Mitochondrial reprogramming through cardiac oxygen sensors in ischaemic heart disease. Cardiovasc Res 88: 219-228.

Cadenas S, Buckingham JA, Samec S, Seydoux J, Din N, Dulloo AG, Brand MD. 1999. UCP2 and UCP3 rise in starved rat skeletal muscle but mitochondrial proton conductance is unchanged. FEBS Lett 462: 257-260.

Cadenas S, Echtay KS, Harper JA, Jekabsons MB, Buckingham JA, Grau E, Abuin A, Chapman H, Clapham JC, Brand MD. 2002. The basal proton conductance of skeletal muscle mitochondria from transgenic mice overexpressing or lacking uncoupling protein-3. J Biol Chem 277: 2773-2778.

Cai Z, Zhong H, Bosch-Marce M, Fox-Talbot K, Wang L, Wei C, Trush MA, Semenza GL. 2008. Complete loss of ischaemic preconditioning-induced cardioprotection in mice with partial deficiency of HIF-1 alpha. Cardiovasc Res 77: 463-470.

Cannon B, Nedergaard J. 2004. Brown adipose tissue: function and physiological significance. Physiol Rev 84: 277-359.

Cassard-Doulcier AM, Gelly C, Fox N, Schrementi J, Raimbault S, Klaus S, Forest C, Bouillaud F, Ricquier D. 1993. Tissue-specific and beta-adrenergic regulation of the mitochondrial uncoupling protein gene: control by cis-acting elements in the 5'-flanking region. Mol Endocrinol 7: 497-506.

Cohen MV, Yang XM, Liu GS, Heusch G, Downey JM. 2001. Acetylcholine, bradykinin, opioids, and phenylephrine, but not adenosine, trigger preconditioning by generating free radicals and opening mitochondrial K(ATP) channels. Circ Res 89: 273-278.

Conklin D, Prough R, Bhatanagar A. 2007. Aldehyde metabolism in the cardiovascular system. Mol Biosyst 3: 136-150.

Crescenzo R, Mainieri D, Solinas G, Montani JP, Seydoux J, Liverini G, Iossa S, Dulloo AG. 2003. Skeletal muscle mitochondrial oxidative capacity and uncoupling protein 3 are differently influenced by semistarvation and refeeding. FEBS Lett 544: 138-142.

Cullinan SB, Zhang D, Hannink M, Arvisais E, Kaufman RJ, Diehl JA. 2003. Nrf2 is a direct PERK substrate and effector of PERK-dependent cell survival. Mol Cell Biol 23: 7198-7209.

Cypess AM, et al. 2009. Identification and importance of brown adipose tissue in adult humans. N Engl J Med 360: 1509-1517.

Chan CB, Harper ME. 2006. Uncoupling proteins: role in insulin resistance and insulin insufficiency. Curr Diabetes Rev 2: 271-283.

Chan CB, De Leo D, Joseph JW, McQuaid TS, Ha XF, Xu F, Tsushima RG, Pennefather PS, Salapatek AM, Wheeler MB. 2001. Increased uncoupling protein-2 levels in beta-cells are associated with impaired glucose-stimulated insulin secretion: mechanism of action. Diabetes 50: 1302-1310.

Chance B, Sies H, Boveris A. 1979. Hydroperoxide metabolism in mammalian organs. Physiol Rev 59: 527-605.

Chapple SJ, Cheng X, Mann GE. 2013. Effects of 4-hydroxynonenal on vascular endothelial and smooth muscle cell redox signaling and function in health and disease. Redox Biol 1: 319-331.

Chen CH, Budas GR, Churchill EN, Disatnik MH, Hurley TD, Mochly-Rosen D. 2008. Activation of Aldehyde Dehydrogenase-2 Reduces Ischemic Damage to the Heart. Science 321: 1493-1495.

Chen W, Sun Z, Wang XJ, Jiang T, Huang Z, Fang D, Zhang DD. 2009. Direct interaction between Nrf2 and p21(Cip1/WAF1) upregulates the Nrf2-mediated antioxidant response. Mol Cell 34: 663-673.

Churchill EN, Disatnik MH, Mochly-Rosen D. 2009. Time-dependent and ethanol-induced cardiac protection from ischemia mediated by mitochondrial translocation of varepsilonPKC and activation of aldehyde dehydrogenase 2. J Mol Cell Cardiol 46: 278-284.

Davies KJ. 1995. Oxidative stress: the paradox of aerobic life. Biochem Soc Symp 61: 1-31.

de Luis DA, Aller R, Izaola O, Sagrado MG, Conde R, Primo D, de la Fuente B, Ovalle HF, Mambrilla MR. 2012. Relationship of -55C/T polymorphism of uncoupling protein 3 (UCP3) gene with metabolic syndrome by ATP III classification. J Clin Lab Anal 26: 272-278.

del Arco A, Satrústegui J. 2013. Mitochondrial Carriers.

Demple B, Harrison L. 1994. Repair of oxidative damage to DNA: enzymology and biology. Annu Rev Biochem 63: 915-948.

Dinkova-Kostova AT, Holtzclaw WD, Wakabayashi N. 2005. Keap1, the sensor for electrophiles and oxidants that regulates the phase 2 response, is a zinc metalloprotein. Biochemistry 44: 6889-6899.

Dinkova-Kostova AT, Holtzclaw WD, Cole RN, Itoh K, Wakabayashi N, Katoh Y, Yamamoto M, Talalay P. 2002. Direct evidence that sulfhydryl groups of Keap1 are the sensors regulating induction of phase 2 enzymes that protect against carcinogens and oxidants. Proc Natl Acad Sci U S A 99: 11908-11913.

Drose S, Hanley PJ, Brandt U. 2009. Ambivalent effects of diazoxide on mitochondrial ROS production at respiratory chain complexes I and III. Biochim Biophys Acta 1790: 558-565.

Duval C, Negre-Salvayre A, Dogilo A, Salvayre R, Penicaud L, Casteilla L. 2002. Increased reactive oxygen species production with antisense oligonucleotides directed against uncoupling protein 2 in murine endothelial cells. Biochem Cell Biol 80: 757-764.

Eaton P, Li JM, Hearse DJ, Shattock MJ. 1999. Formation of 4-hydroxy-2-nonenal-modified proteins in ischemic rat heart. Am J Physiol 276: H935-943.

Echtay KS, Winkler E, Frischmuth K, Klingenberg M. 2001. Uncoupling proteins 2 and 3 are highly active H(+) transporters and highly nucleotide sensitive when activated by coenzyme Q (ubiquinone). Proc Natl Acad Sci U S A 98: 1416-1421.

Echtay KS, Pakay JL, Esteves TC, Brand MD. 2005. Hydroxynonenal and uncoupling proteins: a model for protection against oxidative damage. Biofactors 24: 119-130.

Echtay KS, et al. 2003. A signalling role for 4-hydroxy-2-nonenal in regulation of mitochondrial uncoupling. EMBO J 22: 4103-4110.

Echtay KS, et al. 2002. Superoxide activates mitochondrial uncoupling proteins. Nature 415: 96-99.

Ellis AK. 1991. Serum protein measurements and the diagnosis of acute myocardial infarction. Circulation 83: 1107-1109.

Enerback S, Jacobsson A, Simpson EM, Guerra C, Yamashita H, Harper ME, Kozak LP. 1997. Mice lacking mitochondrial uncoupling protein are cold-sensitive but not obese. Nature 387: 90-94.

Esterbauer H, Schaur RJ, Zollner H. 1991. Chemistry and biochemistry of 4-hydroxynonenal, malonaldehyde and related aldehydes. Free Radic Biol Med 11: 81-128.

Esteves TC, Brand MD. 2005. The reactions catalysed by the mitochondrial uncoupling proteins UCP2 and UCP3. Biochim Biophys Acta 1709: 35-44.

Finkel T. 2011. Signal transduction by reactive oxygen species. J Cell Biol 194: 7-15.

Fleury C, et al. 1997. Uncoupling protein-2: a novel gene linked to obesity and hyperinsulinemia. Nat Genet 15: 269-272.

Fourquet S, Guerois R, Biard D, Toledano MB. 2010. Activation of NRF2 by nitrosative agents and H2O2 involves KEAP1 disulfide formation. J Biol Chem 285: 8463-8471.

Freeman BA, Crapo JD. 1982. Biology of disease: free radicals and tissue injury. Lab Invest 47: 412-426.

Fu J, Taubman MB. 2010. Prolyl hydroxylase EGLN3 regulates skeletal myoblast differentiation through an NF-kappaB-dependent pathway. J Biol Chem 285: 8927-8935.

Galluzzi L, Kroemer G. 2008. Necroptosis: a specialized pathway of programmed necrosis. Cell 135: 1161-1163.

Galluzzi L, Kepp O, Trojel-Hansen C, Kroemer G. 2012. Mitochondrial control of cellular life, stress, and death. Circ Res 111: 1198-1207.

Gargiulo S, et al. 2014. Genetic deletion in uncoupling protein 3 augments 18F-fluorodeoxyglucose cardiac uptake in the ischemic heart. BMC Cardiovasc Disord 14: 98.

Garlick PB, Davies MJ, Hearse DJ, Slater TF. 1987. Direct detection of free radicals in the reperfused rat heart using electron spin resonance spectroscopy. Circ Res 61: 757-760.

Garlid KD, Jaburek M, Jezek P. 1998. The mechanism of proton transport mediated by mitochondrial uncoupling proteins. FEBS Lett 438: 10-14.

Giardina TM, Steer JH, Lo SZ, Joyce DA. 2008. Uncoupling protein-2 accumulates rapidly in the inner mitochondrial membrane during mitochondrial reactive oxygen stress in macrophages. Biochim Biophys Acta 1777: 118-129.

Gong DW, et al. 2000. Lack of obesity and normal response to fasting and thyroid hormone in mice lacking uncoupling protein-3. J Biol Chem 275: 16251-16257.

Gross GJ, Auchampach JA. 1992. Blockade of ATP-sensitive potassium channels prevents myocardial preconditioning in dogs. Circ Res 70: 223-233.

Grune T, Reinheckel T, Joshi M, Davies KJ. 1995. Proteolysis in cultured liver epithelial cells during oxidative stress. Role of the multicatalytic proteinase complex, proteasome. J Biol Chem 270: 2344-2351.

Gutierrez-Aguilar M, Baines CP. 2013. Physiological and pathological roles of mitochondrial SLC25 carriers. Biochem J 454: 371-386.

Guzy RD, Hoyos B, Robin E, Chen H, Liu L, Mansfield KD, Simon MC, Hammerling U, Schumacker PT. 2005. Mitochondrial complex III is required for hypoxia-induced ROS production and cellular oxygen sensing. Cell Metab 1: 401-408.

Hafner RP, Nobes CD, McGown AD, Brand MD. 1988. Altered relationship between protonmotive force and respiration rate in non-phosphorylating liver mitochondria isolated from rats of different thyroid hormone status. Eur J Biochem 178: 511-518.

Halestrap AP. 2010. A pore way to die: the role of mitochondria in reperfusion injury and cardioprotection. Biochem Soc Trans 38: 841-860.

Halestrap AP, Pasdois P. 2009. The role of the mitochondrial permeability transition pore in heart disease. Biochim Biophys Acta 1787: 1402-1415.

Halestrap AP, Clarke SJ, Khaliulin I. 2007. The role of mitochondria in protection of the heart by preconditioning. Biochim Biophys Acta 1767: 1007-1031.

Halliwell B. 2011. Free radicals and antioxidants - quo vadis? Trends Pharmacol Sci 32: 125-130.

Halliwell B, Gutteridge JM. 1990. Role of free radicals and catalytic metal ions in human disease: an overview. Methods Enzymol 186: 1-85.

Hausenloy DJ, Yellon DM. 2011. The therapeutic potential of ischemic conditioning: an update. Nat Rev Cardiol 8: 619-629.

Hausenloy DJ, Tsang A, Yellon DM. 2005. The reperfusion injury salvage kinase pathway: a common target for both ischemic preconditioning and postconditioning. Trends Cardiovasc Med 15: 69-75.

Hekimi S, Lapointe J, Wen Y. 2011. Taking a "good" look at free radicals in the aging process. Trends Cell Biol 21: 569-576.

Hill Bradford G, Dranka Brian P, Zou L, Chatham John C, Darley-Usmar Victor M. 2009a. Importance of the bioenergetic reserve capacity in response to cardiomyocyte stress induced by 4-hydroxynonenal. Biochemical Journal 424: 99-107.

Hill BG, Awe SO, Vladykovskaya E, Ahmed Y, Liu SQ, Bhatnagar A, Srivastava S. 2009b. Myocardial ischaemia inhibits mitochondrial metabolism of 4-hydroxy-trans-2-nonenal. Biochem J 417: 513-524.

Himms-Hagen J, Harper ME. 2001. Physiological role of UCP3 may be export of fatty acids from mitochondria when fatty acid oxidation predominates: an hypothesis. Exp Biol Med (Maywood) 226: 78-84.

Hoerter J, Gonzalez-Barroso MD, Couplan E, Mateo P, Gelly C, Cassard-Doulcier AM, Diolez P, Bouillaud F. 2004. Mitochondrial uncoupling protein 1 expressed in the heart of transgenic mice protects against ischemic-reperfusion damage. Circulation 110: 528-533.

Huang HC, Nguyen T, Pickett CB. 2002. Phosphorylation of Nrf2 at Ser-40 by protein kinase C regulates antioxidant response element-mediated transcription. J Biol Chem 277: 42769-42774.

Hulbert AJ, Else PL, Manolis SC, Brand MD. 2002. Proton leak in hepatocytes and liver mitochondria from archosaurs (crocodiles) and allometric relationships for ectotherms. J Comp Physiol B 172: 387-397.

Hurtaud C, Gelly C, Bouillaud F, Levi-Meyrueis C. 2006. Translation control of UCP2 synthesis by the upstream open reading frame. Cell Mol Life Sci 63: 1780-1789.

Huttemann M, Lee I, Pecinova A, Pecina P, Przyklenk K, Doan JW. 2008. Regulation of oxidative phosphorylation, the mitochondrial membrane potential, and their role in human disease. J Bioenerg Biomembr 40: 445-456.

Huttemann M, Pecina P, Rainbolt M, Sanderson TH, Kagan VE, Samavati L, Doan JW, Lee I. 2011. The multiple functions of cytochrome c and their regulation in life and death decisions of the mammalian cell: From respiration to apoptosis. Mitochondrion 11: 369-381.

Indo HP, Davidson M, Yen HC, Suenaga S, Tomita K, Nishii T, Higuchi M, Koga Y, Ozawa T, Majima HJ. 2007. Evidence of ROS generation by mitochondria in cells with impaired electron transport chain and mitochondrial DNA damage. Mitochondrion 7: 106-118.

Ishii T, Itoh K, Yamamoto M. 2002. Roles of Nrf2 in activation of antioxidant enzyme genes via antioxidant responsive elements. Methods Enzymol 348: 182-190.

Itoh K, Wakabayashi N, Katoh Y, Ishii T, Igarashi K, Engel JD, Yamamoto M. 1999. Keap1 represses nuclear activation of antioxidant responsive elements by Nrf2 through binding to the amino-terminal Neh2 domain. Genes Dev 13: 76-86.

Itoh K, et al. 1997. An Nrf2/small Maf heterodimer mediates the induction of phase II detoxifying enzyme genes through antioxidant response elements. Biochem Biophys Res Commun 236: 313-322.

Jain AK, Mahajan S, Jaiswal AK. 2008. Phosphorylation and dephosphorylation of tyrosine 141 regulate stability and degradation of INrf2: a novel mechanism in Nrf2 activation. J Biol Chem 283: 17712-17720.

Jaiswal AK. 2004. Nrf2 signaling in coordinated activation of antioxidant gene expression. Free Radic Biol Med 36: 1199-1207.

Javadov SA, Clarke S, Das M, Griffiths EJ, Lim KH, Halestrap AP. 2003. Ischaemic preconditioning inhibits opening of mitochondrial permeability transition pores in the reperfused rat heart. J Physiol 549: 513-524.

Jezek P, Hlavata L. 2005. Mitochondria in homeostasis of reactive oxygen species in cell, tissues, and organism. Int J Biochem Cell Biol 37: 2478-2503.

Jiang N, Zhang G, Bo H, Qu J, Ma G, Cao D, Wen L, Liu S, Ji LL, Zhang Y. 2009. Upregulation of uncoupling protein-3 in skeletal muscle during exercise: a potential antioxidant function. Free Radic Biol Med 46: 138-145.

Jimenez-Jimenez J, Ledesma A, Zaragoza P, Gonzalez-Barroso MM, Rial E. 2006. Fatty acid activation of the uncoupling proteins requires the presence of the central matrix loop from UCP1. Biochim Biophys Acta 1757: 1292-1296.

Kang KW, Lee SJ, Park JW, Kim SG. 2002. Phosphatidylinositol 3-kinase regulates nuclear translocation of NF-E2-related factor 2 through actin rearrangement in response to oxidative stress. Mol Pharmacol 62: 1001-1010.

Kawai Y, Garduno L, Theodore M, Yang J, Arinze IJ. 2011. Acetylation-deacetylation of the transcription factor Nrf2 (nuclear factor erythroid 2-related factor 2) regulates its transcriptional activity and nucleocytoplasmic localization. J Biol Chem 286: 7629-7640.

Kehrer JP. 1993. Free radicals as mediators of tissue injury and disease. Crit Rev Toxicol 23: 21-48.

Khailova LS, Prikhodko EA, Dedukhova VI, Mokhova EN, Popov VN, Skulachev VP. 2006. Participation of ATP/ADP antiporter in oleate- and oleate hydroperoxide-induced uncoupling suppressed by GDP and carboxyatractylate. Biochim Biophys Acta 1757: 1324-1329.

Kloner RA, Bolli R, Marban E, Reinlib L, Braunwald E. 1998. Medical and cellular implications of stunning, hibernation, and preconditioning: an NHLBI workshop. Circulation 97: 1848-1867.

Kobayashi A, Kang MI, Watai Y, Tong KI, Shibata T, Uchida K, Yamamoto M. 2006. Oxidative and electrophilic stresses activate Nrf2 through inhibition of ubiquitination activity of Keap1. Mol Cell Biol 26: 221-229.

Kobayashi A, Kang MI, Okawa H, Ohtsuji M, Zenke Y, Chiba T, Igarashi K, Yamamoto M. 2004. Oxidative stress sensor Keap1 functions as an adaptor for Cul3-based E3 ligase to regulate proteasomal degradation of Nrf2. Mol Cell Biol 24: 7130-7139.

Komatsu M, et al. 2010. The selective autophagy substrate p62 activates the stress responsive transcription factor Nrf2 through inactivation of Keap1. Nat Cell Biol 12: 213-223.

Korshunov SS, Skulachev VP, Starkov AA. 1997. High protonic potential actuates a mechanism of production of reactive oxygen species in mitochondria. FEBS Lett 416: 15-18.

Kozak UC, Kopecky J, Teisinger J, Enerback S, Boyer B, Kozak LP. 1994. An upstream enhancer regulating brown-fat-specific expression of the mitochondrial uncoupling protein gene. Mol Cell Biol 14: 59-67.

Krauss S, Zhang CY, Lowell BB. 2002. A significant portion of mitochondrial proton leak in intact thymocytes depends on expression of UCP2. Proc Natl Acad Sci U S A 99: 118-122.

Krauss S, Zhang C-Y, Lowell BB. 2005. The mitochondrial uncoupling-protein homologues. Nature Reviews Molecular Cell Biology 6: 248-261.

Krauss S, Zhang CY, Scorrano L, Dalgaard LT, St-Pierre J, Grey ST, Lowell BB. 2003. Superoxide-mediated activation of uncoupling protein 2 causes pancreatic beta cell dysfunction. J Clin Invest 112: 1831-1842.

Kuzuya T, Hoshida S, Yamashita N, Fuji H, Oe H, Hori M, Kamada T, Tada M. 1993. Delayed effects of sublethal ischemia on the acquisition of tolerance to ischemia. Circ Res 72: 1293-1299.

Langendorff O. 1895. Untersuchungen am uberlebenden Saugethierherzen. Pflugers Arch 61: 291–332.

Lanni A, Beneduce L, Lombardi A, Moreno M, Boss O, Muzzin P, Giacobino JP, Goglia F. 1999. Expression of uncoupling protein-3 and mitochondrial activity in the transition from hypothyroid to hyperthyroid state in rat skeletal muscle. FEBS Lett 444: 250-254.

Larkin S, Mull E, Miao W, Pittner R, Albrandt K, Moore C, Young A, Denaro M, Beaumont K. 1997. Regulation of the third member of the uncoupling protein family, UCP3, by cold and thyroid hormone. Biochem Biophys Res Commun 240: 222-227.

Lemasters JJ, Bond JM, Chacon E, Harper IS, Kaplan SH, Ohata H, Trollinger DR, Herman B, Cascio WE. 1996. The pH paradox in ischemia-reperfusion injury to cardiac myocytes. EXS 76: 99-114.

Leonard MO, Kieran NE, Howell K, Burne MJ, Varadarajan R, Dhakshinamoorthy S, Porter AG, O'Farrelly C, Rabb H, Taylor CT. 2006. Reoxygenation-specific activation of the antioxidant transcription factor Nrf2 mediates cytoprotective gene expression in ischemia-reperfusion injury. The FASEB Journal.

Levraut J, Iwase H, Shao ZH, Vanden Hoek TL, Schumacker PT. 2003. Cell death during ischemia: relationship to mitochondrial depolarization and ROS generation. Am J Physiol Heart Circ Physiol 284: H549-558.

Li LX, Skorpen F, Egeberg K, Jorgensen IH, Grill V. 2002. Induction of uncoupling protein 2 mRNA in beta-cells is stimulated by oxidation of fatty acids but not by nutrient oversupply. Endocrinology 143: 1371-1377.

Liao R, Podesser BK, Lim CC. 2012. The continuing evolution of the Langendorff and ejecting murine heart: new advances in cardiac phenotyping. Am J Physiol Heart Circ Physiol 303: H156-167.

Liesa M, Shirihai OS. 2013. Mitochondrial dynamics in the regulation of nutrient utilization and energy expenditure. Cell Metab 17: 491-506.

Liu GS, Thornton J, Van Winkle DM, Stanley AW, Olsson RA, Downey JM. 1991. Protection against infarction afforded by preconditioning is mediated by A1 adenosine receptors in rabbit heart. Circulation 84: 350-356.

Locke RM, Rial E, Nicholls DG. 1982. The acute regulation of mitochondrial proton conductance in cells and mitochondria from the brown fat of cold-adapted and warm-adapted guinea pigs. Eur J Biochem 129: 381-387.

Lombardi A, Busiello RA, Napolitano L, Cioffi F, Moreno M, de Lange P, Silvestri E, Lanni A, Goglia F. 2010. UCP3 translocates lipid hydroperoxide and mediates lipid hydroperoxide-dependent mitochondrial uncoupling. J Biol Chem 285: 16599-16605.

Ma Q. 2010. Transcriptional responses to oxidative stress: pathological and toxicological implications. Pharmacol Ther 125: 376-393.

Ma Q, He X. 2012. Molecular basis of electrophilic and oxidative defense: promises and perils of Nrf2. Pharmacol Rev 64: 1055-1081.

Mailloux RJ, Harper M-E. 2011. Uncoupling proteins and the control of mitochondrial reactive oxygen species production. Free Radical Biology and Medicine 51: 1106-1115.

Mailloux RJ, Xuan JY, Beauchamp B, Jui L, Lou M, Harper ME. 2013. Glutaredoxin-2 is required to control proton leak through uncoupling protein-3. J Biol Chem 288: 8365-8379.

Mak S, Lehotay DC, Yazdanpanah M, Azevedo ER, Liu PP, Newton GE. 2000. Unsaturated aldehydes including 4-OH-nonenal are elevated in patients with congestive heart failure. J Card Fail 6: 108-114.

Malhotra D, et al. 2010. Global mapping of binding sites for Nrf2 identifies novel targets in cell survival response through ChIP-Seq profiling and network analysis. Nucleic Acids Res 38: 5718-5734.

Marber MS, Latchman DS, Walker JM, Yellon DM. 1993. Cardiac stress protein elevation 24 hours after brief ischemia or heat stress is associated with resistance to myocardial infarction. Circulation 88: 1264-1272.

Mari M, Morales A, Colell A, Garcia-Ruiz C, Fernandez-Checa JC. 2009. Mitochondrial glutathione, a key survival antioxidant. Antioxid Redox Signal 11: 2685-2700.

Maynard S, de Souza-Pinto NC, Scheibye-Knudsen M, Bohr VA. 2010. Mitochondrial base excision repair assays. Methods 51: 416-425.

McCord JM, Roy RS, Schaffer SW. 1985. Free radicals and myocardial ischemia. The role of xanthine oxidase. Adv Myocardiol 5: 183-189.

McLeod CJ, Aziz A, Hoyt RF, Jr., McCoy JP, Jr., Sack MN. 2005. Uncoupling proteins 2 and 3 function in concert to augment tolerance to cardiac ischemia. J Biol Chem 280: 33470-33476.

Minners J, van den Bos EJ, Yellon DM, Schwalb H, Opie LH, Sack MN. 2000. Dinitrophenol, cyclosporin A, and trimetazidine modulate preconditioning in the isolated rat heart: support for a mitochondrial role in cardioprotection. Cardiovasc Res 47: 68-73.

Minners J, Lacerda L, McCarthy J, Meiring JJ, Yellon DM, Sack MN. 2001. Ischemic and Pharmacological Preconditioning in Girardi Cells and C2C12 Myotubes Induce Mitochondrial Uncoupling. Circulation Research 89: 787-792.

Mitchell P. 1966. Chemiosmotic coupling in oxidative and photosynthetic phosphorylation. Biol Rev Camb Philos Soc 41: 445-502.

Mitchell P. 2011. Chemiosmotic coupling in oxidative and photosynthetic phosphorylation. Biochimica et Biophysica Acta (BBA) - Bioenergetics 1807: 1507-1538.

Mookerjee SA, Brand MD. 2011. Characteristics of the turnover of uncoupling protein 3 by the ubiquitin proteasome system in isolated mitochondria. Biochim Biophys Acta 1807: 1474-1481.

Motohashi H, Yamamoto M. 2004. Nrf2-Keap1 defines a physiologically important stress response mechanism. Trends Mol Med 10: 549-557.

Motohashi H, O'Connor T, Katsuoka F, Engel JD, Yamamoto M. 2002. Integration and diversity of the regulatory network composed of Maf and CNC families of transcription factors. Gene 294: 1-12.

Murphy E, Steenbergen C. 2008. Mechanisms underlying acute protection from cardiac ischemia-reperfusion injury. Physiol Rev 88: 581-609.

Murphy MP. 2009. How mitochondria produce reactive oxygen species. Biochem J 417: 1-13.

Murphy MP, et al. 2003. Superoxide activates uncoupling proteins by generating carbon-centered radicals and initiating lipid peroxidation: studies using a mitochondria-targeted spin trap derived from alpha-phenyl-N-tert-butylnitrone. J Biol Chem 278: 48534-48545.

Murray AJ, Anderson RE, Watson GC, Radda GK, Clarke K. 2004. Uncoupling proteins in human heart. The Lancet 364: 1786-1788.

Murry CE, Jennings RB, Reimer KA. 1986. Preconditioning with ischemia: a delay of lethal cell injury in ischemic myocardium. Circulation 74: 1124-1136.

Nabben M, Hoeks J. 2008. Mitochondrial uncoupling protein 3 and its role in cardiac- and skeletal muscle metabolism. Physiol Behav 94: 259-269.

Nabben M, Shabalina IG, Moonen-Kornips E, van Beurden D, Cannon B, Schrauwen P, Nedergaard J, Hoeks J. 2011. Uncoupled respiration, ROS production, acute lipotoxicity and oxidative damage in isolated skeletal muscle mitochondria from UCP3-ablated mice. Biochim Biophys Acta 1807: 1095-1105.

Nadtochiy SM, Tompkins AJ, Brookes PS. 2006. Different mechanisms of mitochondrial proton leak in ischaemia/reperfusion injury and preconditioning: implications for pathology and cardioprotection. Biochem J 395: 611-618.

Nakamura K, et al. 2002. Carvedilol decreases elevated oxidative stress in human failing myocardium. Circulation 105: 2867-2871.

Negre-Salvayre A, Hirtz C, Carrera G, Cazenave R, Troly M, Salvayre R, Penicaud L, Casteilla L. 1997. A role for uncoupling protein-2 as a regulator of mitochondrial hydrogen peroxide generation. FASEB J 11: 809-815.

Nguyen T, Sherratt PJ, Pickett CB. 2003. Regulatory mechanisms controlling gene expression mediated by the antioxidant response element. Annu Rev Pharmacol Toxicol 43: 233-260.

Nickel A, Kohlhaas M, Maack C. 2014. Mitochondrial reactive oxygen species production and elimination. J Mol Cell Cardiol 73: 26-33.

Nicholls DG. 2001. A history of UCP1. Biochem Soc Trans 29: 751-755.

Nicholls DG. 2006. The physiological regulation of uncoupling proteins. Biochim Biophys Acta 1757: 459-466.

Nicholls and Ferguson. 2013. Bioenergetics 4th Ed. AP Elsevier.

Nicholls DG, Locke RM. 1984. Thermogenic mechanisms in brown fat. Physiol Rev 64: 1-64.

Nioi P, McMahon M, Itoh K, Yamamoto M, Hayes JD. 2003. Identification of a novel Nrf2-regulated antioxidant response element (ARE) in the mouse NAD(P)H:quinone oxidoreductase 1 gene: reassessment of the ARE consensus sequence. Biochem J 374: 337-348.

Niture SK, Jain AK, Jaiswal AK. 2009. Antioxidant-induced modification of INrf2 cysteine 151 and PKC-delta-mediated phosphorylation of Nrf2 serine 40 are both required for stabilization and nuclear translocation of Nrf2 and increased drug resistance. J Cell Sci 122: 4452-4464.

Nobes CD, Brown GC, Olive PN, Brand MD. 1990. Non-ohmic proton conductance of the mitochondrial inner membrane in hepatocytes. J Biol Chem 265: 12903-12909.

Noji H, Yasuda R, Yoshida M, Kinosita K, Jr. 1997. Direct observation of the rotation of F1-ATPase. Nature 386: 299-302.

Nunnari J, Suomalainen A. 2012. Mitochondria: in sickness and in health. Cell 148: 1145-1159.

Opie LH, Sack MN. 2002. Metabolic plasticity and the promotion of cardiac protection in ischemia and ischemic preconditioning. J Mol Cell Cardiol 34: 1077-1089.

Orrenius S, McConkey DJ, Bellomo G, Nicotera P. 1989. Role of Ca2+ in toxic cell killing. Trends Pharmacol Sci 10: 281-285.

Ozcan C, Palmeri M, Horvath TL, Russell KS, Russell RR, 3rd. 2013. Role of uncoupling protein 3 in ischemia-reperfusion injury, arrhythmias, and preconditioning. Am J Physiol Heart Circ Physiol 304: H1192-1200.

Palmieri F. 2014. Mitochondrial transporters of the SLC25 family and associated diseases: a review. Journal of Inherited Metabolic Disease.

Paradis E, Clavel S, Bouillaud F, Ricquier D, Richard D. 2003. Uncoupling protein 2: a novel player in neuroprotection. Trends Mol Med 9: 522-525.

Park JW, Chun YS, Kim YH, Kim CH, Kim MS. 1997. Ischemic preconditioning reduces Op6 generation and prevents respiratory impairment in the mitochondria of post-ischemic reperfused heart of rat. Life Sci 60: 2207-2219.

Parker N, Vidal-Puig A, Brand MD. 2008a. Stimulation of mitochondrial proton conductance by hydroxynonenal requires a high membrane potential. Biosci Rep 28: 83-88.

Parker N, Affourtit C, Vidal-Puig A, Brand MD. 2008b. Energization-dependent endogenous activation of proton conductance in skeletal muscle mitochondria. Biochem J 412: 131-139.

Parker N, Crichton PG, Vidal-Puig AJ, Brand MD. 2009. Uncoupling protein-1 (UCP1) contributes to the basal proton conductance of brown adipose tissue mitochondria. J Bioenerg Biomembr 41: 335-342.

Parton LE, et al. 2007. Glucose sensing by POMC neurons regulates glucose homeostasis and is impaired in obesity. Nature 449: 228-232.

Pedraza N, Rosell M, Villarroya J, Iglesias R, Gonzalez FJ, Solanes G, Villarroya F. 2006. Developmental and tissue-specific involvement of peroxisome proliferator-activated receptor-alpha in the control of mouse uncoupling protein-3 gene expression. Endocrinology 147: 4695-4704.

Pescador N, Cuevas Y, Naranjo S, Alcaide M, Villar D, Landazuri MO, Del Peso L. 2005. Identification of a functional hypoxia-responsive element that regulates the expression of the egl nine homologue 3 (egln3/phd3) gene. Biochem J 390: 189-197.

Piper HM, Garcia-Dorado D, Ovize M. 1998. A fresh look at reperfusion injury. Cardiovasc Res 38: 291-300.

Porter RK, Hulbert AJ, Brand MD. 1996. Allometry of mitochondrial proton leak: influence of membrane surface area and fatty acid composition. Am J Physiol 271: R1550-1560.

Purdom-Dickinson SE, Lin Y, Dedek M, Morrissy S, Johnson J, Chen QM. 2007. Induction of antioxidant and detoxification response by oxidants in cardiomyocytes: Evidence from gene expression profiling and activation of Nrf2 transcription factor. J Mol Cell Cardiol 42: 159-176.

Raedschelders K, Ansley DM, Chen DD. 2012. The cellular and molecular origin of reactive oxygen species generation during myocardial ischemia and reperfusion. Pharmacol Ther 133: 230-255.

Razeghi P, Young ME, Alcorn JL, Moravec CS, Frazier OH, Taegtmeyer H. 2001. Metabolic gene expression in fetal and failing human heart. Circulation 104: 2923-2931.

Rial E, Poustie A, Nicholls DG. 1983. Brown-adipose-tissue mitochondria: the regulation of the 32000-Mr uncoupling protein by fatty acids and purine nucleotides. Eur J Biochem 137: 197-203.

Rial E, Aguirregoitia E, Jimenez-Jimenez J, Ledesma A. 2004. Alkylsulfonates activate the uncoupling protein UCP1: implications for the transport mechanism. Biochim Biophys Acta 1608: 122-130.

Rial E, Gonzalez-Barroso M, Fleury C, Iturrizaga S, Sanchis D, Jimenez-Jimenez J, Ricquier D, Goubern M, Bouillaud F. 1999. Retinoids activate proton transport by the uncoupling proteins UCP1 and UCP2. EMBO J 18: 5827-5833.

Ricquier D, Bouillaud F. 2000. The uncoupling protein homologues: UCP1, UCP2, UCP3, StUCP and AtUCP. Biochem J 345 Pt 2: 161-179.

Rich PR, Marechal A. 2010. The mitochondrial respiratory chain. Essays Biochem 47: 1-23.

Robidoux J, Martin TL, Collins S. 2004. Beta-adrenergic receptors and regulation of energy expenditure: a family affair. Annu Rev Pharmacol Toxicol 44: 297-323.

Robinson AJ, Overy C, Kunji ER. 2008. The mechanism of transport by mitochondrial carriers based on analysis of symmetry. Proc Natl Acad Sci U S A 105: 17766-17771.

Rodrigo GC, Lawrence CL, Standen NB. 2002. Dinitrophenol pretreatment of rat ventricular myocytes protects against damage by metabolic inhibition and reperfusion. J Mol Cell Cardiol 34: 555-569.

Rolfe DF, Brand MD. 1996. Contribution of mitochondrial proton leak to skeletal muscle respiration and to standard metabolic rate. Am J Physiol 271: C1380-1389.

Rolfe DF, Brand MD. 1997. The physiological significance of mitochondrial proton leak in animal cells and tissues. Biosci Rep 17: 9-16.

Rousset S, Emre Y, Join-Lambert O, Hurtaud C, Ricquier D, Cassard-Doulcier AM. 2006. The uncoupling protein 2 modulates the cytokine balance in innate immunity. Cytokine 35: 135-142.

Rushmore TH, Morton MR, Pickett CB. 1991. The antioxidant responsive element. Activation by oxidative stress and identification of the DNA consensus sequence required for functional activity. J Biol Chem 266: 11632-11639.

Sack M. 2006. Mitochondrial depolarization and the role of uncoupling proteins in ischemia tolerance. Cardiovasc Res 72: 210-219.

Safari F, Anvari Z, Moshtaghioun S, Javan M, Bayat G, Forosh SS, Hekmatimoghaddam S. 2014. Differential expression of cardiac uncoupling proteins 2 and 3 in response to myocardial ischemia-reperfusion in rats. Life Sci 98: 68-74.

Samec S, Seydoux J, Dulloo AG. 1998. Role of UCP homologues in skeletal muscles and brown adipose tissue: mediators of thermogenesis or regulators of lipids as fuel substrate? FASEB J 12: 715-724.

Schoutsen B, De Jong JW, Harmsen E, De Tombe PP, Achterberg PW. 1983. Myocardial xanthine oxidase/dehydrogenase. Biochim Biophys Acta 762: 519-524.

Schrauwen P, Hesselink MK. 2004. The role of uncoupling protein 3 in fatty acid metabolism: protection against lipotoxicity? Proc Nutr Soc 63: 287-292.

Schrauwen P, Hoeks J, Hesselink MK. 2006. Putative function and physiological relevance of the mitochondrial uncoupling protein-3: involvement in fatty acid metabolism? Prog Lipid Res 45: 17-41.

Seifert EL, Bezaire V, Estey C, Harper ME. 2008. Essential role for uncoupling protein-3 in mitochondrial adaptation to fasting but not in fatty acid oxidation or fatty acid anion export. J Biol Chem 283: 25124-25131.

Semenza GL. 2011. Hypoxia-inducible factor 1: regulator of mitochondrial metabolism and mediator of ischemic preconditioning. Biochim Biophys Acta 1813: 1263-1268.

Shabalina IG, Nedergaard J. 2011. Mitochondrial ('mild') uncoupling and ROS production: physiologically relevant or not? Biochem Soc Trans 39: 1305-1309.

Shabalina IG, Ost M, Petrovic N, Vrbacky M, Nedergaard J, Cannon B. 2010. Uncoupling protein-1 is not leaky. Biochim Biophys Acta 1797: 773-784.

Shi W, Vinten-Johansen J. 2012. Endogenous cardioprotection by ischaemic postconditioning and remote conditioning. Cardiovasc Res 94: 206-216.

Shinmura K, Xuan YT, Tang XL, Kodani E, Han H, Zhu Y, Bolli R. 2002. Inducible nitric oxide synthase modulates cyclooxygenase-2 activity in the heart of conscious rabbits during the late phase of ischemic preconditioning. Circ Res 90: 602-608.

Sies H. 1997. Oxidative stress: oxidants and antioxidants. Exp Physiol 82: 291-295.

Skulachev VP. 1991. Fatty acid circuit as a physiological mechanism of uncoupling of oxidative phosphorylation. FEBS Lett 294: 158-162.

Solaini G, Harris DA. 2005. Biochemical dysfunction in heart mitochondria exposed to ischaemia and reperfusion. Biochem J 390: 377-394.

Solanes G, Pedraza N, Iglesias R, Giralt M, Villarroya F. 2003. Functional relationship between MyoD and peroxisome proliferator-activated receptor-dependent regulatory pathways in the control of the human uncoupling protein-3 gene transcription. Mol Endocrinol 17: 1944-1958.

Solanes G, Pedraza N, Calvo V, Vidal-Puig A, Lowell BB, Villarroya F. 2005. Thyroid hormones directly activate the expression of the human and mouse uncoupling protein-3 genes through a thyroid response element in the proximal promoter region. Biochem J 386: 505-513.

Son C, Hosoda K, Ishihara K, Bevilacqua L, Masuzaki H, Fushiki T, Harper ME, Nakao K. 2004. Reduction of diet-induced obesity in transgenic mice overexpressing uncoupling protein 3 in skeletal muscle. Diabetologia 47: 47-54.

Spickett CM. 2013. The lipid peroxidation product 4-hydroxy-2-nonenal: Advances in chemistry and analysis. Redox Biol 1: 145-152.

Srivastava S, Chandrasekar B, Gu Y, Luo J, Hamid T, Hill BG, Prabhu SD. 2007. Downregulation of CuZn-superoxide dismutase contributes to beta-adrenergic receptor-mediated oxidative stress in the heart. Cardiovasc Res 74: 445-455.

Stadtman ER. 2006. Protein oxidation and aging. Free Radic Res 40: 1250-1258.

Stein AB, Bolli R, Guo Y, Wang OL, Tan W, Wu WJ, Zhu X, Zhu Y, Xuan YT. 2007. The late phase of ischemic preconditioning induces a prosurvival genetic program that results in marked attenuation of apoptosis. J Mol Cell Cardiol 42: 1075-1085.

Stock D, Leslie AG, Walker JE. 1999. Molecular architecture of the rotary motor in ATP synthase. Science 286: 1700-1705.

Suleman N, Somers S, Smith R, Opie LH, Lecour SC. 2008. Dual activation of STAT-3 and Akt is required during the trigger phase of ischaemic preconditioning. Cardiovasc Res 79: 127-133.

Sun JZ, Tang XL, Knowlton AA, Park SW, Qiu Y, Bolli R. 1995. Late preconditioning against myocardial stunning. An endogenous protective mechanism that confers resistance to postischemic dysfunction 24 h after brief ischemia in conscious pigs. J Clin Invest 95: 388-403.

Sun Z, Zhang S, Chan JY, Zhang DD. 2007. Keap1 controls postinduction repression of the Nrf2-mediated antioxidant response by escorting nuclear export of Nrf2. Mol Cell Biol 27: 6334-6349.

Sutherland FJ, Shattock MJ, Baker KE, Hearse DJ. 2003. Mouse isolated perfused heart: characteristics and cautions. Clin Exp Pharmacol Physiol 30: 867-878.

Taguchi K, Motohashi H, Yamamoto M. 2011. Molecular mechanisms of the Keap1-Nrf2 pathway in stress response and cancer evolution. Genes Cells 16: 123-140.

Talalay P, Dinkova-Kostova AT, Holtzclaw WD. 2003. Importance of phase 2 gene regulation in protection against electrophile and reactive oxygen toxicity and carcinogenesis. Adv Enzyme Regul 43: 121-134.

Talbot DA, Hanuise N, Rey B, Rouanet JL, Duchamp C, Brand MD. 2003. Superoxide activates a GDP-sensitive proton conductance in skeletal muscle mitochondria from king penguin (Aptenodytes patagonicus). Biochem Biophys Res Commun 312: 983-988.

Teshima Y, Akao M, Jones SP, Marban E. 2003. Uncoupling protein-2 overexpression inhibits mitochondrial death pathway in cardiomyocytes. Circ Res 93: 192-200.

Toime LJ, Brand MD. 2010. Uncoupling protein-3 lowers reactive oxygen species production in isolated mitochondria. Free Radic Biol Med 49: 606-611.

Turrens JF. 2003. Mitochondrial formation of reactive oxygen species. J Physiol 552: 335-344.

Vidal-Puig AJ, et al. 2000. Energy metabolism in uncoupling protein 3 gene knockout mice. J Biol Chem 275: 16258-16266.

Villarroya F, Iglesias R, Giralt M. 2007. PPARs in the Control of Uncoupling Proteins Gene Expression. PPAR Res 2007: 74364.

Vozza A, et al. 2014. UCP2 transports C4 metabolites out of mitochondria, regulating glucose and glutamine oxidation. Proceedings of the National Academy of Sciences 111: 960-965.

Wang X, Gong J, Liu X, Zhan R, Kong R, Zhao Y, Wan D, Leng X, Chen M, Qian L. 2010. Expression of uncoupling protein 3 in mitochondria protects against stress-induced myocardial injury: a proteomic study. Cell Stress Chaperones 15: 771-779.

Whelan RS, Kaplinskiy V, Kitsis RN. 2010. Cell death in the pathogenesis of heart disease: mechanisms and significance. Annu Rev Physiol 72: 19-44.

Winkler E, Klingenberg M. 1994. Effect of fatty acids on H+ transport activity of the reconstituted uncoupling protein. J Biol Chem 269: 2508-2515.

Wojcik M, Burzynska-Pedziwiatr I, Wozniak LA. 2010. A review of natural and synthetic antioxidants important for health and longevity. Curr Med Chem 17: 3262-3288.

Xuan YT, Tang XL, Banerjee S, Takano H, Li RC, Han H, Qiu Y, Li JJ, Bolli R. 1999. Nuclear factor-kappaB plays an essential role in the late phase of ischemic preconditioning in conscious rabbits. Circ Res 84: 1095-1109.

Yamamoto T, Suzuki T, Kobayashi A, Wakabayashi J, Maher J, Motohashi H, Yamamoto M. 2008. Physiological significance of reactive cysteine residues of Keap1 in determining Nrf2 activity. Mol Cell Biol 28: 2758-2770.

Yellon DM, Downey JM. 2003. Preconditioning the myocardium: from cellular physiology to clinical cardiology. Physiol Rev 83: 1113-1151.

Yellon DM, Hausenloy DJ. 2007. Myocardial reperfusion injury. N Engl J Med 357: 1121-1135.

Yu BP. 1994. Cellular defenses against damage from reactive oxygen species. Physiol Rev 74: 139-162.

Yu R, Chen C, Mo YY, Hebbar V, Owuor ED, Tan TH, Kong AN. 2000a. Activation of mitogen-activated protein kinase pathways induces antioxidant response element-mediated gene expression via a Nrf2-dependent mechanism. J Biol Chem 275: 39907-39913.

Yu XX, Mao W, Zhong A, Schow P, Brush J, Sherwood SW, Adams SH, Pan G. 2000b. Characterization of novel UCP5/BMCP1 isoforms and differential regulation of UCP4 and UCP5 expression through dietary or temperature manipulation. FASEB J 14: 1611-1618.

Zackova M, Skobisova E, Urbankova E, Jezek P. 2003. Activating omega-6 polyunsaturated fatty acids and inhibitory purine nucleotides are high affinity ligands for novel mitochondrial uncoupling proteins UCP2 and UCP3. J Biol Chem 278: 20761-20769.

Zhang CY, Parton LE, Ye CP, Krauss S, Shen R, Lin CT, Porco JA, Jr., Lowell BB. 2006. Genipin inhibits UCP2-mediated proton leak and acutely reverses obesity- and high glucose-induced beta cell dysfunction in isolated pancreatic islets. Cell Metab 3: 417-427.

Zhang CY, et al. 2001. Uncoupling protein-2 negatively regulates insulin secretion and is a major link between obesity, beta cell dysfunction, and type 2 diabetes. Cell 105: 745-755.

Zhang Y, et al. 2010. 4-hydroxy-2-nonenal protects against cardiac ischemia-reperfusion injury via the Nrf2-dependent pathway. J Mol Cell Cardiol 49: 576-586.

Zorov DB, Juhaszova M, Sollott SJ. 2014. Mitochondrial Reactive Oxygen Species (ROS) and ROS-Induced ROS Release. Physiol Rev 94: 909-950.

Zweier JL, Talukder MA. 2006. The role of oxidants and free radicals in reperfusion injury. Cardiovasc Res 70: 181-190.

Zweier JL, Flaherty JT, Weisfeldt ML. 1987. Direct measurement of free radical generation following reperfusion of ischemic myocardium. Proc Natl Acad Sci U S A 84: 1404-1407.

Zweier JL, Kuppusamy P, Williams R, Rayburn BK, Smith D, Weisfeldt ML, Flaherty JT. 1989. Measurement and characterization of postischemic free radical generation in the isolated perfused heart. J Biol Chem 264: 18890-18895.

ANNEX

APPENDED ARTICLE

Anedda A, Lopez-Bernardo E, Acosta-Iborra B, Saadeh Suleiman M, Landazuri MO, Cadenas S. 2013. The transcription factor Nrf2 promotes survival by enhancing the expression of uncoupling protein 3 under conditions of oxidative stress. Free Radic Biol Med 61C: 395-407.